

3-26-2010

Design and development of an enzyme-linked biosensor for detection and quantification of phosphate species

Serkan Akar

Florida International University

DOI: 10.25148/etd.FI13101554

Follow this and additional works at: <https://digitalcommons.fiu.edu/etd>

 Part of the [Biomedical Engineering and Bioengineering Commons](#)

Recommended Citation

Akar, Serkan, "Design and development of an enzyme-linked biosensor for detection and quantification of phosphate species" (2010). *FIU Electronic Theses and Dissertations*. 1213.
<https://digitalcommons.fiu.edu/etd/1213>

This work is brought to you for free and open access by the University Graduate School at FIU Digital Commons. It has been accepted for inclusion in FIU Electronic Theses and Dissertations by an authorized administrator of FIU Digital Commons. For more information, please contact dcc@fiu.edu.

FLORIDA INTERNATIONAL UNIVERSITY

Miami, Florida

DESIGN AND DEVELOPMENT OF AN ENZYME-LINKED BIOSENSOR FOR
DETECTION AND QUANTIFICATION OF PHOSPHATE SPECIES

A thesis submitted in partial fulfillment of the
requirements for the degree of

MASTER OF SCIENCE

in

BIOMEDICAL ENGINEERING

by

Serkan Akar

2010

To: Dean Amir Mirmiran
College of Engineering and Computing


This thesis, written by Serkan Akar, and entitled Design and Development of an Enzyme-Linked Biosensor for Detection and Quantification of Phosphate Species, having been approved in respect to style and intellectual content, is referred to you for judgment.

We have read this thesis and recommend that it be approved.

 Wei-Chiang Lin

 Leonel Lagos

 Nezh Pala

 Vekalet Tek, Major Professor

Date of Defense: March 26, 2010

The thesis of Serkan Akar is approved.

Dean Amir Mirmiran
College of Engineering and Computing

Interim Dean Kevin O'Shea
University Graduate School

Florida International University, 2010

DEDICATION

I would like to dedicate this work to my family. To my loving wife Kasia for her emotional support, to my siblings, especially my sister Tülüş for never ending encouragement, my parents Güllü and Ibrahim for instilling in me the importance of good education, and finally to my parents-in-law Maggie and Sam for cheering me up along this journey.

ACKNOWLEDGMENT

It is a pleasure to thank those who made this thesis possible. First and foremost, I would like to acknowledge my major professor Dr. Vekalet Tek for her tremendous help and dedication to my project. It was an honor for me to work with such a great professor and a scientist. Dr. Tek was not only a professor to me; she was also a very professional mentor and a supervisor who walked me through the thesis research. I appreciate her immense knowledge, guidance, honesty, openness and friendship. I thank her for being there for me whenever I needed her even at 2 am in the morning.

I am also indebted to Dr. Leonel Lagos, for giving me the chance of joining the Department of Energy (DOE) as Fellow Program. He has made his support available in a number of ways including various learning opportunities, hands on experiences at Applied Research Center (ARC), internships at Oak Ridge National Laboratory, Tennessee and Pacific Northwest National Laboratory, Washington, most importantly projected DOE Head Quarters internship possibility. I appreciate his concern about my future and his recommendation for a position at Department of Energy.

A special thanks to Dr. Wei-Chiang Lin who is my committee member for his valuable advice in science discussion, supervision in sensing techniques and furthermore, using his precious times to review my presentations, read this thesis and gave his critical comments about it.

I also gratefully acknowledge Dr. Nezhil Pala who is my other committee member for his advice and crucial contribution, which made him a valuable part of this research and so to this thesis. His involvement with his originality has triggered and nourished my intellectual maturity that I will benefit from, for a long time to come.

In addition, I would like to express the deepest appreciation Dr. Thomas G. Thundat (Oak Ridge National Lab (ORNL) -Nano Scale group leader) allowed me to work in his labs and provided me assistance more importantly he inspired me all the time. Most importantly, he always inspired me with his positive comments which helped me to lay the ground foundations of this research.

I am heartily thankful to Dr. Adam Bange (Xavier University, Associate Professor) who was a post doctoral staff at the ORNL for assisting me to assemble the foundation of this biosensor research with his broad knowledge.

I am forever grateful to my friend and colleague Krishnatej Vedala for helping me with the computer programming used in my thesis work (Mat-Lab). I value the time he took off from his own studies in order to assist me.

Professor and Research Director, Dr. Norman Munroe and his group member MSc. Puneet Gill and Dr. Waseem Haider essential thanks for preparing the nano-materials as well as helping me throughout the thesis.

Last but not least, my deepest gratitude goes to my beloved wife, Kasia (Ayşe) Akar for her unflagging love and support throughout my education life; this dissertation is simply impossible without you. I am forever grateful for those sleepless days and night to stand by me during this thesis work.

I can never forget the help of those Department of Energy (DOE) Fellows support and help especially those Merlin Ngachin, Jose Matos, Lee Brady and Charles Castello.

I would like to thank Florida International University's Engineering Department for allowing me the use of their facilities and providing of a productive environment for a student to grow.

ABSTRACT OF THE THESIS

DESIGN AND DEVELOPMENT OF AN ENZYME-LINKED BIOSENSOR FOR DETECTION AND QUANTIFICATION OF PHOSPHATE SPECIES

by

Serkan Akar

Florida International University, 2010

Miami, Florida

Professor Vekalet Tek, Major Professor

The objective of this study is to design and development of an enzyme-linked biosensor for detection and quantification of phosphate species. Various concentrations of phosphate species were tested and completed for this study.

Phosphate is one of the vital nutrients for all living organisms. Phosphate compounds can be found in nature (e.g., water sediments), and they often exist in an inorganic form. The amount of phosphates in the environment strongly influences the operations of living organisms. Excess amount of phosphate in the environment causes eutrophication which in turn causes oxygen deficit for the other living organisms. Fish die and degradation of habitat in the water occurs as a result of eutrophication. In contrast, low phosphate concentration causes death of vegetation since plants utilize the inorganic phosphate for photosynthesis, respiration, and regulation of enzymes. Therefore, the phosphate quantity in lakes and rivers must be monitored.

Result demonstrated that phosphate species could be detected in various organisms via enzyme-linked biosensor in this research.

TABLE OF CONTENTS

CHAPTER	PAGE
1.0 INTRODUCTION	1
2.0 MATERIALS AND METHODS.....	6
2.1 Materials	6
2.1.1 Chemicals.....	6
2.2 Methods.....	7
2.2.1 Buffer preparations	7
2.2.2 Construction of Experimental Cell	11
2.2.3 Construction of Electrode Housing.....	12
2.2.4 Solid work design of cell and housing.....	16
2.2.5 Electrochemical Measuring Device	18
2.2.6 Electrodes.....	18
2.2.7 Protein-linked polymers and nano structured materials.....	20
2.2.8 Pyruvate Oxidase Enzyme	25
2.2.9 Enzyme de-salting column:.....	25
2.2.10 Enzyme Immobilization on Materials.....	28
3.0 EXPERIMENTS	33
3.1 Cyclic Voltammetry (CV).....	33
3.2 Amperometry	34
3.3 Detection of Phosphate Concentration in the Cell.....	35
4.0 RESULTS AND DISCUSSIONS.....	37
4.1 Results.....	37
4.2.1 Amperometric measurements of phosphate.....	41
4.2.2 Raw Data:.....	42
4.2.3 Filtered Data:	46
4.2.4 Normalized Signal	55
4.2.4.1 Normalized signal for 10mM Phosphate Titration Responses	57
4.2.4.2 Normalized signal for 1mM Phosphate Titration Responses	60
4.2.4.3 Normalized signal for 0.01mM Phosphate Titration Responses	63

4.2.4.4 Normalized signal for 0.0001mM Phosphate Titration Responses	66
4.2.4.5 Normalized signal for 0.00001mM Phosphate Titration Responses	69
4.2.5 Current magnitude change obtained from amperometry	72
4.2.6 Calibration Curves	76
4.3 Discussions	79
4.3.1 CV System and Background Test (Negative Control).....	79
4.3.2 Amperometric System and Background (Negative Control) Test.....	80
4.3.3 Amperometric Results for Phosphate Detection.....	81
5.0 CONCLUSION.....	85
6.0 FUTURE WORK.....	87
BIBLIOGRAPHY.....	88

LIST OF TABLES

TABLE	PAGE
Table 1. Test plan for the current obtained from H ₂ O ₂ Respect to Different Materials.....	36
Table 2. Amperometric Magnitude Change in Current (nA) for 10mM PO ₄ ³⁻ Titration	73
Table 3. Amperometric Magnitude Change in Current (nA) for 1mM PO ₄ ³⁻ Titration	73
Table 4. Amperometric Magnitude Change in Current (nA) for 0.01mM PO ₄ ³⁻ Titration	73
Table 5. Amperometric Magnitude Change in Current (nA) for 0.0001mM PO ₄ ³⁻ Titration	73
Table 6. Amperometric Magnitude Change in Current (nA) for 0.00001mM PO ₄ ³⁻ Titration	75
Table 7. Summary of Current Change versus Concentration	75
Table 8. Current Magnitude Changes (nA) for Silica Polymer in Various Concentrations.....	76
Table 9. Current Magnitude Changes (nA) for CuCrAgNi Alloyed CNT in Various Concentrations.....	77
Table 10. Current Magnitude Changes (nA) for CuCr Alloyed MWCNT in Various Concentrations.....	78
Table 11. Phosphate Concentration Detection Limits with Different Methods (Akar,Development of a biosensor for detection of phosphate species in uranium contaminated groundwater and wastewater sediments 2010).....	84

LIST OF FIGURES

FIGURE	PAGE
Figure 1. Chemical Structure of Dithiobis [succinimidyl propionate] (DSP)	9
Figure 2. Chemical Structure of Na ₂ HPO ₄	11
Figure 3. The First Experimental Cell Made at the Oak Ridge National Lab's Machine Shop.....	13
Figure 4. Experimental Cell with Four Compartments and Oxygen Ports.....	14
Figure 5. Increased Amount of Oxygen Ports	15
Figure 6. Cell from Bottom View	15
Figure 7. Computer Program "Solid Works" Drawings of the Cell.	16
Figure 8. Computer Program "Solid Works" Drawing of the Housing for the Electrodes.....	16
Figure 9. Top and Profile Views of the Cell.....	17
Figure 10. (a) Cells with Electrodes, (b) Electrode Housing and (c) Cell with the Housing.....	17
Figure 11. Epsilon Electrochemical Work Station (Facility 2005).	18
Figure 12. Three Molar (3M) Potassium Chloride (KCL).....	20
Figure 13. Working Electrode (Glassy Carbon) (a, b), Reference Electrode (Ag/AgCl) (c, d), Counter Electrode (Platinum Wire) (e, f).....	21
Figure 14. Au Deposited on Silica Substrate.....	21
Figure 15. Actual Picture of the Gold-Coated Silica Polymer	22
Figure 16. Actual View of the Nano-Structured Highly Conductive Material.....	23
Figure 17. Four Point Probe Resistivity Measurements Sketch	24
Figure 18. Authentic View of the Highly Conductive Nano Structured MWCNT	24
Figure 19. De-salting Columns.....	26

Figure 20. Chemicals Used for the Immobilization Process.....	29
Figure 21. Gold Coated Silica Polymer Incubated in DSP+DMSO	30
Figure 22. POX Immobilized on MWCNT and Kept in Tris Buffer After Experiments.....	32
Figure 23. Nano Materials Kept in Tris Buffer Over Three Months Period.....	32
Figure 24. Computer Drawing of Experimental Cell and Magnetic Bar Placed in the Housing.....	34
Figure 25. Cyclic Voltammetry (CV) of Ferricyanide.....	37
Figure 26. CV Recording of Tris Buffer Background	38
Figure 27: Amperometric Background Test Recording for 1ml, 50mM Tris-HCl pH 7.5.....	39
Figure 28. Continuous Titration of 20 μ l, 20% H ₂ O ₂ in 1ml Tris Buffer	39
Figure 29. Enzymatic Reaction Mechanism of Pyruvate Oxidase (Villalba, Bioelectroanalytical determination of phosphate 2009).....	40
Figure 30. Single Titration of 50 mM Tris-HCl with 20 μ l, 20% H ₂ O ₂	41
Figure 31. Amperometric Recordings for Silica Polymer, CuCrNiAg Alloyed with CNT, CuCr Alloyed with MWCNT by titration of 10mM [PO ₄ ³⁻] Solution.....	43
Figure 32. Amperometric Recordings for Silica Polymer, CuCrNiAg Alloyed with CNT, CuCr Alloyed with MWCNT by titration of 1mM [PO ₄ ³⁻] Solution.....	44
Figure 33. Amperometric Recordings for Silica Polymer, CuCrNiAg Alloyed with CNT, CuCr Alloyed with MWCNT by titration of 0.01mM [PO ₄ ³⁻] Solution.....	45
Figure 34. Amperometric Recordings for Silica Polymer, CuCrNiAg Alloyed with CNT, CuCr Alloyed with MWCNT by titration of 0.0001mM [PO ₄ ³⁻] Solution.....	45
Figure 35. Amperometric Recordings for Silica Polymer, CuCrNiAg Alloyedwith CNT, CuCr Alloyed with MWCNT by titration of 0.00001mM [PO ₄ ³⁻] Solution.....	46
Figure 36. ECG Signal, Raw Data (a), Filtered Data (b) and Normalized Data (c), (Wu 2009).....	47

Figure 37. Filtered Data for Silica Polymer, CuCrNiAg Alloyed with CNT, CuCr Alloyed with MWCNT by titration of 10mM [PO ₄ ³⁻] Solution.....	52
Figure 38. Filtered Data for Silica Polymer, CuCrNiAg Alloyed with CNT, CuCr Alloyed with MWCNT by titration of 1mM [PO ₄ ³⁻] Solution.....	53
Figure 39. Filtered Data for Silica Polymer, CuCrNiAg Alloyed with CNT, CuCr Alloyed with MWCNT by titration of 0.01mM [PO ₄ ³⁻] Solution.....	54
Figure 40. Filtered Data for Silica Polymer, CuCrNiAg Alloyed with CNT, CuCr Alloyed with MWCNT by titration of 0.0001mM [PO ₄ ³⁻] Solution.....	55
Figure 41. Filtered Data for Silica Polymer, CuCrNiAg Alloyed with CNT, CuCr Alloyed with MWCNT by titration of 0.00001mM [PO ₄ ³⁻] Solution.....	56
Figure 42. Normalized Data for Silica Polymer by titration of 10mM [PO ₄ ³⁻] Solution.....	58
Figure 43. Normalized Data for Cu Cr Ni Ag Alloyed with CNT by titration of 10mM [PO ₄ ³⁻] Solution.....	59
Figure 44. Normalized Data for CuCr Alloyed with MWCNT by titration of 10mM [PO ₄ ³⁻] Solution.....	60
Figure 45. Normalized Data for Silica Polymer by titration of 1mM [PO ₄ ³⁻] Solution.....	61
Figure 46. Normalized Data for CuCrNiAg Alloyed with CNT by titration of 1mM [PO ₄ ³⁻] Solution.....	62
Figure 47. Normalized Data for CuCr Alloyed with MWCNT by titration of 1mM [PO ₄ ³⁻] Solution.....	63
Figure 48. Normalized Data for Silica Polymer by titration of 0.01mM [PO ₄ ³⁻] Solution.....	64
Figure 49. Normalized Data for CuCrNiAg Alloyed with CNT by titration of 0.01mM [PO ₄ ³⁻] Solution.....	65
Figure 50. Normalized Data for CuCr Alloyed with MWCNT by titration of 0.01mM [PO ₄ ³⁻] Solution.....	66
Figure 51. Normalized Data for Silica Polymer by titration of 0.0001mM [PO ₄ ³⁻] Solution.....	67

Figure 52. Normalized Data for CuCrNiAg Alloyed with CNT by titration of 0.0001mM [PO ₄ ³⁻] Solution.....	68
Figure 53. Normalized Data for CuCr Alloyed with MWCNT by titration of 0.0001mM [PO ₄ ³⁻] Solution.....	69
Figure 54. Normalized Data for Silica Polymer by titration of 0.00001mM [PO ₄ ³⁻] Solution.....	70
Figure 55. Normalized Data for CuCrNiAg Alloyed with CNT by titration of 0.00001mM [PO ₄ ³⁻] Solution.....	71
Figure 56. Normalized Data for CuCr Alloyed with MWCNT by titration of 0.0001mM [PO ₄ ³⁻] Solution.....	72
Figure 57. Phosphate Calibration Curve for Silica Polymer.....	76
Figure 58. Phosphate Calibration Curve for CuCrAgNi Alloyed with CNT.....	77
Figure 59. Phosphate Calibration Curve for CuCr Alloyed with MWCNT	78

1.0 INTRODUCTION

Phosphate is one of the vital nutrients for all living organisms (Schropp 2007). The phosphate compound is an ion, formed with four oxygen atoms binding to a phosphorus atom. The central element of phosphate is phosphorus and never found free in the environment since it is highly reactive (Weiner 2001). Phosphate compound can be found in nature (e.g., water sediments) (Ragothama 1999), and they often exist in an-inorganic form. The amount of phosphates in the environment strongly influences the operations of living organisms. Excess amount of phosphate in the environment causes eutrophication which in turn causes oxygen deficit for the other living organisms. Fish die and degradation of habitat in the water occurs as a result of eutrophication (Khan 2002). In contrast, low phosphate concentration causes death of vegetation since plants utilize the inorganic phosphate for photosynthesis, respiration, and regulation of enzymes (Ragothama 1999). Therefore, the phosphate quantity in lakes and rivers must be monitored continuously (Engblom, The phosphate sensor 1998). Human beings daily attain approximately 700-1600 mg of phosphates, as a dietary supply, through the food consumption (Weisinger 1998). In human body, phosphates are found in both the organic and inorganic forms. About 85 percent of the organic phosphates are stored in human body in the form of hydroxyapatite ($\text{Ca}_{10}(\text{PO}_4)_6\text{OH}_2$) which is the main component of bones and teeth (Shiber 2002), (Weisinger 1998). The remaining 15 percent is found in the backbone of DNA, in the structure of phospholipids (component of cellular membrane) and in some proteins (Weiner 2001), (Weisinger 1998). Organic phosphate compounds also play significant roles in metabolic energy conversion in the form of

adenosine triphosphate (ATP), guanosine triphosphate (GTP), cyclic adenosine monophosphate (cAMP). In addition, phosphate is found in the red blood cells in the form of 2,3-bisphosphoglycerates (2,3BPG), which is an essential element to release the oxygen from hemoglobin in the tissue. On the other hand, phosphate exists in the inorganic form as H_3PO_4 and H_2PO_4 in the plasma (Weiner 2001). As a result of phosphate deficiency in vegetation, human phosphate intake reduces significantly. Some of the phosphate related illnesses are: hyperparathyroidism, vitamin D deficiency, Fanconi syndrome, etc (Engblom, The phosphate sensor 1998). Since low and the excess amount of phosphate cause malfunctions in environment and the living organisms, an accurate and sensitive way of measuring phosphates is required (Engblom, The phosphate sensor 1998). Enzymatic biosensors for detection of phosphate became very attractive in last three decades. As the scientists reveal new discoveries about the importance of phosphate, the design and development of phosphate detection devices gained popularity. Throughout the years, all these factors mentioned above encouraged scientists to investigate methods for phosphate detection (Villalba, Bioelectroanalytical determination of phosphate 2009), (Engblom, The phosphate sensor 1998). Up to now, several sensor technologies for monitoring phosphate species have been implemented. Among these, a microfluidic system with a 0.7 ppb detection limit, an autonomous microfluidic system with a $3\mu M$ detection limit, a biosensor based on the pyruvate oxidase modified conducting polymer for phosphate ion determination with a $3\mu M$ detection limit, and a thick-film phosphate biosensor based hydrogel immobilized pyruvate oxidase with a $5\mu M$ detection limit are a few that have drawn particular attention (Akar, Development of a biosensor for detection of phosphate species in uranium contaminated groundwater and

wastewater sediments 2010), (Daykin 1995), (McGraw 2007), (Rahman, The biosensor based on the pyruvate oxidase modified conducting polymer for phosphate ions determination 2006), (Mak 2003). Although these sensors have successfully detected the phosphate, they have peculiar drawbacks. For instance, conventional colorimetric and potentiometric techniques have disadvantages in sensing. The prominent downside is that the systems are too complicated for frequent use or low selectivity (Villalba, Bioelectroanalytical determination of phosphate 2009), (Mozaz 2006) and (Allan 2006). Enzyme-immobilized biosensors are the most applicable ones for the phosphate detection and quantification because of their substrate specificity and lower detection limits. In terms of frequent use, the enzyme utilized in the biosensor has to be replaced due to the descending or limited time of enzyme activity. Although the bio- catalytic sensors have these types of weaknesses, they offer a quick response and provide very rapid results. The first enzymatic phosphate biosensor was developed employing double enzymes by Guilbalut et al. (Engblom, The phosphate sensor 1998) (Guilbalut 1975). As it is reported, this group utilized both alkaline phosphatase and glucose oxidase for their biosensor. However, alkaline phosphatase becomes active on the functionalities of phosphate ester and the derivatives of alcohol by opening the bond between them which lowers the enzyme specificity to the substrates. Then again, this type of sensing system could not be used efficiently in the aquatic environment for the lower concentrations of phosphate detection (Villalba, Bioelectroanalytical determination of phosphate 2009). Later, Wollenberger et al. attempted to lower the detection limit of the phosphate concentration by employing three different enzymes simultaneously in their research (Engblom, The phosphate sensor 1998), (Gavalas 2001). Although this group was able to

decrease the detection limit by 10-fold as compared to Guilbalut's design, the response time of the multiple enzymatic sensors was about three minutes for a single measurement as opposed to seconds with biosensors. Furthermore, the function of its selectivity negatively affected the long term stability of the sensor (Rahman, The biosensor based on the pyruvate oxidase modified conducting polymer for phosphate ions determination 2006), (Gavalas 2001). The single enzymatic method using pyruvate oxidase, first introduced by Mizutani et al. in 1983, is the most efficient and highly selective to phosphate (Akyilmaz, Construction of an Amperometric Pyruvate Oxidase Enzyme Electrode for Determination of Pyruvate and Phosphate 2007). Moreover, the immobilization of a single enzyme is simpler than the immobilization of double or triple enzymes to the surface and is more effective. It is reported that the double and the triple enzyme-immobilized sensor technology has some disadvantages because the enzyme shelf lives are not harmonious. Also, the conventional pyruvate oxidase method suffered from storage stability, low reproducibility, and selectivity due to their poor design (Akyilmaz, Construction of an Amperometric Pyruvate Oxidase Enzyme Electrode for Determination of Pyruvate and Phosphate 2007), (Kubo 1991), (Akar, Development of a biosensor for detection of phosphate species in uranium contaminated groundwater and wastewater sediments 2010). One of the main focuses of this research is to develop an environmental biosensor for detection of phosphate. United States Department of Energy (USDOE) has several sites where radio-active nuclear materials (i.e., uranium and plutonium) have contaminated the ground water throughout the nation. Major source for drinking water mostly comes from ground water via emerging to the rivers. At many of these sites, the concentration of uranium exceeds the standards (30µg/L) set by the U.S.

Environmental Protection Agency (USEPA 2001). Currently, DOE scientists are focusing on polyphosphate attachment techniques for immobilizing uranium in the soil. The stabilization is based on the direct binding of the polyphosphate compounds to uranium via ionic bonds with a highly positive charged element. Uranium is usually available in the environment either as a reduced form, U^{4+} , or as the oxidized form, U^{6+} . Uranium +6 has a tendency to bind polyphosphate and oxidize to the +4 state (Akar, Development of a biosensor for detection of phosphate species in uranium contaminated groundwater and wastewater sediments 2010), (Merkel 2006), (Zhang 2002) and (Jager 1998). When polyphosphate is added to the uranium contaminated area, stabilization of the uranium as apatite and sequestered as autunite is reported by Wellman et al. This research revealed that the reduced concentrations of phosphate can reduce the uranium stabilization (Wellman 2005).

The current phosphate detection method used at Hanford is sampling and analysis at the laboratory which has many disadvantages (i.e., potential cross contamination, longer turnaround time and high cost). For these reasons, we are developing a new biosensor to detect phosphate in groundwater by employing advanced materials and nano-materials to surmount these problems.

2.0 MATERIALS AND METHODS

2.1 Materials

2.1.1 Chemicals

- HEPES; (4-(2-hydroxyethyl)-1-piperazineethanesulfonic acid), MW 238 g/mol, Sigma Aldrich, Catalog number 83264-500ML-F.
- Tris; (hydroxymethyl amino methane), MW 121.14 g/mol, Sigma Aldrich, Catalog number 252859-500G.
- Pyruvic Acid (2-oxopropanoic acid or α -ketopropionic acid), MW 88.06 g/mol, Sigma Aldrich, Catalog number 204-824-3.
- Dimethyl Sulfoxide (DMSO; methylsulfinylmethane), MW 78.13 g/mol, Sigma Aldrich, Catalog number D8418-250ML.
- Dithiobis [succinimidyl propionate] (DSP), MW404.42, Piercenet, Catalog number 22585.
- Flavin Adenine Dinucleotide (FAD), MW829.51g/mol, Sigma Aldrich, Catalog number F6625-100MG.
- Thiamine Pyrophosphate (TPP), MW460.77g/mol, Sigma Aldrich, Catalog number C8754-100G.
- Magnesium (Mg^{2+}), MW24.31g/mol, Sigma Aldrich, Catalog number 254118-250G.
- Pyruvate Oxidase (POX) (EC. 1.2.3.3, 100 units mg^{-1}) from aerococcus species, Sigma Aldrich, Catalog number P4591-100UN.
- Dibasic Hydrogen Phosphate (Na_2HPO_4), MW 141.96, Sigma Aldrich, Catalog number S7907-100G.

2.2 Methods

2.2.1 Buffer preparations

For the entire experiment two types of buffers were prepared and used.

1. HEPES BUFFER; 100 ml , 0,5M of pH 7 HEPES buffer as suggested by (Rahman, The biosensor based on the pyruvate oxidase modified conducting polymer for phosphate ions determination 2006) was prepared at the lab from the equation and the procedure below:

$$\text{Molar Mass} = \text{Volume} \times \text{Molarity} \times \text{Molecular Weight}$$

Equation 1. Calculation of Molar Mass

$$\text{Mass} = (90\text{ml}/1000\text{ml}) \times (0.5\text{M}) \times (238\text{g/mol}) = 11.915\text{grams of HEPES}$$

11.915 grams of HEPES was dissolved in 90 ml of de-ionized water measuring $18\text{M}\Omega/\text{cm}^3$ (for purity purposes) obtained from Milli-Q water purifying system in a 100 ml beaker. The solution was stirred for about 5 min at 5000 rpm for complete homogenous mixture. The pH of the buffer was adjusted to pH 7.0 by titrating with hydrochloric acid (HCl) while continuously stirring. The entire solution used for this project was prepared and used at the ambient temperature. The final volume of the buffer was adjusted to 100 ml with de-ionized water in a 100 ml glass volumetric flask.

2. TRIS BUFFER; 1000 ml, 50 mM, pH 7.5 TRIS buffer as suggested by (Akyilmaz, Construction of an Amperometric Pyruvate Oxidase Enzyme Electrode for Determination of Pyruvate and Phosphate 2007) was prepared at the laboratory following the procedure below:

6.057grams of the Tris base, calculated based on the Equation 1, was dissolved in 900 ml of de-ionized water measuring $18\text{M}\Omega/\text{cm}^3$ (for purity purposes) obtained from Milli-Q water purifying system in a 1 L glass beaker. In order to homogenize the mixture, the solution was stirred for about 5min at 5000rpm. For final volume measuring, it was then transferred into a 1L glass volumetric flask. The pH of the obtained Tris buffer was adjusted to pH 7.5 (Rahman, The biosensor based on the pyruvate oxidase modified conducting polymer for phosphate ions determination 2006) by titrating with 1 mM HCl solution while stirring with a stir bar. The finally volume of the tris-HCL solution was completed to 100ml while pH is observed. Solutions were prepared at room temperature.

Pyruvate (CH_3COCOOH): a substrate of pyruvate oxidase essential for enzymatic reaction to occur and it is a vital compound in production of byproduct H_2O_2 . According to the literature, $0.05\mu\text{M}$ Pyruvic acid is the optimum concentration for pyruvate oxidase enzymatic reaction (Akyilmaz, Construction of an Amperometric Pyruvate Oxidase Enzyme Electrode for Determination of Pyruvate and Phosphate 2007). The 10 ml, pyruvate solution was prepared as followed:

To attain 10ml, $0.05\mu\text{M}$, Pyruvate solution, first 50mM stock solution was prepared and diluted to $0.05\mu\text{M}$. To prepare 50mM stock solution 2.20mg of Pyruvic acid was dissolved in 50ml de-ionized water measuring $18\text{M}\Omega/\text{cm}^3$ (for purity purposes) obtained from Milli-Q water purifying system. Then, the solution was stirred for about 5min at 5000rpm for complete homogenous mixture.

$$C_1 \times V_1 = C_2 \times V_2$$

Equation 2. Dilution Formula

Where:

C_1 : The concentration of the stock solution,

C_2 : The concentration of the final solution,

V_1 : The volume of the stock solution,

V_2 : The volume of the final solution.

Dimethyl Sulfoxide (DMSO) ($(\text{CH}_3)_2\text{S}$): a colorless, liquid organic compound which is a very necessary polar aprotic solvent. It plays an important role for dissolving both polar and non polar compounds such as proteins. In our experiment it is utilized during the protein attachment process to dissolve Dithiobis [succinimidyl propionate] DSP. Dithiobis [succinimidyl propionate] DSP ($\text{C}_{14}\text{H}_{16}\text{N}_2\text{O}_8\text{S}_2$): a homo-bi-functional crosslinker exploited for thiol cleavable and membrane permeable crosslinking. During crosslinking procedure, DSP undergoes a reaction with any amine-containing molecule.

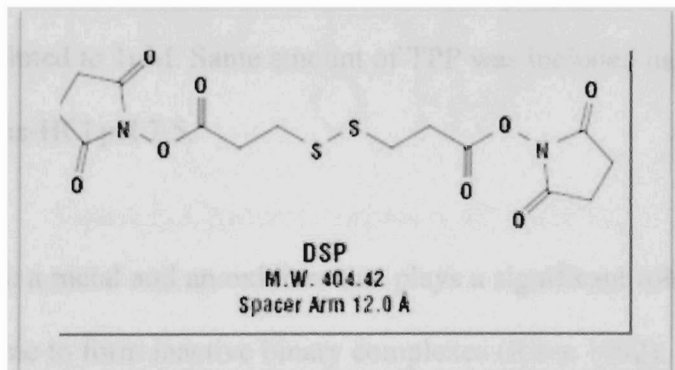


Figure 1. Chemical Structure of Dithiobis [succinimidyl propionate] (DSP)

Flavin Adenine Dinucleotide (FAD): a co-enzyme that stabilizes the pyruvate oxidase while the enzyme catalyzes that reaction to produce H_2O_2 . FAD and Thiamine Pyrophosphate (TPP), divalent cations, bind to apoenzyme to form inactive binary

complexes. It is also reported that divalent cations affect quaternary structure and shift the equilibrium (Risse 1992). 20ml, 1mM FAD solution was prepared and diluted to 0.4 μ M (Equation 2) according to Rahman et al (Rahman, The biosensor based on the pyruvate oxidase modified conducting polymer for phosphate ions determination 2006). For this procedure, Equation 1 was used to calculate the mass to be 16.5mg and by using Equation 2, FAD diluted to 0.4 μ M. Same amount of FAD was included in experiments along with 1ml, 50mM tris-HCl pH 7.5.

Thiamine Pyrophosphate (TPP): as explained above, it is one of the divalent cations that help to stabilize the pyruvate oxidase activity. 20ml, 1mM TPP solution was prepared and diluted to 1 μ M according to Rahman et al (Rahman, The biosensor based on the pyruvate oxidase modified conducting polymer for phosphate ions determination 2006). For this procedure, Equation 1 was used to calculate the mass to be 9.21mg and by using Equation 2, TPP diluted to 1 μ M. Same amount of TPP was included in experiments along with 1ml, 50mM tris-HCl pH 7.5.

Magnesium (Mg^{2+}): a metal and an oxidizer that plays a significant role in TPP and FAD to bind to apoenzyme to form inactive binary complexes (Risse 1992). 50ml, 2mM Mg^{2+} solution was prepared as suggested by Rahman et al (Rahman, The biosensor based on the pyruvate oxidase modified conducting polymer for phosphate ions determination 2006). For this procedure, Equation 1 was used to calculate the mass to be 2.5mg and same amount of Mg^{2+} was included in experiments along with 1ml, 50mM tris-HCl pH 7.5.

The purpose of employing FAD, TPP and Mg is that pyruvate oxidase has poor functionality under 40°C. To overcome this matter, co-factors (FAD, TPP and Mg) are utilized to stabilize the enzymatic reaction (Yamamoto 1987).

Dibasic Sodium Hydrogen Phosphate (Na_2HPO_4): a water soluble, white colored powder is a phosphoric acid sodium salt that has a chemical structure seen in Figure 2. In this experiment, it is applied as a phosphate source to complete the chemical reaction as shown in Equation 5 and Equation 6. It is explained in depth in the amperometry section.

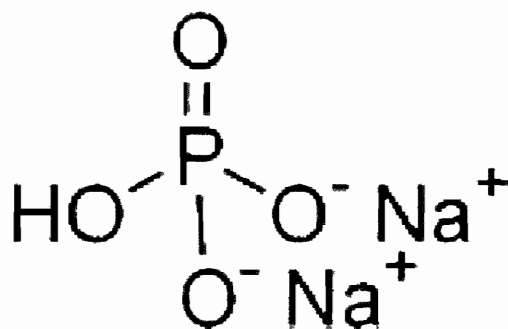


Figure 2. Chemical Structure of Na_2HPO_4

2.2.2 Construction of Experimental Cell

An experimental cell had to be custom built due to the unavailability of the commercial product to accommodate the design. Some of the constraints were: positioning of a non-disturbing stir bar that simultaneously homogenizes the solution, a placement of an enzyme linked material directly under the electrode for maximum sensitivity and a construction of an electrode housing that positions the electrodes perpendicular to the bottom of the experimental cell as well as 2-3mm directly above to the enzyme linked

material. These limiting factors made the cell design one of the most challenging and evolving parts of the entire experiment. Modifications to the cell have been done throughout the investigation. The volume of the cell had to be rendered in to specifications to be able to accommodate small sizes of materials and chemicals as well as relatively larger three electrodes (Working Electrode, Reference Electrode and Counter Electrode). Electrodes are explained in depth under the “Electrodes” section.

Each electrode has a diameter that must be accounted for during the design. In addition, available pyruvate oxidase was only 100 units (59mg) which had to last for the full investigation due to the high cost. After analyzing all the constraints and the standards, the first design emerged as a trial cell seen on the Figure 3.

2.2.3 Construction of Electrode Housing

As stated above, electrodes have relatively large dimensions and they must be positioned directly above the enzyme-linked material, perpendicular to the bottom, and locate about 2-3mm above the linked materials. The electrode housing was constructed from the plexy-glass material and it was able to accommodate working electrode (GCE), Reference Electrode (Ag/AgCl), and counter electrode (platinum wire). In Figure 8, the housing dimensions and specifications are displayed. The Preliminary electrochemical studies were successfully performed with the first stage of the design. Some of the accomplishments included adjustment of volume, creation of electrode housing and achievement of place for magnetic stir bar. Although the dimensions of the cell fit to the specifications, the cell could accommodate one experiment at a time.

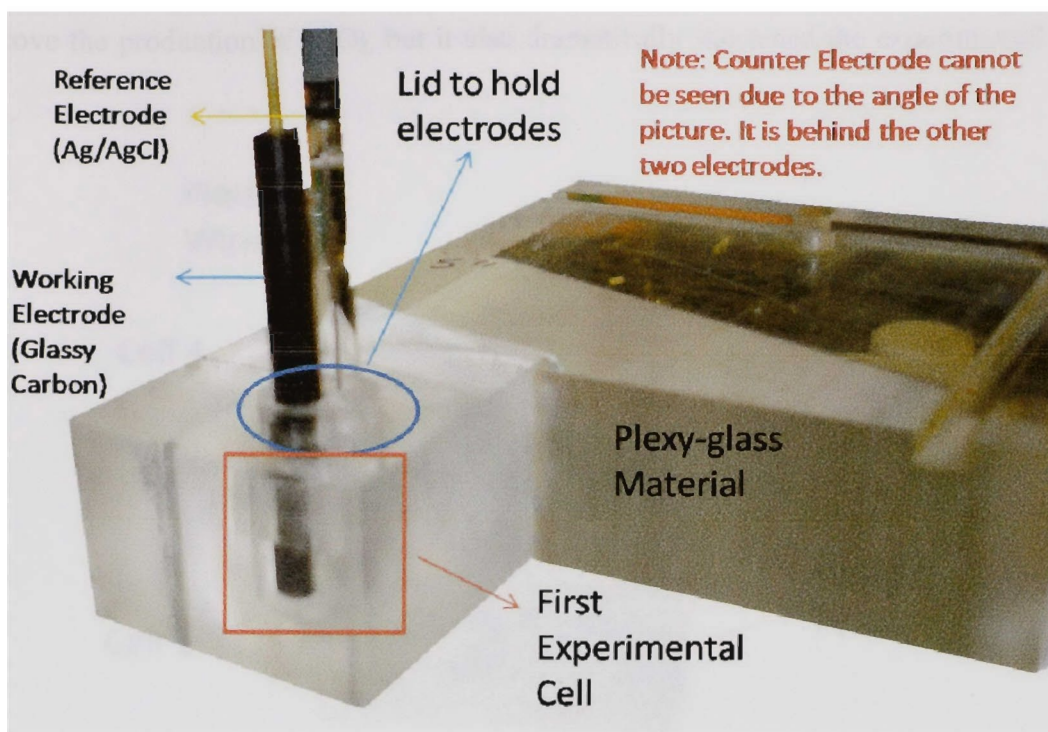


Figure 3. The First Experimental Cell Made at the Oak Ridge National Lab's Machine Shop.

Therefore, more cells had to be constructed in order to perform multiple analyses without cross contamination and frequent sanitization. Subsequently, three extra cells were assembled in to the system to reduce the cleaning time and to avoid any contamination possibilities during the current measurements. On the other hand, according to the chemical Equation 6 indicates that oxygen is an essential element for H_2O_2 production. Considering all the rationale, modification to the cell became inevitable which evolved to the stage shown in Figure 4. Consistent experimental data was obtained via the newly designed experimental cells with the increased number of oxygen ports. Furthermore, the by-product of the enzymatic reaction, H_2O_2 , was successfully generated which helped in troubleshooting to determine the reason of predicament. The new design did not only

improve the production of H_2O_2 , but it also dramatically shortened the experimental test time.

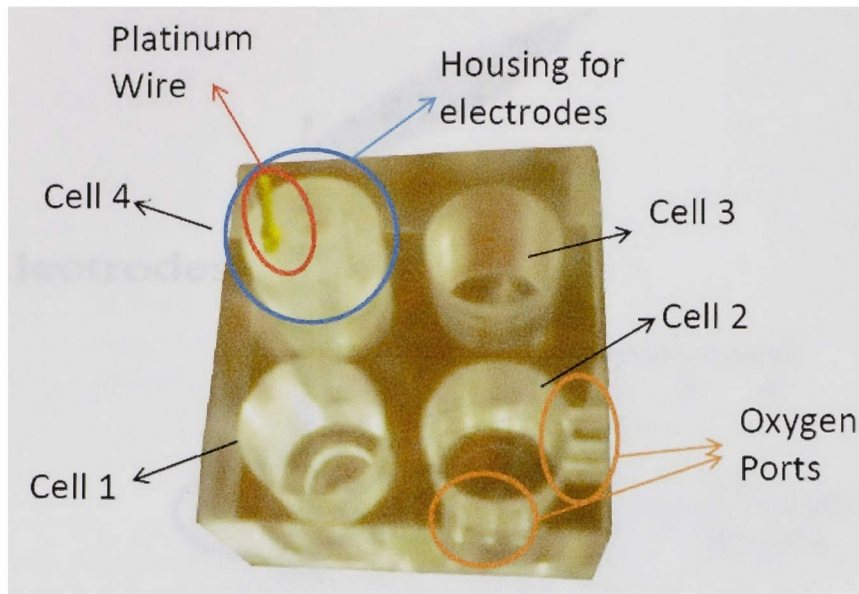


Figure 4. Experimental Cell with Four Compartments and Oxygen Ports.

Conducting a single experiment with the cell shown in Figure 3, took about 80 – 110 minutes from start to finish. In addition, after each test, the cell had to be cleaned to avoid any possible cross-contamination from previous experiment. This cleaning procedure took about 15 to 30 minutes. As opposed to the first stage of the cell, the newly designed cells reduce the number of cleaning steps between each measurement since there are three more compartments available. Later, the data obtained from the modified cell were compared with previously obtained data and a spectacular increase in current was noticed. Eventually, the new data which were obtained by using the novel electrochemistry cell was compared with related literature data. The consistency was observed between the obtained data and published data. This observation confirmed that

the transition of the sufficient amount of oxygen gas, which was critical for fully efficient enzymatic reaction, was supplied via newly designed oxygen ports (Figure 5).

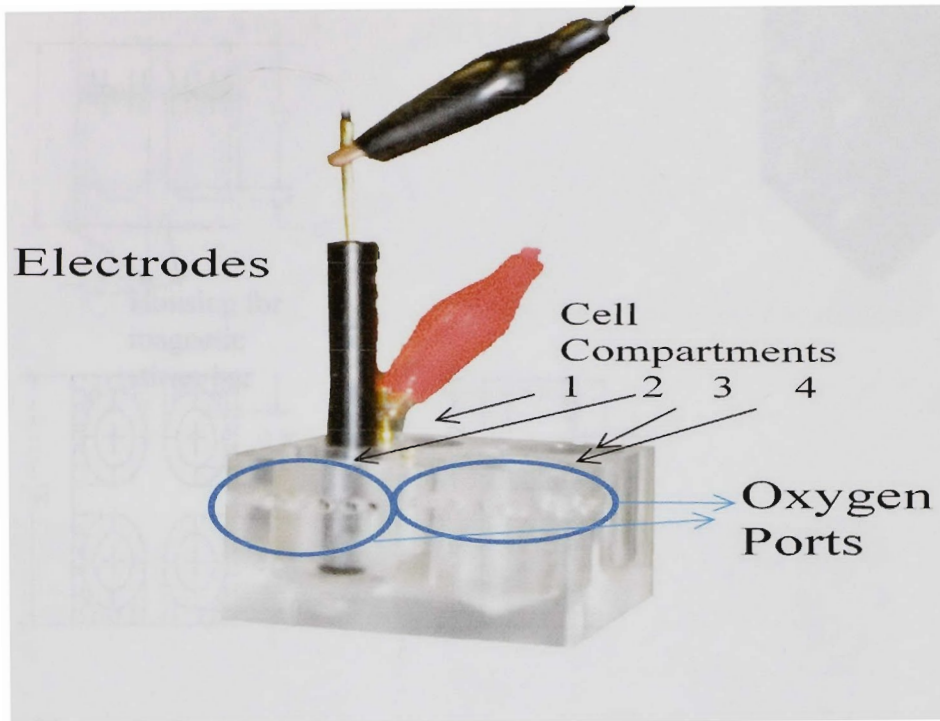


Figure 5. Increased Amount of Oxygen Ports

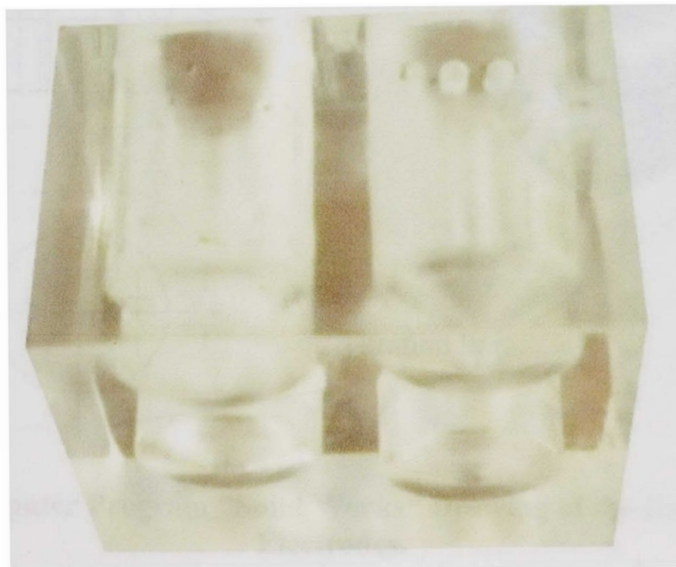


Figure 6. Cell from Bottom View

2.2.4 Solid work design of cell and housing

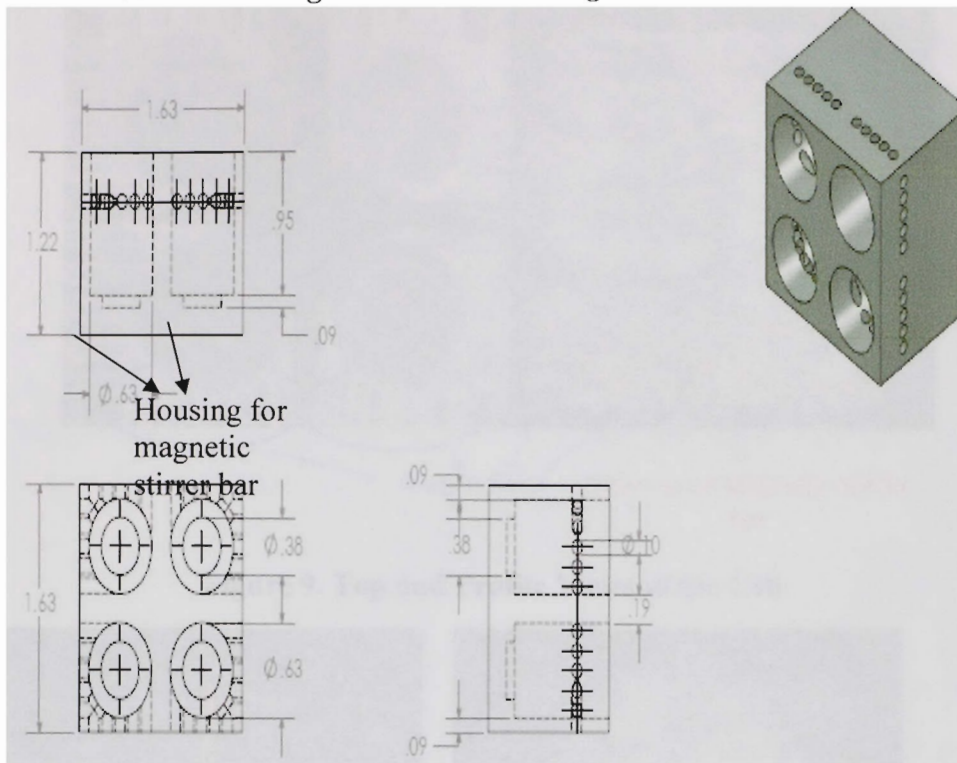


Figure 7. Computer Program "Solid Works" Drawings of the Cell.

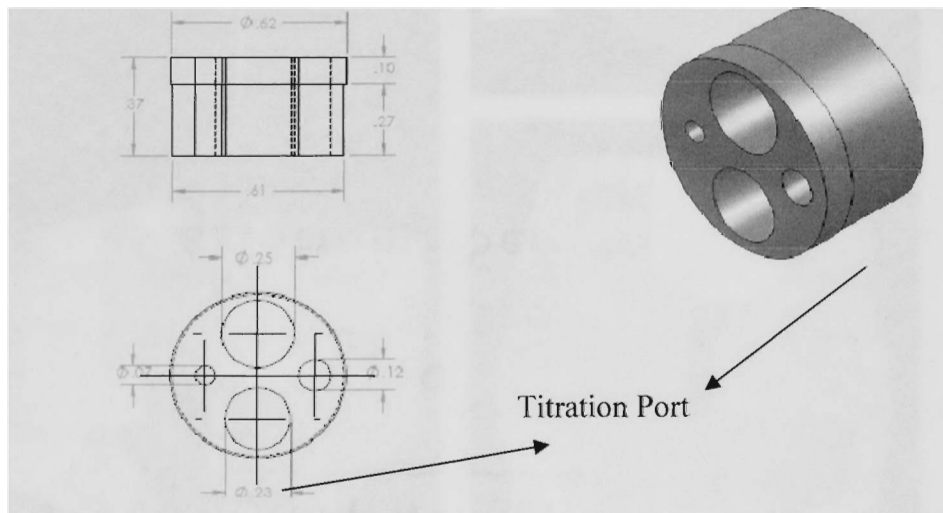


Figure 8. Computer Program "Solid Works" Drawing of the Housing for the Electrodes.

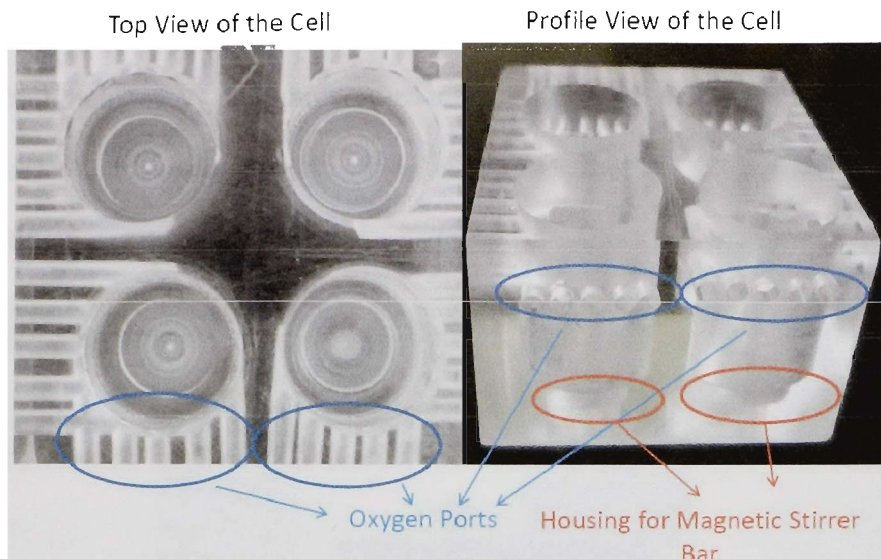


Figure 9. Top and Profile Views of the Cell.

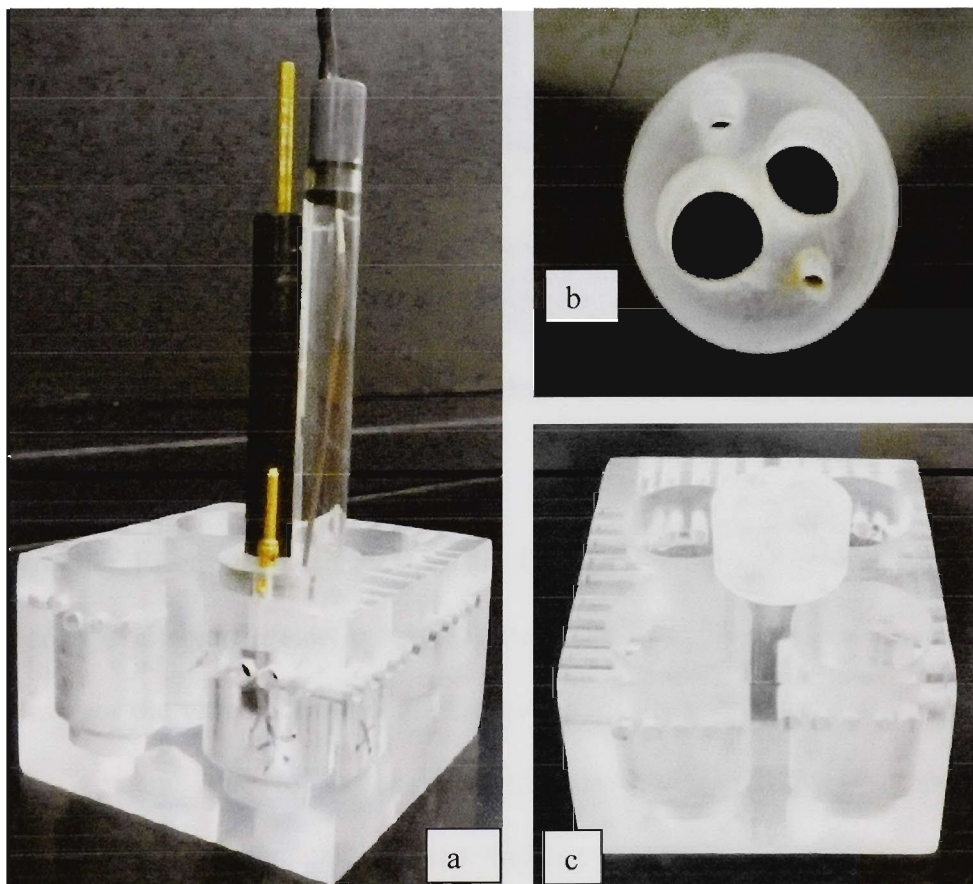


Figure 10. (a) Cells with Electrodes, (b) Electrode Housing and (c) Cell with the Housing.

2.2.5 Electrochemical Measuring Device

Cyclic voltammetry (CV) and amperometric measurements were performed with the use of Potentiostat/Galvanostat Epsilon model as an electrochemical measuring instrument.

Figure 11 illustrates the actual view of the electrochemical work station.



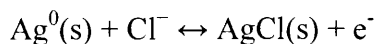
Figure 11. Epsilon Electrochemical Work Station (Facility 2005).

2.2.6 Electrodes

Working Electrode; according to the literature, there are several types of electrodes readily available for electrochemical measurements. The most common electrode is the glassy or the vitreous carbon electrode (GCE). It is very widely used in electrochemical measurements due to its excellent mechanical and electrical properties, extended potential range, chemical inertness (solvent resistant) and reproducibility (Instrument 2005). GCE is prepared by heating the material in very small increments in controlled

environment (inert environment). Slowly, the temperature increment is applied from 300 °C to 1200 °C to eradicate the oxygen, nitrogen, and the hydrogen which might build up in the process. The GCE has to be polished after each use by polishing cloth and then rinsed with DI water to obtain a maximum performance. Although few other pretreatment methods have been proposed in the literature, the most effective treatment was determined to be the polishing cloth (J. Wang, Analytical Electrochemistry 2000) (Instrument 2005). In this thesis work, the treatment procedure stated above was followed before performing a new analysis. Specifications and the picture of a working electrode are illustrated in Figure 13(a, b).

Reference Electrode - Silver/Silver Chloride (Ag/AgCl); it is a very commonly used electrode in electrochemical measurements. The reference electrode tests a cathodic protection corrosion control systems in the aqueous environments. The chemical equation (Equation 3) undergoes a redox reaction and the electron is detected between silver metal and the salt which is silver chloride.



Equation 3. Reference Electrode Chemical Reaction

The electrochemistry device uses this reaction as a reference to determine the analyte being studied. Specifications and the picture of a reference electrode are demonstrated in Figure 13 (c and d). The electrode was kept in 3M Potassium Chloride (KCl) solution for the entire time, as seen in Figure 12, in order to obtain the best results from the reference electrode.



Figure 12. Three Molar (3M) Potassium Chloride (KCL)

Counter Electrode – Platinum Wire; platinum is a widely used counter electrode in conventional three electrode system due to its inertness, resistance to corrosion, high temperature characteristic and stable electrical properties. Specifications and the picture of a counter electrode are exemplified in Figure 13 (e and f). Platinum wire was purchased from Omega Inc. The three inches of wire was folded three times and bounded together to achieve a uniform conduction throughout the experiments.

2.2.7 Protein-linked polymers and nano structured materials

2.2.7.1 Silica polymer

A 1 inch by 3 inch composite inorganic substrate material with silica as a main ingredient was purchased from Edmund Scientific Inc. Then gold (Au) was deposited on to silica via vapor deposition process. The gold and the silica (substrate) were placed inside of a

chamber. Then, the pressure of the chamber was reduced from the atmospheric pressure to -5 torr and the gold was heated to its melting point (1337.33 K).

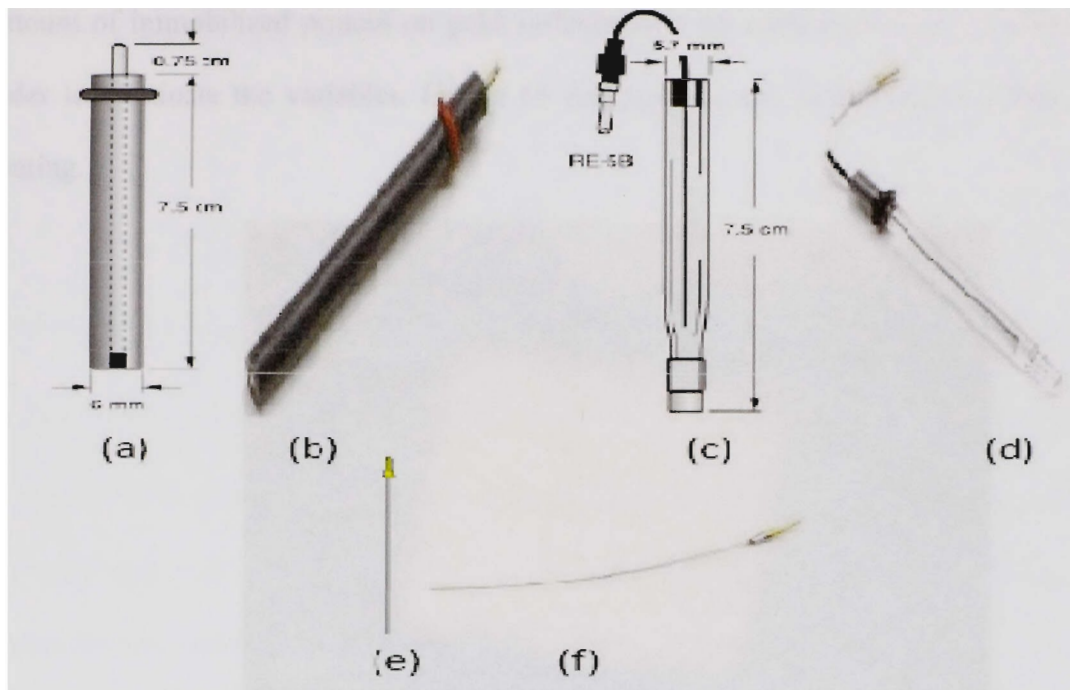


Figure 13. Working Electrode (Glassy Carbon) (a, b), Reference Electrode (Ag/AgCl) (c, d), Counter Electrode (Platinum Wire) (e, f).

Next, the melted Au was adhered on to the substrate via thermionic vacuum system and the deposition amount was determined to be 0.1 mm as seen on the Figure 14 below. The Au deposited substrate was then cut into 10 mm x 10 mm pieces in order to attach equal amount of protein on the surface area.

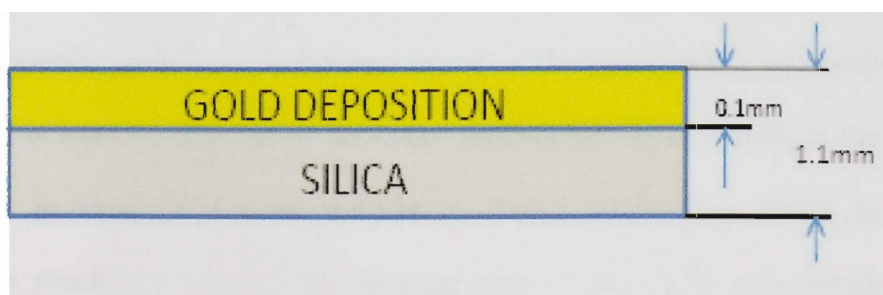


Figure 14. Au Deposited on Silica Substrate

The amount of pyruvate oxidase enzyme affects the production of H_2O_2 and one of the aims of this research is to evaluate the conductivity of the materials. Therefore, the amount of immobilized protein on gold surfaces must be consistent on all substrates in order to eliminate the variables. Figure 15 demonstrates the actual polymer with gold coating.

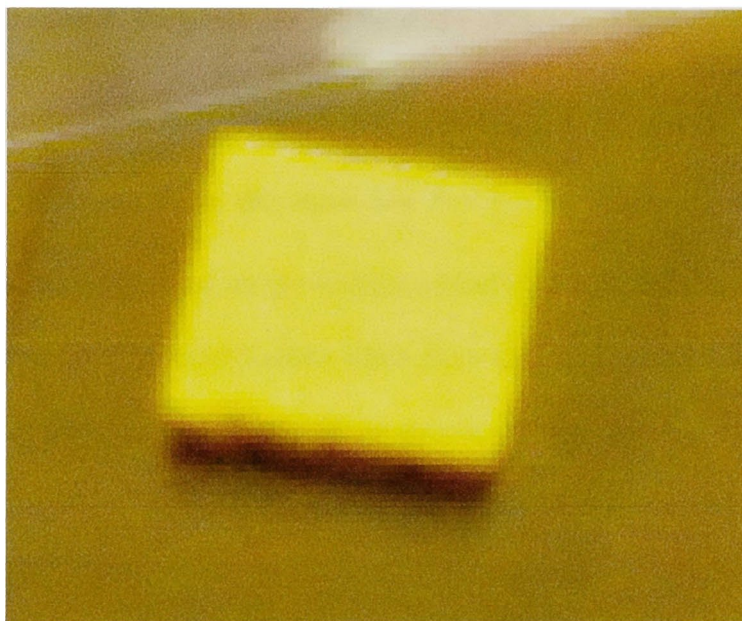


Figure 15. Actual Picture of the Gold-Coated Silica Polymer

2.2.7.2 Highly Conductive Multi Wall Carbon Nano-Tube (CNT) combined with Copper (Cu), Chromium (Cr), Nickel (Ni) and Silver (Ag) metal alloys

These materials are composed of CuCrAgNi, metals and CNT were prepared by employing powder metallurgy techniques based on the metal matrix composite (MMC) compacts. It is reported that one of the major limiting factors in sensing is the electrical conductivity in terms of electron transfer (P. Wang 2009), (Liu 2007). In order to increase the sensitivity towards the measurement of the H_2O_2 concentration in the reaction cell, several highly conductive materials were investigated for the role of

electron transferring materials from the buffer system to the electrodes. The conventional four probe method was performed to determine the conductivity of the materials; calculation was executed using the formula below:

$$\rho = \frac{(\frac{\pi t}{\ln 2})V}{I}$$

Equation 4. Formula of Conductivity (Munroe 2008)

Where ρ is the resistivity, V is the voltage, I is the current, s is the spacing between the probes, and t is the thickness. From the ohms law $R = \frac{V}{I}$, the resistivity was obtained (Munroe 2008). Gold was deposited on the surface of CuCrAgNi based alloys with CNT the same way it is described in Gold-Coated silica from the previous section. Figure 16 shows the real view of the highly conductive nano structured material.

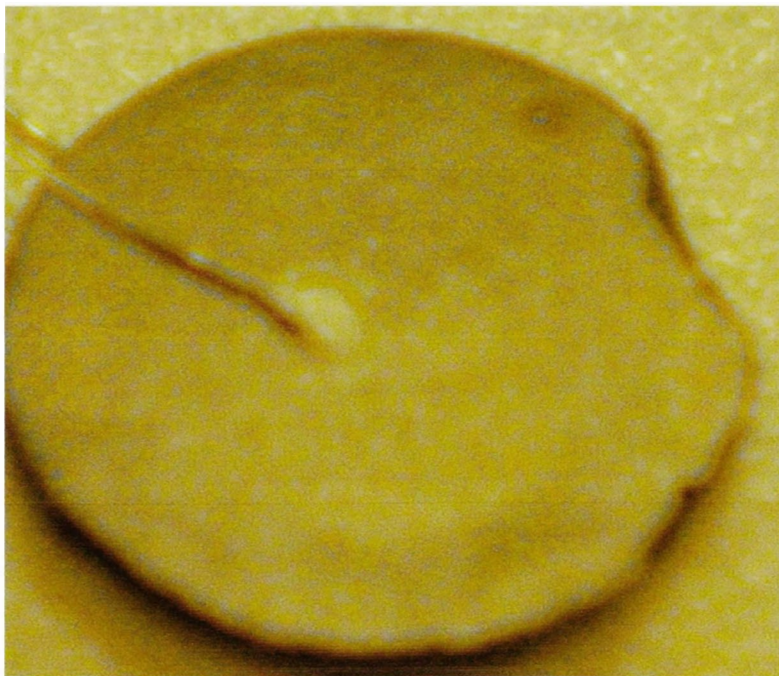


Figure 16. Actual View of the Nano-Structured Highly Conductive Material

2.2.7.3 Highly Conductive material composed of Copper (Cu), Chromium (Cr) with Multi Wall Carbon Nano-Tube (MWCNT)

The groundwork of this material is the same as the Highly Conductive Carbon Nano-Tube (CNT) with Nickel (Ni) and Silver (Ag) (CuCrAgNiCNT) explained in the previous section. The calculations were executed based on the Equation 4. Same procedure was followed respectively below for the calculating the conductivity. The actual view of the material is shown in Figure 18.

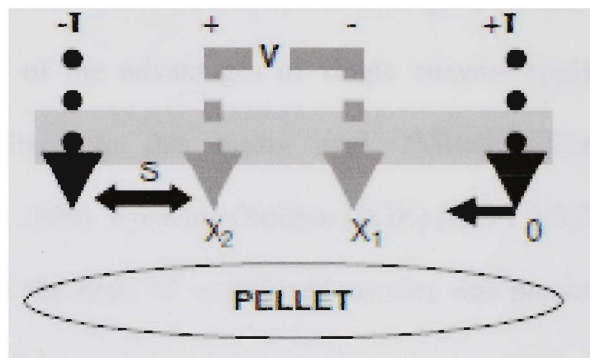


Figure 17. Four Point Probe Resistivity Measurements Sketch

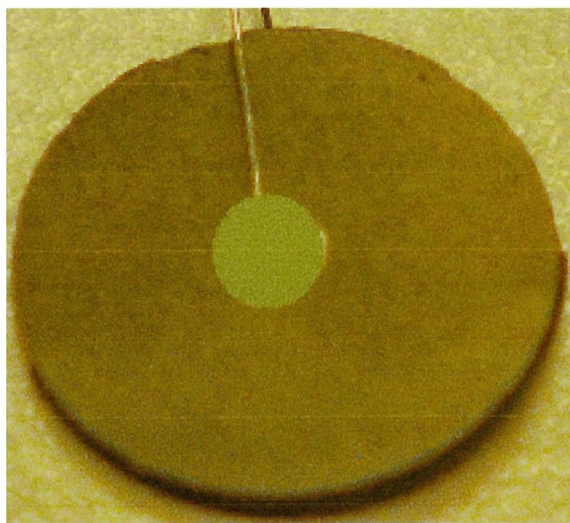


Figure 18. Authentic View of the Highly Conductive Nano Structured MWCNT

2.2.8 Pyruvate Oxidase Enzyme

Even though researchers have been working on the enzyme-linked biosensors for decades, these instruments still need to be improved in their sensitivity, durability, and selectivity. Literature review reveals that there are many different single and multi enzyme applications utilized to develop enzyme attached biosensors. However, the single enzyme conjugated sensors have superiority over the multi enzyme dependent sensors due to their simple application and immobilization (Akar, Development of a biosensor for detection of phosphate species in uranium contaminated groundwater and wastewater sediments 2010). Because of the advantages of single enzyme application, Pyruvate Oxidase (POX) was utilized in this thesis work (Villalba, Bioelectroanalytical determination of phosphate 2009). Pyruvate Oxidase (POX) (EC. 1.2.3.3, 100 units mg⁻¹) from aerococcus species in the form of lyophilized powder was purchased from Sigma Aldrich and used upon receiving.

As stated above, in order for this thesis to work, Pyruvate Oxidase (POX) was determined and attached to the metal surface to be employed. Pyruvate Oxidase (POX) (EC. 1.2.3.3, 100 units mg⁻¹) from aerococcus species in the form of lyophilized powder was purchased from Sigma Aldrich and used upon receiving.

2.2.9 Enzyme de-salting column:

When an enzyme is purchased in the lyophilized form, the supplier provides specific buffer to revive the enzyme for its longer shelf-life. Since the buffer contains salt, it can affect the immobilization of the enzyme to the surface of the material. Pyruvate Oxidase

was de-salted via a salting column to surmount the obstacle. De-salting column kit (displayed in Figure 19) was purchased from General Electric (GE) Health Care.

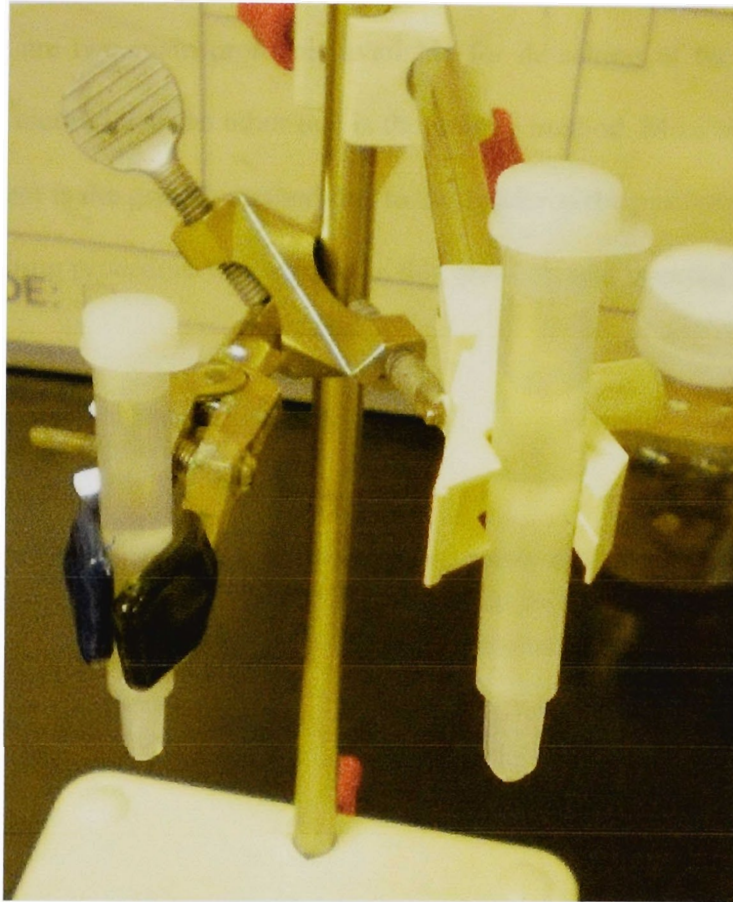


Figure 19. De-salting Columns

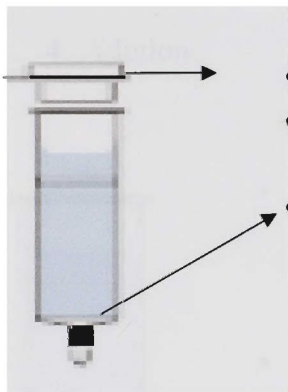
Lyophilized pyruvate oxidase (POX) enzyme, purchased from the Piercenet, contains impurities and buffer salts appended in the vial by the supplier. The enzyme must be extracted from the salts because buffer salts that contain prime amines affect the immobilization process (Fisher 2008). Desalting columns are used for large variety of applications such as removal of large biomolecules, removal of low molecular weight

compounds and buffer exchange. The de-salting process is done via de-salting column purchased from GE Health Care.

2.2.9.1 De-salting column preparation:

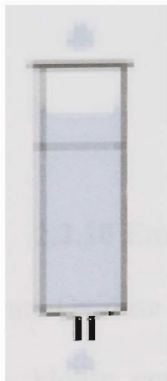
Currently, there are two main protocols available for de-salting of the protein. One of them is the spin method and the other one is the gravity method. Most suitable technique for this experiment is the gravity method due to the nature of the pyruvate oxidase (Fisher 2008). The desalting procedure was applied in this research as it is explained below.

1. Desalting Column Preparation:



- First, the top cap was removed from the column.
- The sealed bottom of the column by the manufacturer for fresh use was cut and discharged.
- The storage solution in the packed column was discharged.

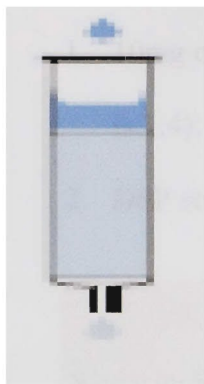
2. Equilibration of the column:



- The column was equilibrated via passing through the equilibrium buffer which was purchased from GE Health Care from the entire packed column.
- The process was repeated four times to achieve the complete equilibrium of the de-salting column.
- The collected equilibrium buffer at the bottom of the column was discarded.
- Note; The entire 25ml of equilibrium buffer was applied to the column.

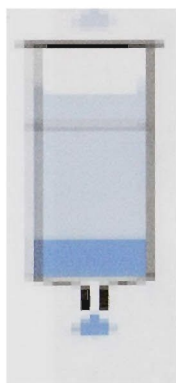
The protein was then immobilized on the surface of the materials right after the elution procedure as suggested by the protocol (Care 2007).

3. De-Salting of the Protein (Pyruvate Oxidase):



4. Elution

- The enzyme solution was applied to the pre- equilibrated column as 2,5ml at a time.
- It is allowed for the total volume, 2.5ml, of the enzyme sample pass-through the column and collected.
- The unbound protein and the impurities were washed out with 2.5ml of de-salting buffer solution.



- In order to collect the enzyme from the column matrix, the elution buffer was loaded to the pre-washed column. The entire de-salted and purified protein was collected from the bottom of the column in a clean vial.
- As soon as the protein was eluted from the column, it was immobilized on top of the materials which we employed according to the protein immobilization procedure (Care 2007).

2.2.10 Enzyme Immobilization on Materials

Pyruvate Oxidase was immobilized on three different material surfaces; polymer (silica) based, highly conductive CNT with Ag and Ni and highly conductive MWCNT.

Immobilization procedure was consistent for each substrate. During the procedure, dimethylsulfoxide (DMSO), enzyme solution (protein), dithiobis (succinimidyl) propionate (DSP), DI water, HEPES buffer and Tris buffer (all the chemicals are presented in Figure 20) were utilized.

Protocol:

1. 10mg of DSP was dissolved in 2.5ml of DMSO (The ratio for DSP to DMSO is 1:4).
2. DSP solution was completely dissolved in the DMSO by stirring.



Figure 20. Chemicals Used for the Immobilization Process

3. Au-coated Silica Polymer material was incubated in DSP+DMSO solution at room temperature.

4. After 30-35 minutes of incubation in DMSO+DSP solution, the material was gently and thoroughly rinsed twice with DI water.
5. The gold-coated substrate was activated with NHS group for protein coupling at this step.
6. In a 10 ml beaker, 5 ml, 0.5M HEPES pH 7 and 100 μ l of protein solution (this amount was strictly kept consistent for all protein conjugations of all three materials to ensure the constant amount of enzyme immobilization) was prepared (enough amount to submerge the material in the mixture).

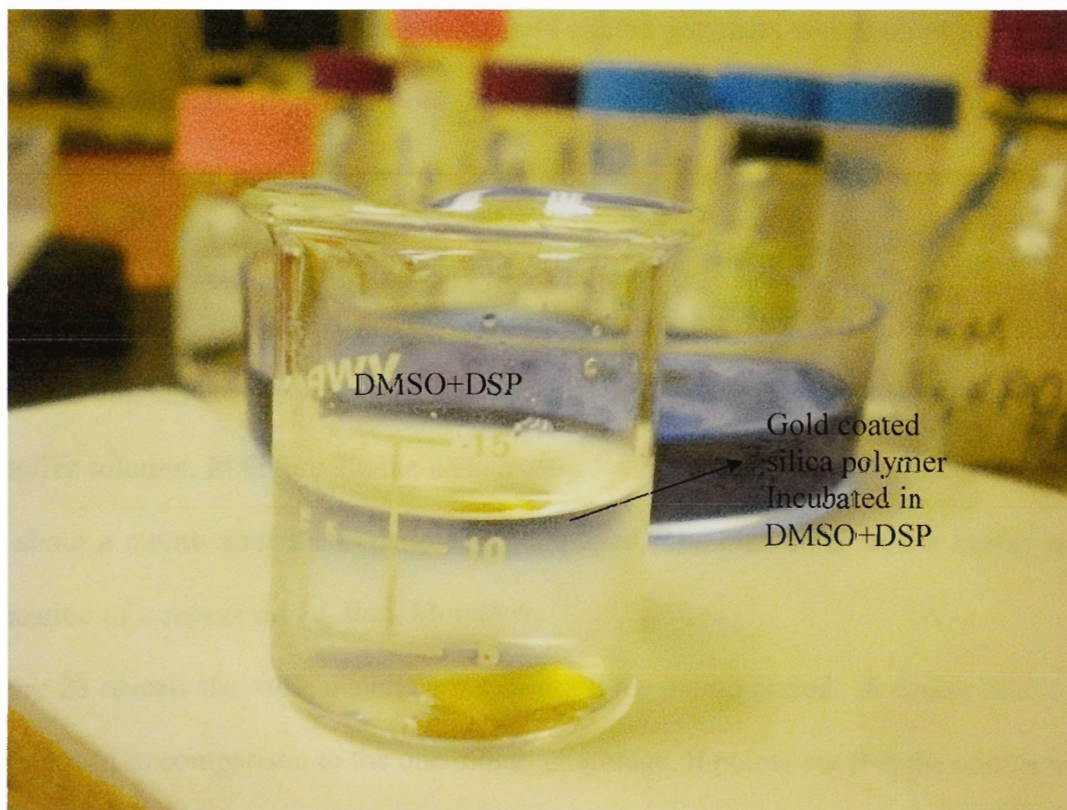


Figure 21. Gold Coated Silica Polymer Incubated in DSP+DMSO

7. The gold substrate was immediately immersed in the HEPES + Protein mixture for incubation to attain maximum amount of protein binding.
8. In order to achieve the optimum result for protein attachment, the carrier was incubated in the buffer and protein mixture solution for 5 hours at room temperature.
9. After 5 hours of incubation, the protein immobilized substrate material was removed from the solution. It was then rinsed with approximately 3ml tris-HCl pH7.5. (This step is very crucial to discard any un-conjugated proteins).

2.2.10.1 Immobilization of nano-structured-highly conductive materials

The same conjugation protocol used for gold-coated polymers was applied to the nano-structured materials. In order to obtain the best results, the immobilized copper-based materials should immediately be used for the electrochemical measurements after the crosslinking (Rahman, The biosensor based on the pyruvate oxidase modified conducting polymer for phosphate ions determination 2006). Highly conductive nano-structured materials contain copper which leached out over approximately two months time period in buffer solution. In Figure 22, the nano material was immobilized and kept in tris buffer for about a month after the experiments completed. The blue color in tris buffer is the indication of a copper dissolution. Moreover,

Figure 23 reveals the same materials but over a three month period. A darker blue color was noticed in comparison to the one month of storage. It points out that the conductivity of the materials deteriorates which also inversely could affect the experimental results.

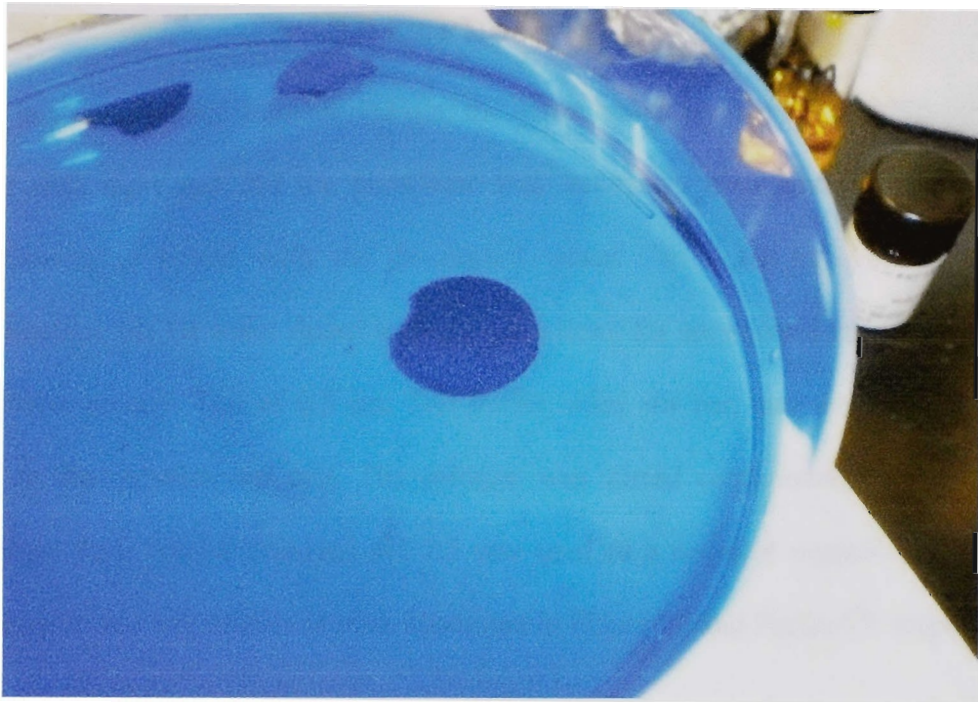


Figure 22. POX Immobilized on MWCNT and Kept in Tris Buffer After Experiments.

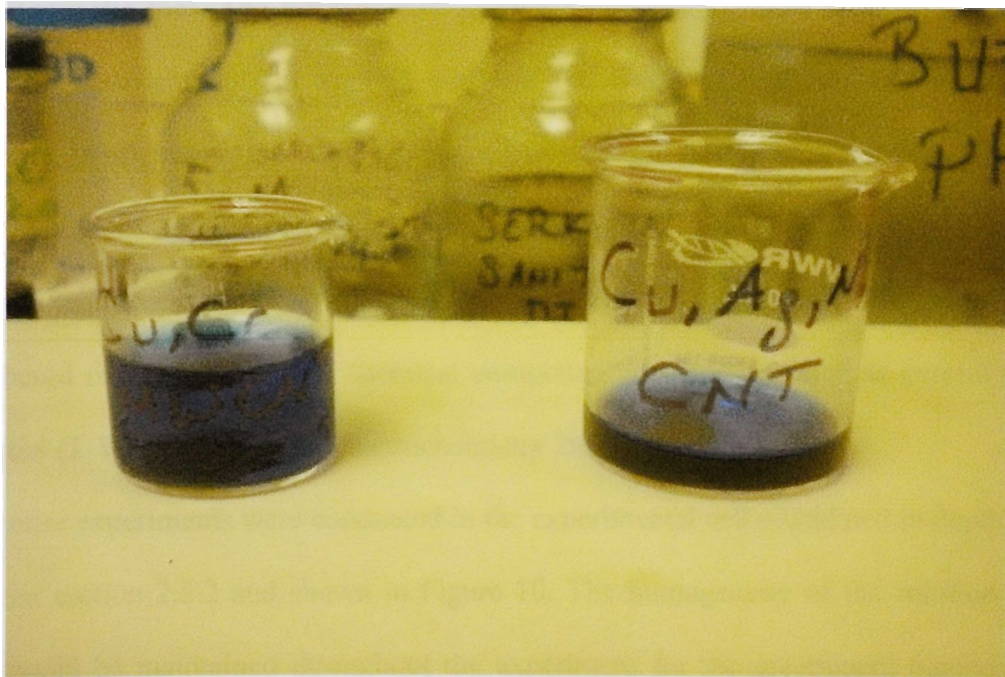


Figure 23. Nano Materials Kept in Tris Buffer Over Three Months Period.

3.0 EXPERIMENTS

Before any experiments were carried out, the entire lab-wares and the supplies were first washed with tap-water and the phosphate free laboratory detergent. Afterwards, they were thoroughly rinsed with the de-ionized water. In order to avoid any cross-contamination, the DI water rinsed supplies were dried for about two hours at 70°C in the oven. Subsequently, 1ml of 0.5 μM Tris buffer, mini stir bar, and the electrodes were placed in the experimental cell. The solution was stirred continuously throughout the recordings. 1ml, 50mM Tris-HCl pH 7.5 was used as a negative control for the entire voltammetric and amperometric tests illustrated in Figure 26 and Figure 27, respectively.

3.1 Cyclic Voltammetry (CV)

It is an electroanalytical technique with conventional three electrode method that is used as a diagnostic tool. The voltammetry provides information about an analyte acquired from the electrical current applied between the working electrode and the counter electrode. In other words, cyclic voltammetry observes the redox behavior of analyte over a wide range of applied potential to the electrodes. CV then scans the analyte between initial potential and the final potential. The instrument's scan range is adjusted by the user based on the investigated chemical compound which is recorded as current versus potential (J. Wang, Analytical Electrochemistry 2000).

The entire experiments were conducted in the experimental cell elucidated in depth in the material section 2.3.2 and shown in Figure 10. The homogeneity of the solution in the cell should be maintained throughout the experiment for the preminent outcome. For that purpose, a stir bar was positioned on the bottom of the cell, where the housing for

magnetic stir bar was constructed (illustrated in Figure 10 and Figure 7). Then, the experimental cell was placed on magnetic stirrer (Figure 24) and tests were conducted while stirring at 3000 rpm. The electrodes (working electrode, reference electrode and the counter electrode) were situated perpendicular to the bottom of the cell (see Figure 10) through the custom constructed electrode housing (Figure 8). The ninety degree angle and the proper height of the electrodes were ensured.

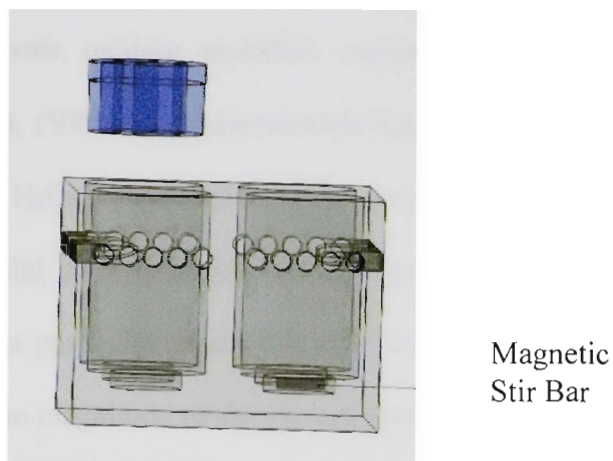


Figure 24. Computer Drawing of Experimental Cell and Magnetic Bar Placed in the Housing.

Detection and quantification of phosphate was performed via electrochemical measurements such as cyclic voltammogram and chronoamperograms with conventional three electrode system. The detailed explanation of electrochemical method is in section 3.1 and 3.2

3.2 Amperometry

Amperometry is also known as chronoamperometry. It is commonly used to determine the diffusion coefficient of electroactive chemical compounds at the surface of the

working electrode (N. Conrath 1995), (Kwan 2005), (Fumio Mizutani 2000). As opposed to cyclic voltammetry, a fixed potential is applied and the current change is recorded versus time (J. Wang, Analytical Electrochemistry 2000). An electrochemical reaction occurs upon the application of potential which in turn alters the magnitude of the current. The concentration of the solution is quantified from the magnitude of the current at indicated time (Christine Mousty 2001), (Engblom, The phosphate sensor 1998), (Fumio Mizutani 2000), (Gavalas 2001), (Kubo 1991), (Kwan 2005), (Rahman, The biosensor based on the pyruvate oxidase modified conducting polymer for phosphate ions determination. 2006), (Villalba, Bioelectroanalytical determination of phosphate 2009). In this investigation, H_2O_2 is produced from the enzymatic reaction that takes place on the enzyme-linked material, directly under the working electrode. The produced H_2O_2 causes a current change at a particular time (time only indicates the reaction moment) on the electrode surface. The magnitude of the current shift determines the concentration of the produced H_2O_2 (Christine Mousty 2001), (Gavalas 2001), (Kubo 1991), (N. Conrath 1995), (Villalba, Bioelectroanalytical determination of phosphate 2009).

3.3 Detection of Phosphate Concentration in the Cell

All the electrochemical measurements to detect and quantify the phosphate concentrations in the fabricated cell were completed with the same amperometric principles as explained in section 3.2.

Magnetic stirrer, 1ml, 50mM tris-HCl buffer, 20 μ l, 0.4 μ M of FAD, 20 μ l, 1 μ M of TPP, 20 μ l 2mM of Mg^{2+} and the electrodes were placed in the constructed experimental cell and stirred continuously at 3000rpm throughout the experiments. Working electrode,

reference electrode and counter electrode were connected to the Epsilon Electrochemical Amperometry, respectively. After the electrodes were positioned on the cell as seen in Figure 10, five various phosphate concentrations were examined (10mM, 1mM, 10 μ M, 100nM, and 10nM).

Table 1. Test plan for the current obtained from H₂O₂ Respect to Different Materials

MATERIAL	Replications		
	Trial 1	Trial 2	Trial 3
Silica Polymer			
CuCrAgNiCNT			
CuCrMWCNT			

Table 1 outlines the testing procedure. First, the silica polymer, subsequently, the nano-structured CuCrAgNi metals alloyed with CNT, and finally, the CuCr metals alloyed with MWCNT were tested with three replications.

All the experiments elucidated in the 3.3 were designed exactly the same way it is described here.

4.0 RESULTS AND DISCUSSIONS

4.1 Results

An enzyme-linked phosphate biosensor was developed for this thesis. The response of the sensor depends on the phosphate concentrations in the cell was investigated via electrochemical amperometric techniques (described in detail in section 3.2) as reported in literature (Serge Cosnier 1998), (M. Sánchez-Paniagua López 2009), (Fumio Mizutani 2000), (Susana Campuzano 2005), (Yaico D. Tanimoto de Albuquerque 2007), (Christine Mousty 2001), (A.T. Lawal 2009), (Mozaz 2006), (N. Conrath 1995). In addition, cyclic voltammetry (CV) was employed (Figure 25, Figure 26) to assess the purity (phosphate free) of the chemical solutions and materials utilized in these experiments (i.e. tris buffer, cells, electrodes and etc.) as well as the system functionality check. CV is often the primary test that is performed to gain information about the electroanalytical investigation (J. Wang, Analytical Electrochemistry 2000).

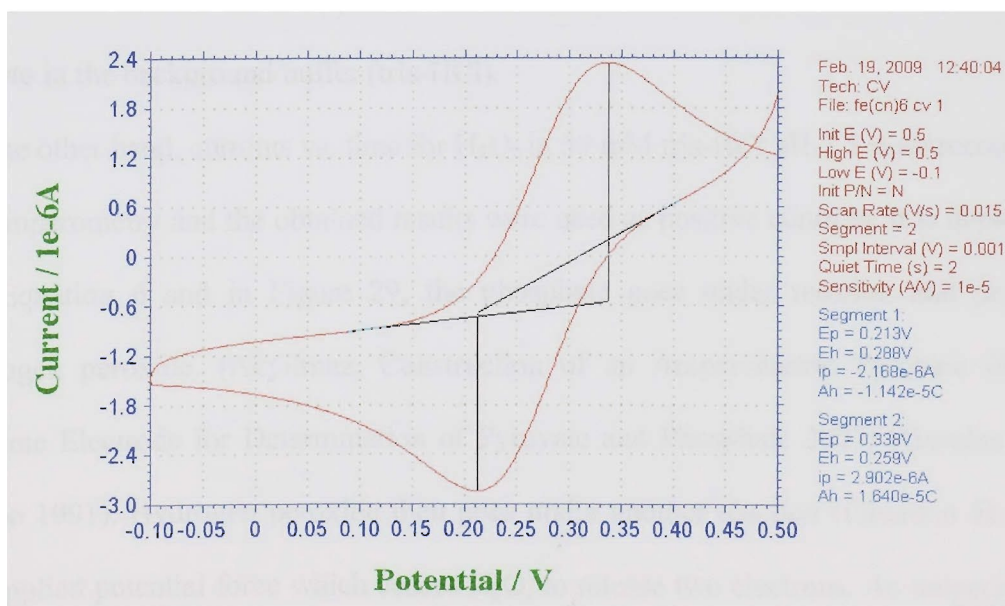


Figure 25. Cyclic Voltammetry (CV) of Ferricyanide

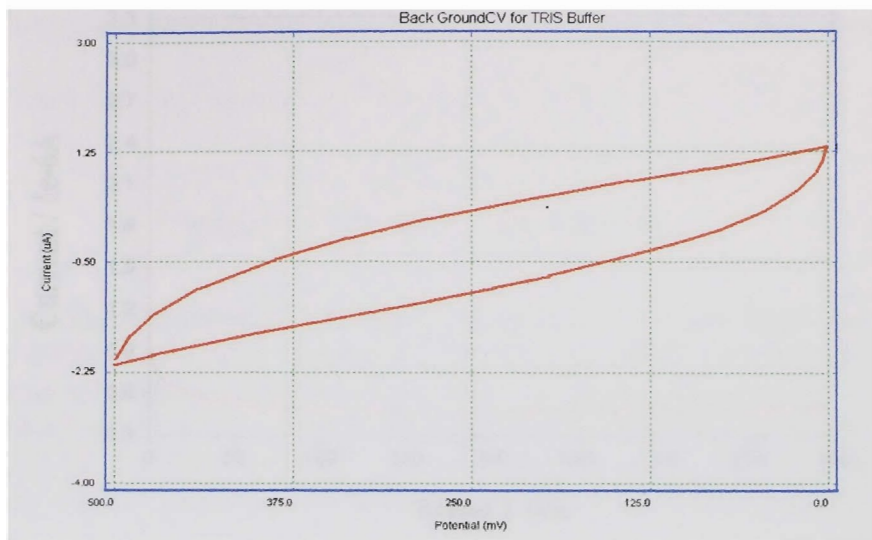


Figure 26. CV Recording of Tris Buffer Background

In order to determine the impurities in the buffers, there were a series of blank tests were often carried out prior to the actual experiments. The negative control experiments were distinguished the difference of the background and the measured substance (J. Wang, Analytical Electrochemistry 2000). Figure 27 depicts a typical amperometric background test for 1ml, 50 mM tris-HCl pH 7.5 and the result demonstrates the inexistence of any analyte in the background buffer (tris-HCl).

On the other hand, currents vs. time for H_2O_2 in 50 mM tris-HCl pH 7.5 were recorded by the amperometry and the obtained results were used as positive controls. It is depicted in the Equation 6 and in Figure 29, the phosphate goes under reaction and produces hydrogen peroxide. (Akyilmaz, Construction of an Amperometric Pyruvate Oxidase Enzyme Electrode for Determination of Pyruvate and Phosphate 2007) (Gavalas 2001) (Kubo 1991). Hydrogen peroxide then goes under another reaction (Equation 5) due to the applied potential force which causes H_2O_2 to release two electrons. An amperometric device captures these released electrons in the form of current change between working

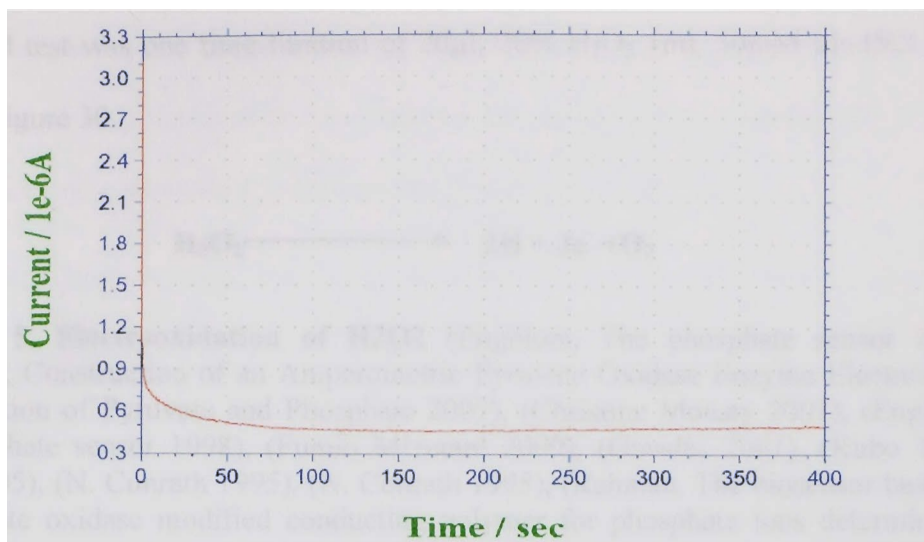


Figure 27: Amperometric Background Test Recording for 1ml, 50mM Tris-HCl pH 7.5

and counter electrodes (Fumio Mizutani 2000), (Serge Cosnier 1998). For this test, two separate techniques under the same conditions were attempted for comparison purposes. The first one was the incessant titration of 20 μ l, 20% H₂O₂ in 1ml, 50mM tris-HCl pH7.5 buffer with 10second intervals seen in Figure 28.

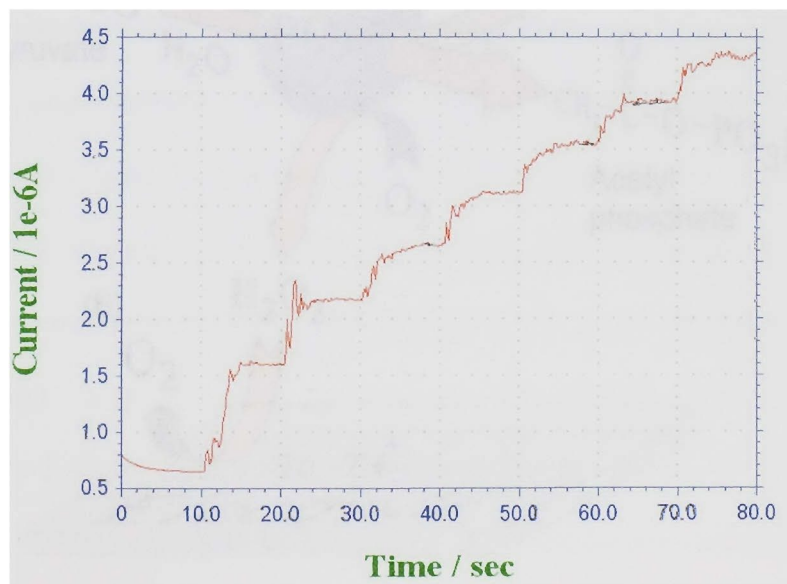
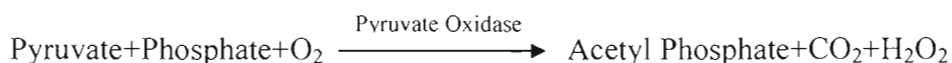


Figure 28. Continuous Titration of 20 μ l, 20% H₂O₂ in 1ml Tris Buffer

The second test was one time titration of 20 μ l, 20% H₂O₂ 1ml, 50mM tris-HCl pH7.5 shown in Figure 30.



Equation 5. Electrooxidation of H₂O₂ (Engblom, The phosphate sensor 1998), (Akyilmaz, Construction of an Amperometric Pyruvate Oxidase Enzyme Electrode for Determination of Pyruvate and Phosphate 2007), (Christine Mousty 2001), (Engblom, The phosphate sensor 1998), (Fumio Mizutani 2000), (Gavalas 2001), (Kubo 1991), (Kwan 2005), (N. Conrath 1995), (N. Conrath 1995), (Rahman, The biosensor based on the pyruvate oxidase modified conducting polymer for phosphate ions determination 2006)



Equation 6. Phosphate Enzymatic Reaction (Akyilmaz, Construction of an Amperometric Pyruvate Oxidase Enzyme Electrode for Determination of Pyruvate and Phosphate 2007), (Engblom, The phosphate sensor 1998), (Fumio Mizutani 2000), (Gavalas 2001), (Guilbalut 1975), (Kubo 1991), (N. Conrath 1995)

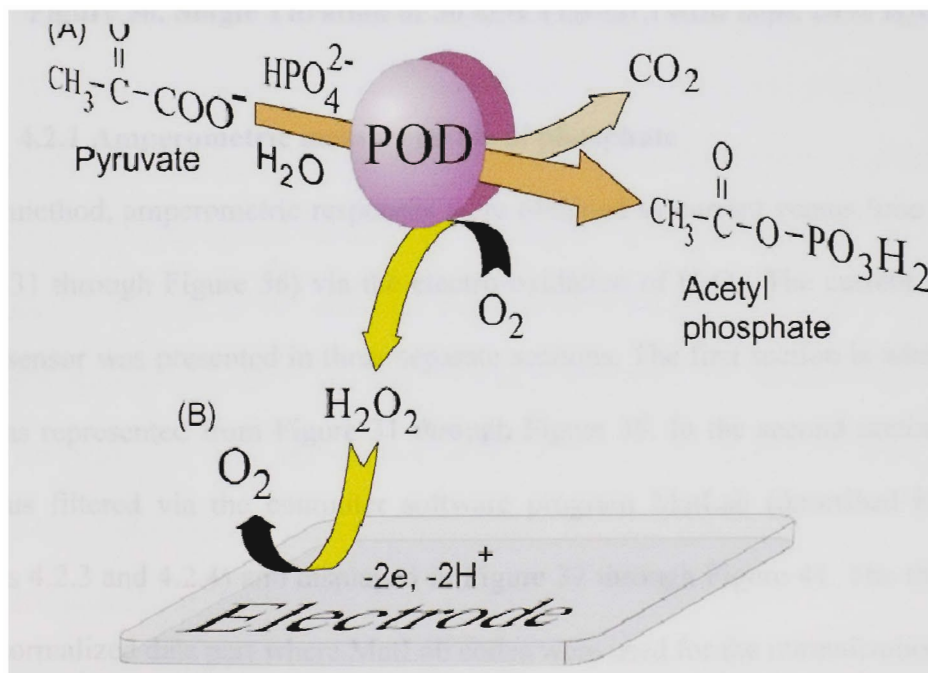


Figure 29. Enzymatic Reaction Mechanism of Pyruvate Oxidase (Villalba, Bioelectroanalytical determination of phosphate 2009)

After completing the instruments test, proper functioning tests, negative control and positive control test, the system was prepared for amperometric experiments for H_2O_2 detection from phosphate solutions (Equation 6 and Figure 29).

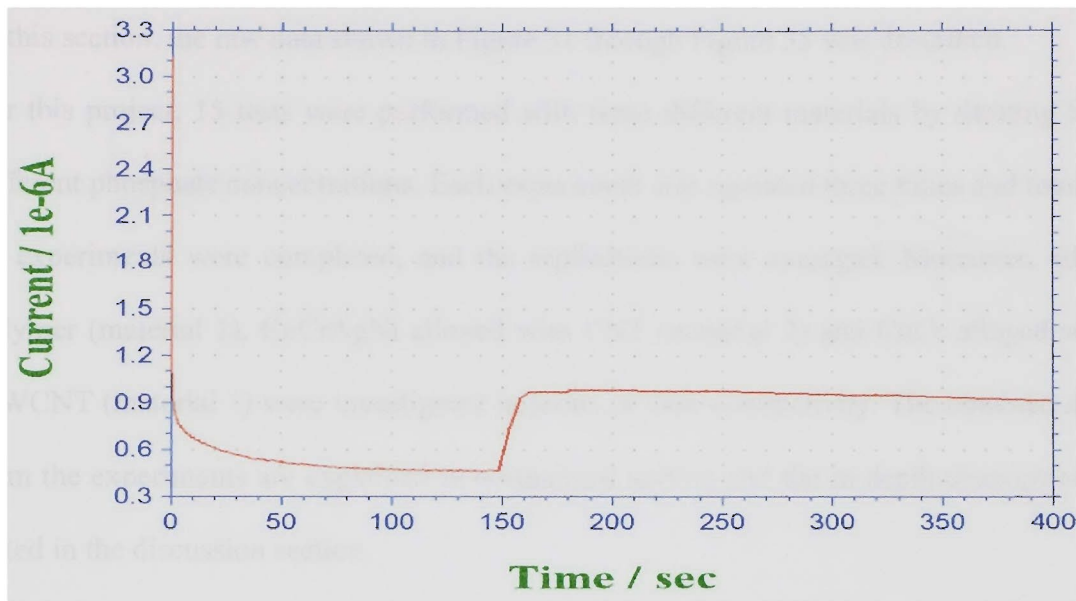


Figure 30. Single Titration of 50 mM Tris-HCl with 20 μ l, 20% H_2O_2

4.2.1 Amperometric measurements of phosphate

In this method, amperometric responses were obtained as current versus time (i-t curve) (Figure 31 through Figure 56) via the electro-oxidation of H_2O_2 . The current response of the biosensor was presented in three separate sections. The first section is where the raw data was represented from Figure 31 through Figure 35. In the second section, the raw data was filtered via the computer software program MatLab (described in detail in sections 4.2.3 and 4.2.4) and displayed in Figure 37 through Figure 41. The third section is the normalized data part where MatLab codes were used for the normalization process

(explained further in section 4.2.5). The normalized data were exhibited in Figure 42 through Figure 56.

4.2.2 Raw Data:

In this section, the raw data shown in Figure 31 through Figure 35 was described.

For this project, 15 tests were performed with three different materials by titrating five different phosphate concentrations. Each experiment was repeated three times and total of 45 experiments were completed, and the replications were averaged. Moreover, silica polymer (material 1), CuCrAgNi alloyed with CNT (material 2) and CuCr alloyed with MWCNT (material 3) were investigated in terms of their conductivity. The obtained data from the experiments are explained in normalized section and the in depth description is stated in the discussion section.

4.2.2.1 Responses for 10 mM Phosphate Titration

Figure 31 represents the amperometric recordings for the three enzyme-linked materials (silica polymer, CuCrAgNi alloyed with CNT and CuCr alloyed with MWCNT) by the titration of 10mM phosphate solution. In the Figure 31, blue line, green line and redline symbolize the average of the obtained amperometric recordings for the silica polymer, CuCrAgNi alloyed with CNT, and CuCr alloyed with MWCNT, respectively. The results are further examined after the normalization of the amperometric recordings obtained from the Mat-Lab programming (section 4.2.5).

4.2.2.2 Responses for 1 mM Phosphate Titration

Up on successful recording of 10mM phosphate detection, 10 folds lower concentration (1mM) was tested.

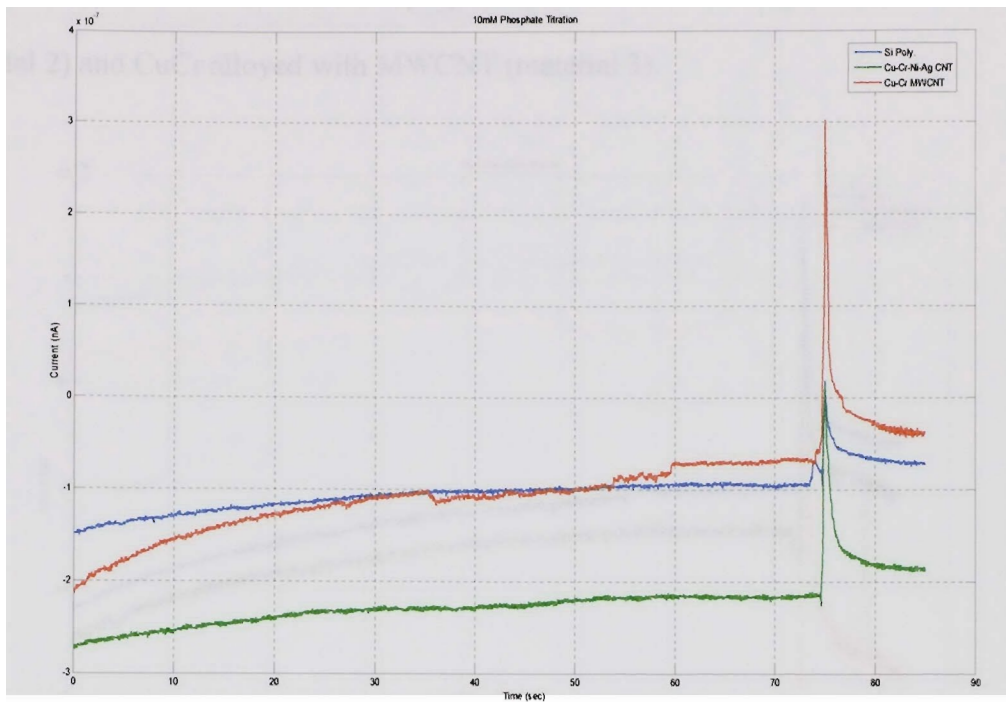


Figure 31. Amperometric Recordings for Silica Polymer, CuCrNiAg Alloyed with CNT, CuCr Alloyed with MWCNT by titration of 10mM $[PO_4^{3-}]$ Solution.

Figure 32 depicts the amperometric recordings for the titration of 1mM phosphate solution. In this part of the investigation, the same procedure in section 4.2.2.1 was applied for 1mM phosphate solution. All the collected data is discussed in depth in the discussion section 4.3.

4.2.2.3 Responses for 0.01 mM Phosphate Titration

In this part of the experiment, the concentration level of phosphate was diluted ten folds from 0.1 mM to 0.01mM (10 μ M) which is more relative to the previous section and the amperometric response of the biosensor was examined. The arrangement of the material testing was exactly in the same order as the sections 4.2.2.1 and 4.2.2.2. The experiments

were conducted in the order of; silica polymer (material 1), CuCrAgNi alloyed with CNT (material 2) and CuCr alloyed with MWCNT (material 3).

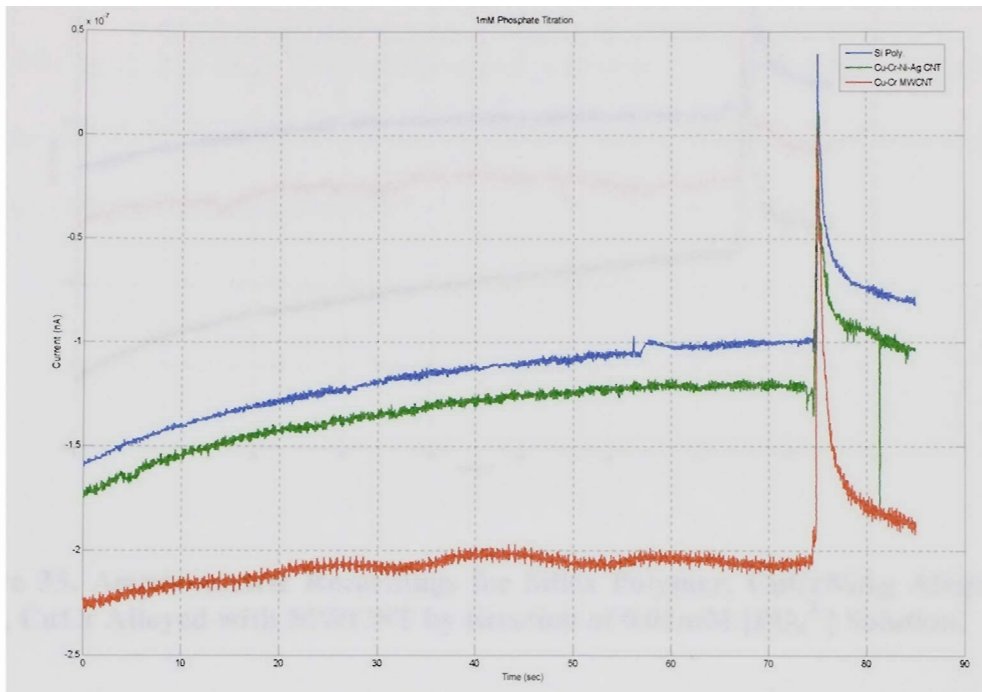


Figure 32. Amperometric Recordings for Silica Polymer, CuCrNiAg Alloyed with CNT, CuCr Alloyed with MWCNT by titration of 1mM $[\text{PO}_4^{3-}]$ Solution.

The attained results are exhibited in Figure 33 and they are further explained in normalized data section 4.2.5.3.

4.2.2.4 Responses for 0.0001 mM Phosphate Titration

0.0001mM phosphate solution was prepared via diluting the stock solution as explained in section 2.3.1. Figure 34 depicts the amperometric recordings for the titration of 0.0001mM phosphate solution. In section 4.2.2.1 experiments were repeated for this phosphate concentration. The further data analysis are elaborated in both normalized data section 4.2.5.4 and the discussion section 4.3.

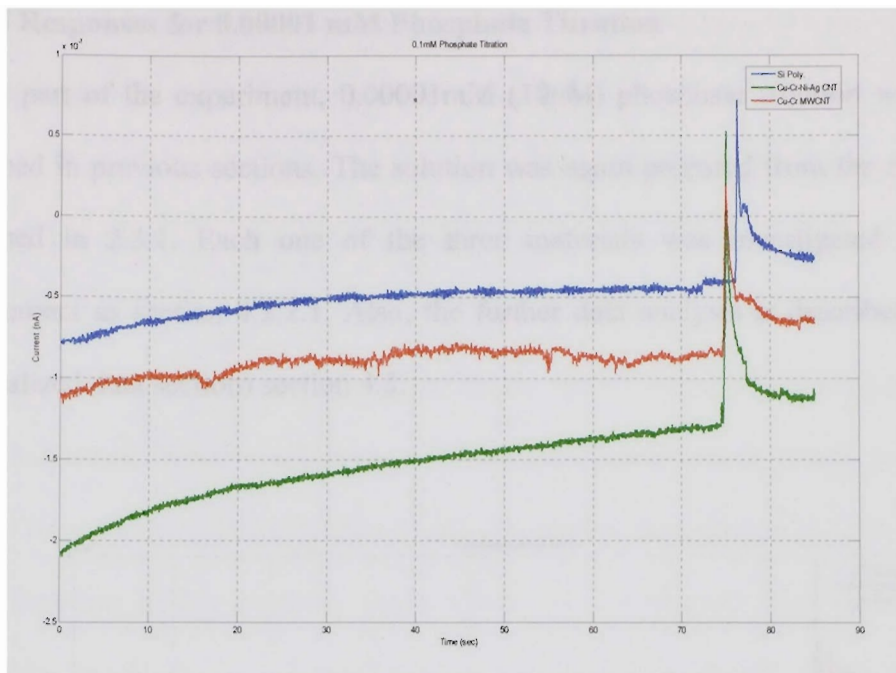


Figure 33. Amperometric Recordings for Silica Polymer, CuCrNiAg Alloyed with CNT, CuCr Alloyed with MWCNT by titration of 0.01mM $[\text{PO}_4^{3-}]$ Solution.

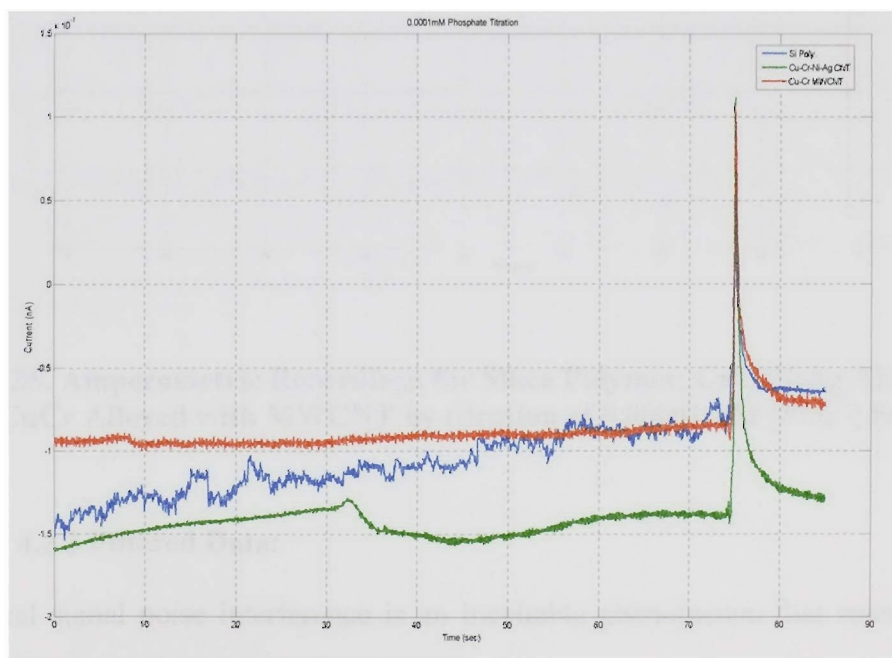


Figure 34. Amperometric Recordings for Silica Polymer, CuCrNiAg Alloyed with CNT, CuCr Alloyed with MWCNT by titration of 0.0001mM $[\text{PO}_4^{3-}]$ Solution.

4.2.2.5 Responses for 0.00001 mM Phosphate Titration

In this part of the experiment, 0.00001mM (10nM) phosphate solution was titrated as described in previous sections. The solution was again prepared from the stock solution described in 2.3.1. Each one of the three materials was investigated in the same arrangement as section 4.2.2.1. Also, the further data analysis is described in depth in (Normalized data section) section 4.3.

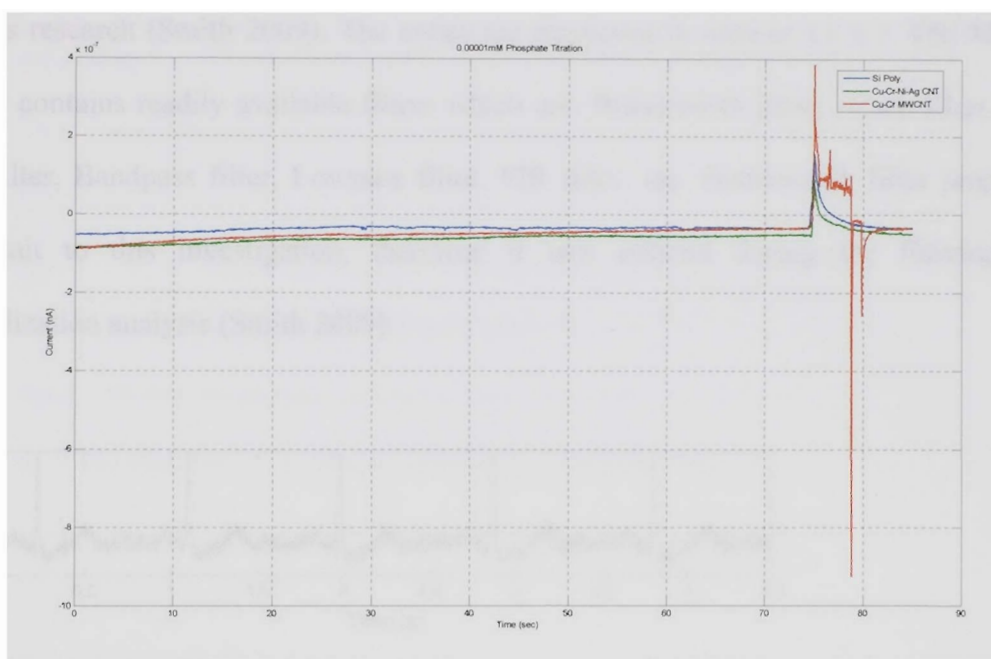


Figure 35. Amperometric Recordings for Silica Polymer, CuCrNiAg Alloyed with CNT, CuCr Alloyed with MWCNT by titration of 0.00001mM $[\text{PO}_4^{3-}]$ Solution.

4.2.3 Filtered Data:

Electrical signal noise interference is an inevitable phenomenon that researchers battle with in their data. Under the optimal conditions, amperometric experiments are performed in a Faraday Cage (Sigmond 2000). Due to the unavailability of the Faraday

Cage in our laboratory, the obtained raw data contained noise as seen in Figure 31 through Figure 35. This filtering process is the same analogy used in EKG signals as seen on Figure 36 (Wu 2009). Figure 36 a, b and c represents the signal with noise, the noise removed via filtering and normalized data respectively. The same exact approach was utilized in this thesis to filter and normalize the noise interfered data obtained from amperometric recordings. Therefore, the results were filtered via the computer software program MatLab. Specific codes were written for filtering and the normalization process for this research (Smith 2009). The codes are displayed in section 4.2.3.1. The MatLab library contains readily available filters which are: Butterworth filter, Notch filter, High pass filter, Bandpass filter, Lowpass filter, FIR filter, etc. Butterworth filter properties best suit to this investigation, therefore it was utilized during the filtering and normalization analysis (Smith 2009).

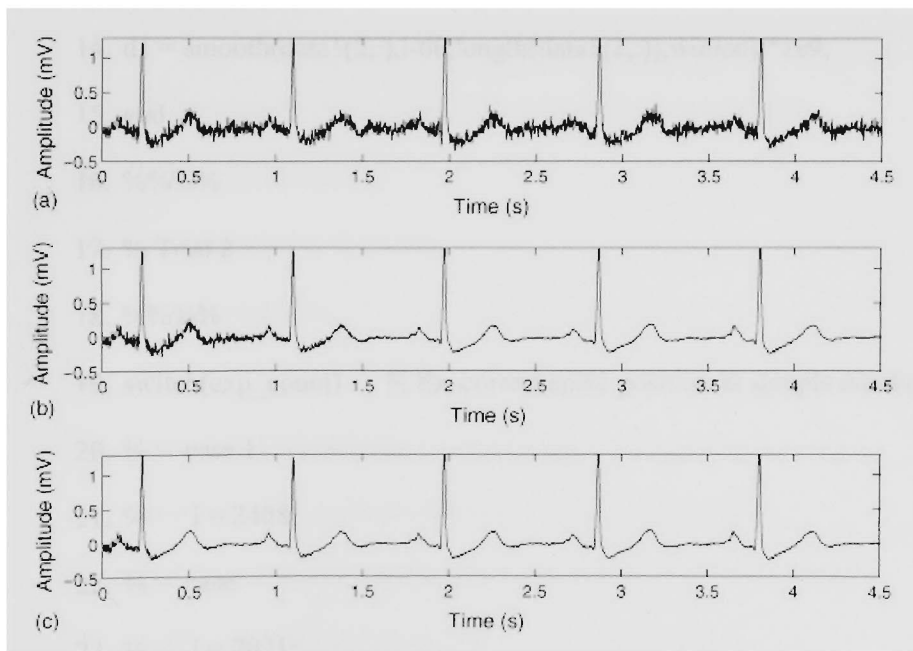


Figure 36. ECG Signal, Raw Data (a), Filtered Data (b) and Normalized Data (c), (Wu 2009)

4.2.3.1 Written Mat-Lab Codes for Signal Filtering and Normalization

```
1. [b,a] = butter(5,0.5); % create Butterworth filter
2. winlen = 10;          % length of window for averaging
3. switch(exp_count) % the correct spike position in sample number for trial# 1
4. %   case 4
5. %   i = 2154;
6. %   case 5
7. %   i = 2065;
8. otherwise          % otherwise, find the maximum value as peak
9. [c,i] = max(data1(2,:));
10. end
11. try              % get 60samples before and 160 samples after the peak
12. d1 = smooth(data1(2,:),i-60,i+120,winlen).*1e9;
13. catch % else, 60 samples before the peak to the end
14. d1 = smooth(data1(2,:),i-60,length(data1(2,:)),winlen).*1e9;
15. end
16. %%%
17. % Trial 2
18. %%%
19. switch(exp_count) % the correct spike position in sample number for trial# 2
20. %   case 1
21. %   i = 2408;
22. %   case
23. %   i = 2021;
24. otherwise          % otherwise, find the maximum value as peak
```

```

25. [c,i] = max(data2(2,:));
26. end
27. d2 = smooth(data2(2,:),i-60,i-61+length(d1),winlen).*1e9;
28. %%%
29. % Trial 3 %%%
30. switch(exp_count) % the correct spike position in sample number for trial# 3
31. % case 4
32. % i = 2017;
33. % case 6
34. % i = 2409;
35. case 15
36. i = 2155;
37. otherwise % otherwise, find the maximum value as peak
38. [c,i] = max(data3(2,:));
39. end
40. d3 = smooth(data3(2,:),i-60,i-61+length(d1),winlen).*1e9;
41. % d3 = filtfilt(b,a,d3);
42. t = (0:length(d1)-1).*0.01;
43. gap = zeros(1,3);
44. clf
45. subplot(311);plot(data1(1,11:end-11),
46. smooth(data1(2,:),11,length(data1(2,:))-11,winlen));
47. title(['\Gamma \rho. ' int2str(exp_count) '. Trial# 1']);
48. grid on; ylabel('Current (nA)');
49. subplot(312);plot(data2(1,11:end-11),

```

```

50. smooth(data2(2,:),11,length(data2(2,:))-11,winlen));
51. title(['Exp. ' int2str(exp_count) ' Trial# 2']);
52. grid on; ylabel('Current (nA)');
53. subplot(313);plot(data3(1,11:end-11),
54. smooth(data3(2,:),11,length(data3(2,:))-11,winlen));
55. title(['Exp. ' int2str(exp_count) ' Trial# 3']);
56. grid on; ylabel('Current (nA)');
57. saveas(gcf,['. Plots Filtered Experiment ' int2str(exp_count)], 'cmf');clf
58. % figure('Position',get(0,'ScreenSize'));
59. subplot(311); plot(t,d1); title(['Exp. ' int2str(exp_count) ' Trial# 1']);
60. grid on; ylabel('Current (nA)');
61. tinit = t;
62. initial = mean(d1(1:25)).*ones(length(tinit),1);
63. tfinal = t(end-25:end);
64. final = mean(d1(end-25:end)).*ones(length(tfinal),1);
65. gap(1) = final(1)-initial(1);
66. hold all; line(tfinal,final,'Color','k');
67. line(tinit,initial,'Color','k');
68. text(mean(tfinal),initial(1)+(gap(1)/2), [num2str(gap(1)) 'nA'], 'VerticalAlignment',...
69. 'Middle', 'HorizontalAlignment','Left');
70. subplot(312); plot(t,d2); title(['Exp. ' int2str(exp_count) ' Trial# 2']);
71. grid on; ylabel('Current (nA)');
72. initial = mean(d2(1:25)).*ones(length(tinit),1);
73. final = mean(d2(end-25:end)).*ones(length(tfinal),1);
74. gap(2) = final(1)-initial(1);

```



```

75. hold all; line(tfinal,final,'Color','k');
76. line(tinit,initial,'Color','k');
77. text(mean(tfinal),initial(1)+(gap(2)/2), [num2str(gap(2)) 'nA'], 'VerticalAlignment',...
78. 'Middle', 'HorizontalAlignment','left');
79. subplot(313); plot(t,d3); title(['Exp ' int2str(exp_count) ' Trial 3']);
80. grid on; ylabel('Current (nA)');
81. initial = mean(d3(1:25)).*ones(length(tinit),1);
82. final = mean(d3(end-25:end)).*ones(length(tfinal),1);
83. gap(3) = final(1)-initial(1);
84. hold all; line(tfinal,final,'Color','k');
85. line(tinit,initial,'Color','k');
86. text(mean(tfinal),initial(1)+(gap(3)/2), [num2str(gap(3)) 'nA'], 'VerticalAlignment',...
87. 'Middle', 'HorizontalAlignment','left');
88. saveas(gcf, ['.. Plots Final Experiment ' int2str(exp_count)], 'emf');
89. % avg = (d1+d2+d3)/3;%
90. % davg = diff(avg);
91. % [c,p2] = find(davg(105:end)>=0,1); p2=105;
92. % % p2 = p2 + 105;
93. % tinit = t;% initial = mean(avg(1:50)).*ones(length(tinit),1);
94. % tfinal = t(p2+25:end);
95. % final = mean(avg(p2+25:end)).*ones(length(tfinal),1);
96. % gap = final(1)-initial(1);%
97. % % subplot(414); plot(t,avg); title(['Exp. ' int2str(exp_count) ' Average']);
98. % % grid on; xlabel('Time (sec)'); ylabel('Current (nA)');
99. % % hold all; line(tfinal,final,'Color','k');

```

```

100. %% line(tinit,initial,'Color','k');
101. %% text(mean(tfinal).0, [num2str(gap) 'nA'], 'VerticalAlignment',...
102. %% 'Middle', 'HorizontalAlignment','Left');

```

4.2.3.2 Description of Filtered Data

In this section, Figure 37 through Figure 41, the filtered data via Mat-Lab codes (presented in section 4.2.4) are illustrated. The list of figures and concentrations order was kept exactly the same with the raw data section for consistency.

4.2.3.2.1 Filtered Data for 10mM Phosphate Titration

The Figure 37 represents the 10mM concentration for three separate enzyme-linked materials. The data presented in section 4.2.2.1 were filtered via the written MatLab codes. The filtered results are further analyzed in the normalized data section 4.2.5.1.

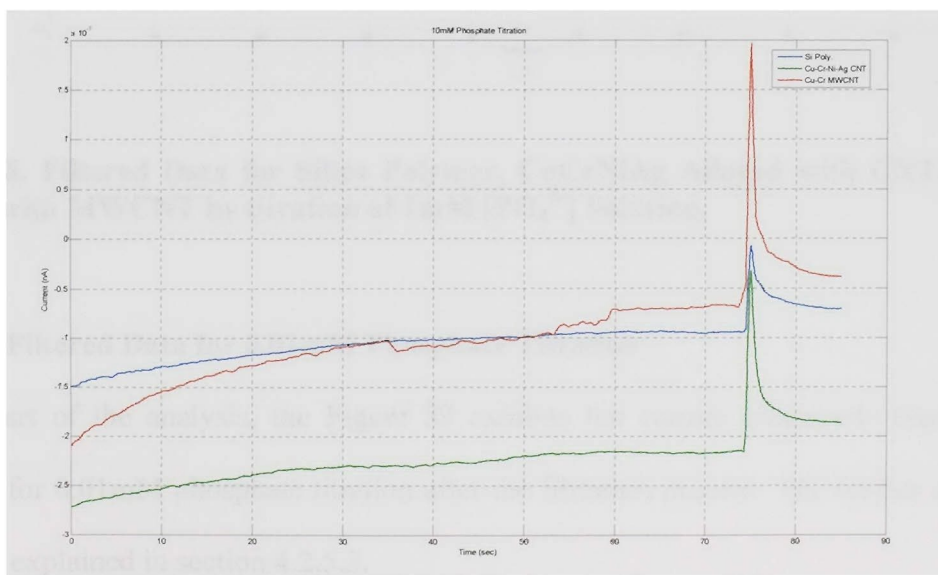


Figure 37. Filtered Data for Silica Polymer, CuCrNiAg Alloyed with CNT, CuCr Alloyed with MWCNT by titration of 10mM $[PO_4^{3-}]$ Solution.

4.2.3.2.2 Filtered Data for 1mM Phosphate Titration

1mM amperometric responses after the Mat-Lab filtration process is displayed in, Figure 38. The data illustrated in section 4.2.2.1 was filtered via the written MatLab codes and the obtained data are further analyzed in normalized data section 4.2.5.2.

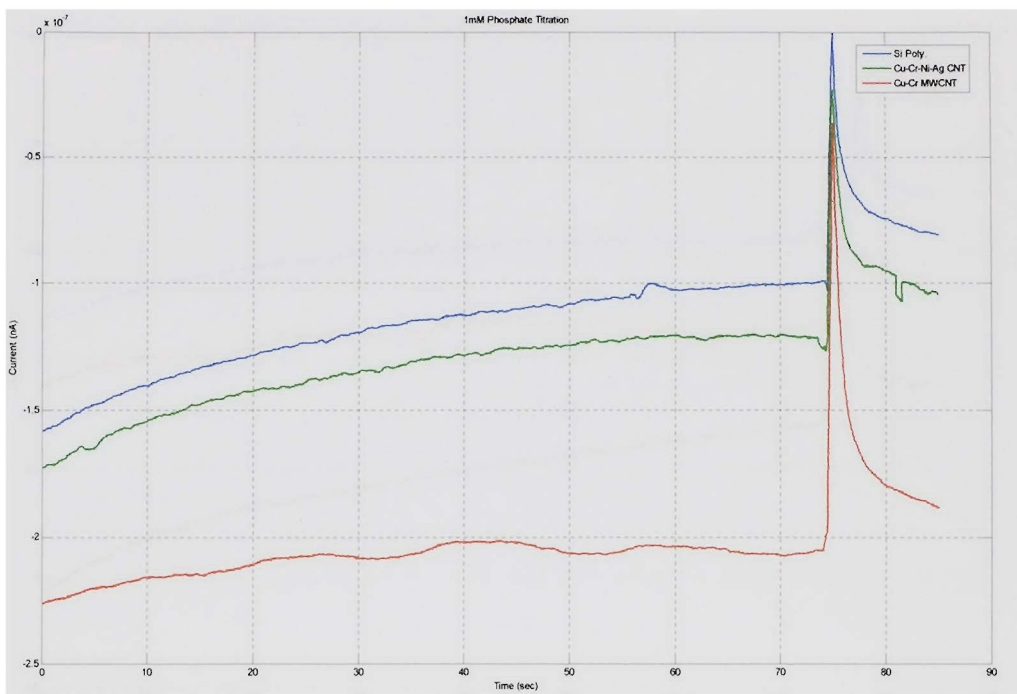


Figure 38. Filtered Data for Silica Polymer, CuCrNiAg Alloyed with CNT, CuCr Alloyed with MWCNT by titration of 1mM $[\text{PO}_4^{3-}]$ Solution.

4.2.3.2.3 Filtered Data for 0.01mM Phosphate Titration

In this part of the analysis, the Figure 39 exhibits the current magnitude changes in response for 0.01mM phosphate titration after the filtration process. The further analysis of data is explained in section 4.2.5.3.

4.2.3.2.4 Filtered Data for 0.0001mM Phosphate Titration

In this part of the study, 0.0001mM phosphate titration responses after filtration process are exhibited. This process is depicted in Figure 40 for the for silica polymer, CuCrAgNi alloyed with CNT and CuCr alloyed with MWCNT by the titration of 0.0001mM phosphate solution.

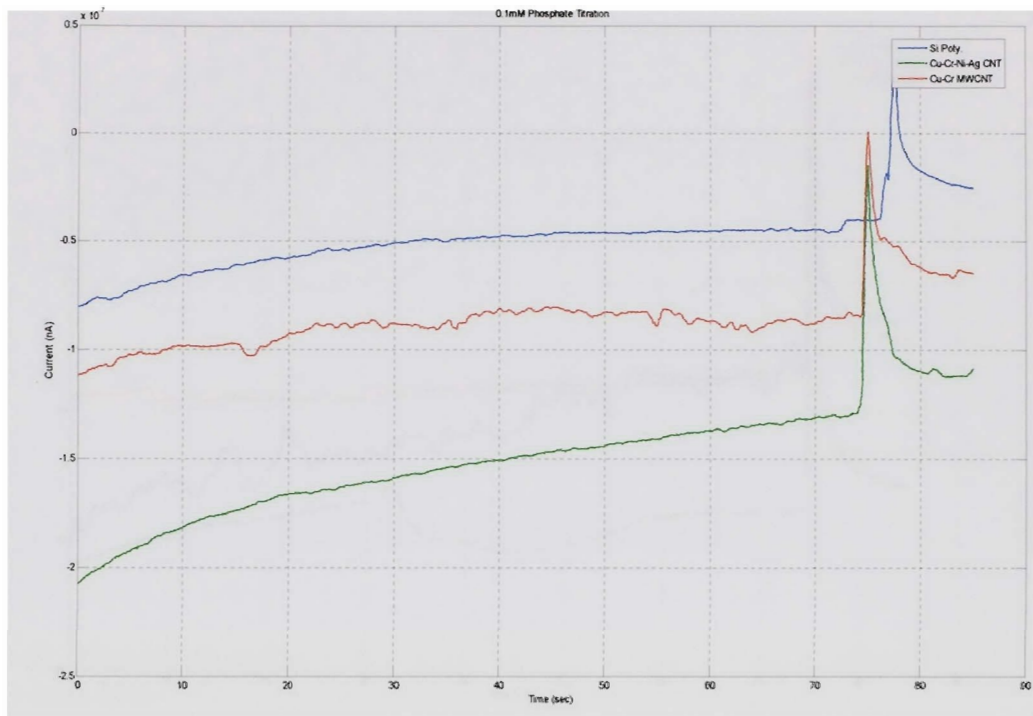


Figure 39. Filtered Data for Silica Polymer, CuCrNiAg Alloyed with CNT, CuCr Alloyed with MWCNT by titration of 0.01mM $[\text{PO}_4^{3-}]$ Solution.

4.2.3.2.5 Filtered Data for 0.00001mM Phosphate Titration

The filtered data for 0.00001mM (10nM) phosphate concentration is obtained and demonstrated in Figure 41. Further analyses of the final results are explained in section 4.2.5.5.

4.2.4 Normalized Signal

Normalization process was performed via Mat-Lab software program described in section 4.2.4. During the normalization process the necessary data is magnified in a bigger scale for better analysis purposes.

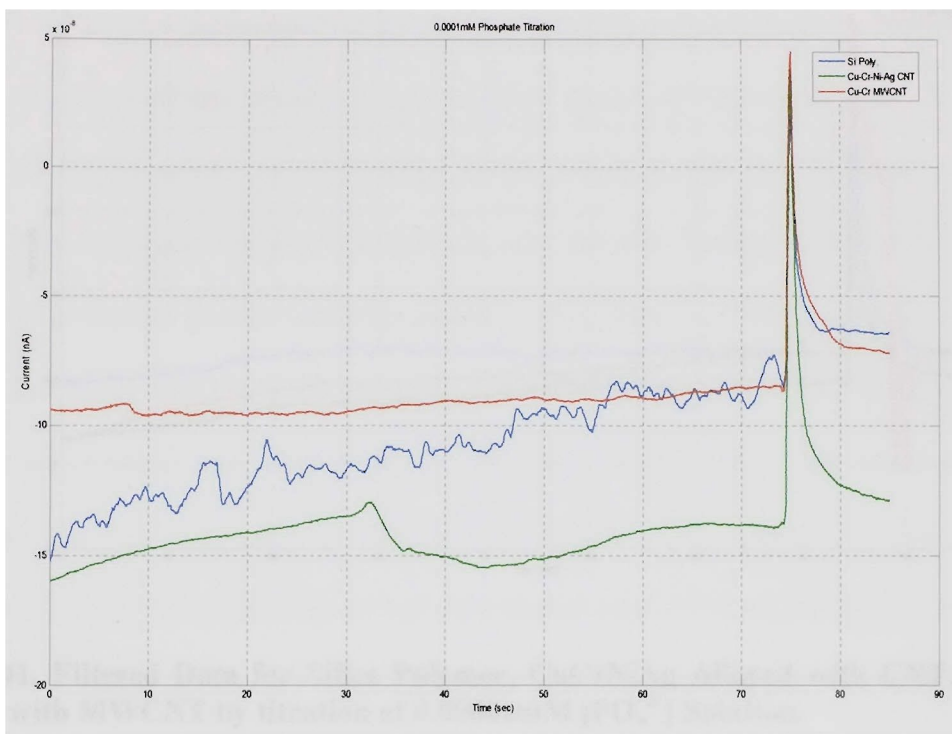


Figure 40. Filtered Data for Silica Polymer, CuCrNiAg Alloyed with CNT, CuCr Alloyed with MWCNT by titration of 0.0001mM $[\text{PO}_4^{3-}]$ Solution.

When data is collected in electrochemical methods, there is a steady state that must be achieved. The electrochemical recordings up to the steady state are not required for any data analysis. There were two steady states and a current magnitude change occurred in the obtained signals. The steady states were achieved before and after the current magnitude change. (J. Wang, Analytical Electrochemistry 2000). In this thesis, the normalization process was as followed: The amperometric instrument was adjusted to

collect data in each 0.05second interval. A complete experiment recording was approximately between 150 seconds to 200 seconds which is equivalent to 2000 data points.

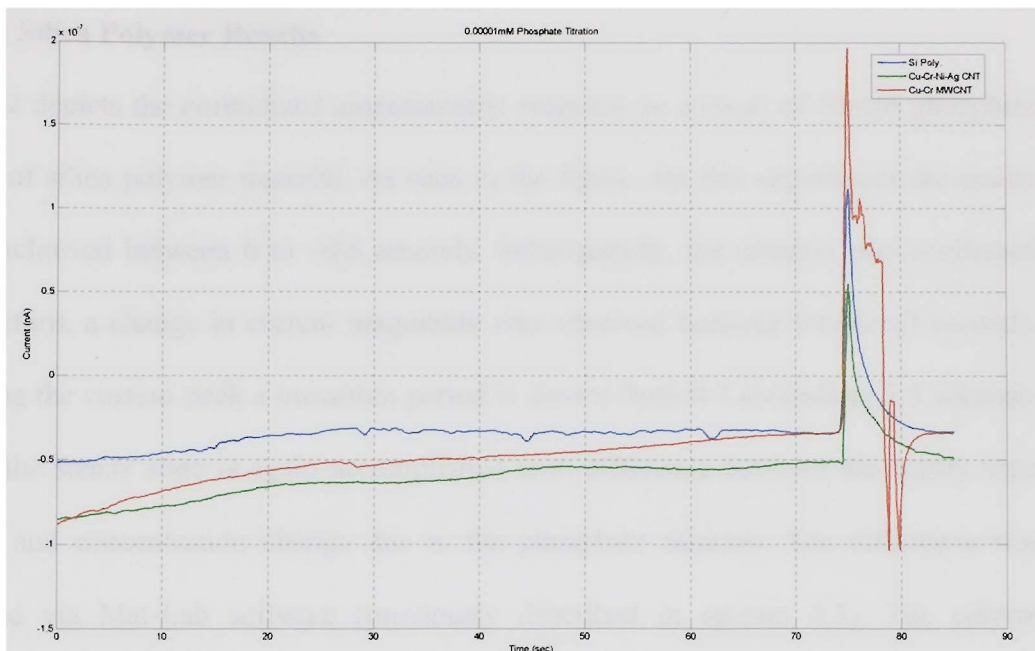


Figure 41. Filtered Data for Silica Polymer, CuCrNiAg Alloyed with CNT, CuCr Alloyed with MWCNT by titration of 0.00001mM $[\text{PO}_4^{3-}]$ Solution.

About 80 seconds to 100 seconds of the experiment time was allowed for the signal to reach a steady state (initialization). No titration was performed during this time period. Once the constant current is attained, titration of phosphate solution was carried out. Due to the titration, change in current magnitude (peak) occurred in signal recording. This current change lasted about 30 seconds to 40 seconds (~200 data points). In the normalization process, the initialization time is discarded and the change in current magnitude (peak) time was amplified for better analysis purposes. Once the data interval

is determined to be processed for analysis, that data is then amplified (exposed) via Mat-Lab (Kim 2002). Figure 42 through Figure 56 represents the normalized data.

4.2.4.1 Normalized signal for 10mM Phosphate Titration Responses

4.2.5.1.1 Silica Polymer Results

Figure 42 depicts the normalized amperometric response as a result of 10mM phosphate titration of silica polymer material. As seen in the figure, for this experiment the steady state is achieved between 0 to ~0.6 seconds. Subsequently, the titration was conducted and in return, a change in current magnitude was observed between 0.6 to 0.7 seconds. Following the current peak a transition period is shown from 0.7 seconds to 1.5 seconds. Finally, the steady state is again accomplished with difference between the steady state baseline and concentration change due to the phosphate titration. The difference was calculated via Mat-Lab software (previously described in section 4.3). The current magnitude change for silica polymer was determined to be 27.33nA which caused by the titration of different phosphate concentration (Christine Mousty 2001), (Fisher 2008), (N. Conrath 1995).

4.2.4.1.2 Cu Cr Ni Ag Alloyed with CNT Results

Figure 43 demonstrates the normalized data for 10mM phosphate titration by employing the enzyme linked CuCrNiAg alloyed with CNT material. The experiment was repeated three times and averaged results are as follows: As seen in the Figure 43 steady state was achieved between 0 to ~0.575 seconds. Afterward, the titration was conducted which caused a change in current magnitude between ~0.58 to 0.68 seconds. The transition

period followed the current peak shown at around 0.7 second to 1.0 second. The current came to the steady state at 1.0 second and stayed on for the rest of the data collection.

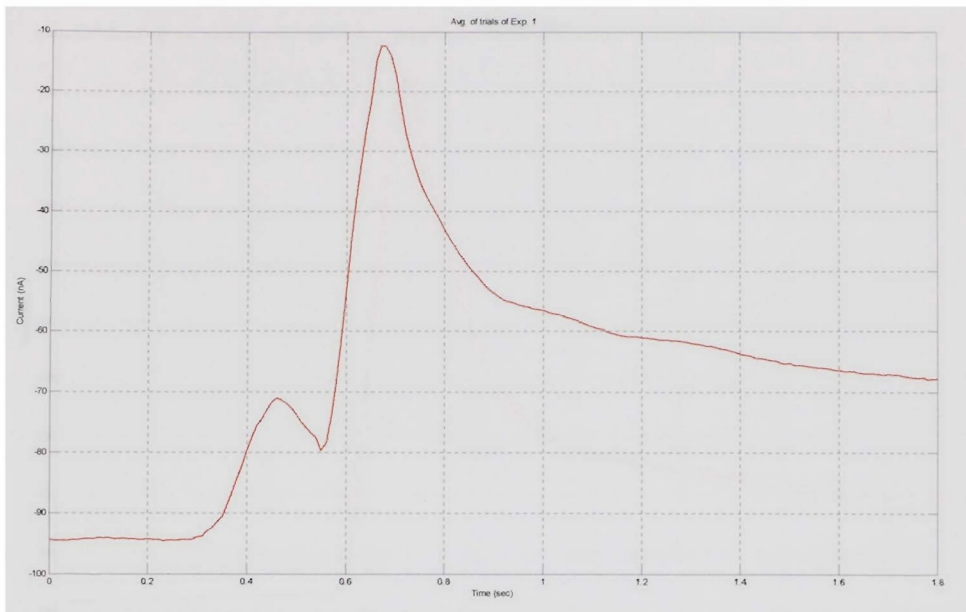


Figure 42. Normalized Data for Silica Polymer by titration of 10mM $[\text{PO}_4^{3-}]$ Solution

The difference between the steady state baseline and concentration change was attributed to the phosphate titration (Christine Mousty 2001), (Fisher 2008), (N. Conrath 1995). The difference was calculated via Mat-Lab software. The current magnitude change was determined to be 34.44nA.

4.2.4.1.3 CuCr Alloyed with MWCNT Results

This was the last experiment one of the three materials for 10mM phosphate detection. The normalized data is exhibited in Figure 44 for the titration of the enzyme-linked Cu Cr alloyed with MWCNT. Under the same conditions experiments were repeated three times

and averaged. In the Figure 44 the steady state was accomplished between 0 to ~0.3 seconds. Later, the phosphate was titrated and a change in current magnitude was

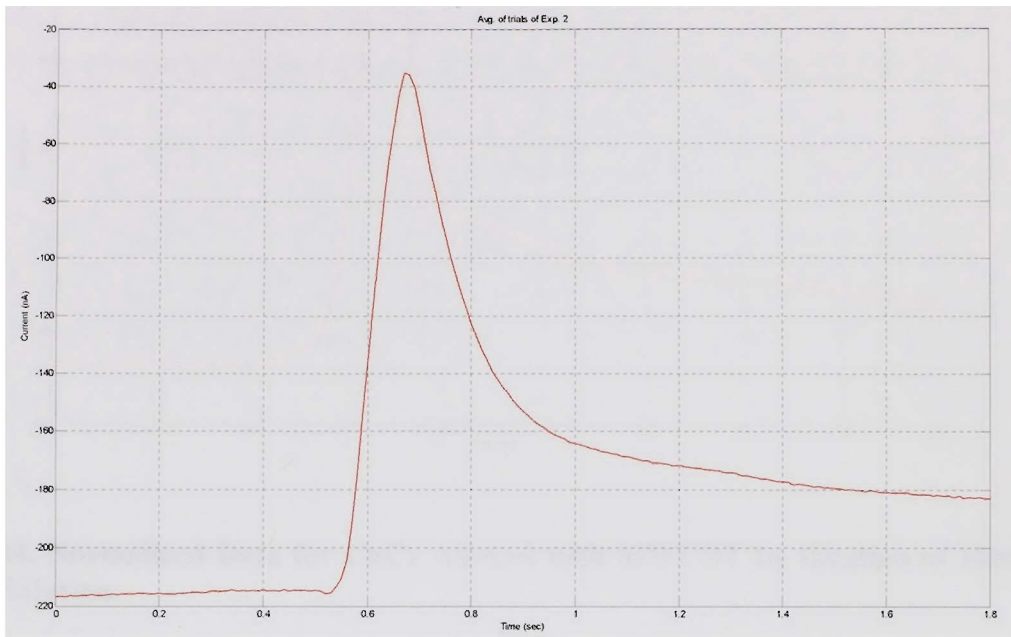


Figure 43. Normalized Data for Cu Cr Ni Ag Alloyed with CNT by titration of 10mM $[\text{PO}_4^{3-}]$ Solution.

observed between ~0.59 to 0.7 seconds. The transition period followed the current peak shown at around 0.7 second to 1.4 seconds. The response signal came to steady state at 1.5 seconds and stayed on for the rest of the data collection. The difference between the steady state baseline and concentration change was attributed to the phosphate titration (Christine Mousty 2001), (Fisher 2008), (N. Conrath 1995). The difference was again calculated via Mat-Lab software. The average current magnitude change was determined to be 38.54nA.

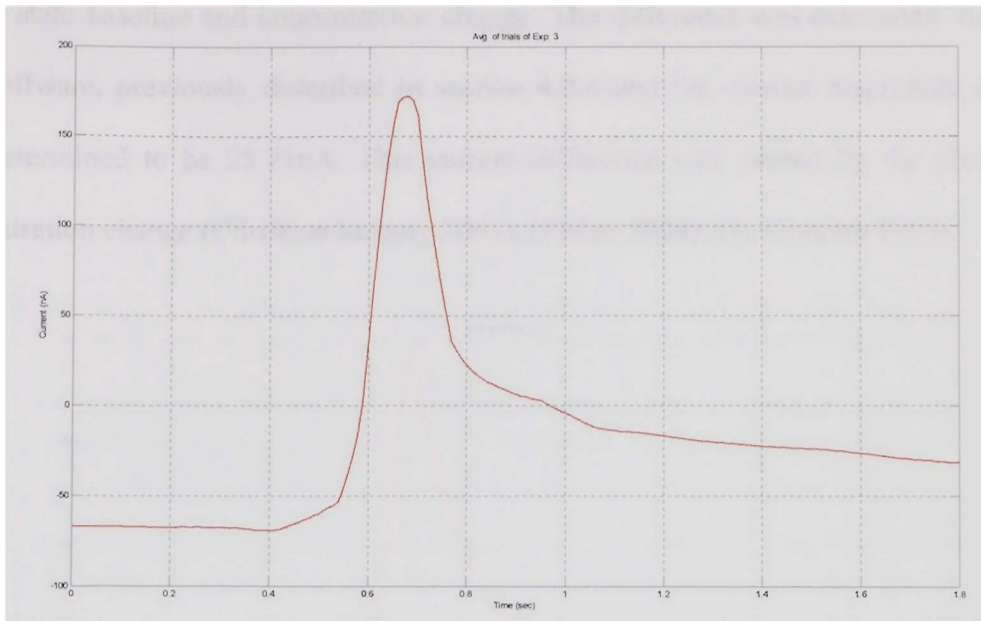


Figure 44. Normalized Data for CuCr Alloyed with MWCNT by titration of 10mM $[\text{PO}_4^{3-}]$ Solution.

4.2.4.2 Normalized signal for 1mM Phosphate Titration Responses

4.2.5.2.1 Silica Polymer Results

In this section 1mM phosphate concentration was titrated in 1ml of tris-HCl and co-enzymes (FAD, TPP, Mg). As mentioned previously, three materials were tested for comparison purposes. In the same order as the other concentration tests, first experiment was conducted for silica polymer. Figure 45 exhibits the normalized data for silica polymer as a result of 1mM phosphate titration. In the figure, a steady state is achieved between 0 to ~0.57 seconds for this material. Subsequently, the phosphate was titrated and in return, a change in current magnitude is observed between approximately 0.57 to 0.72 seconds. Following the current peak, a transition period is seen from 0.72 seconds to 1.4 seconds. Finally, the steady state is again accomplished with difference between the

steady state baseline and concentration change. The difference was calculated via Mat-Lab software, previously described in section 4.2.4 and the current magnitude change was determined to be 25.71nA. This current difference was caused by the phosphate concentration change (Christine Mousty 2001), (Fisher 2008), (N. Conrath 1995).

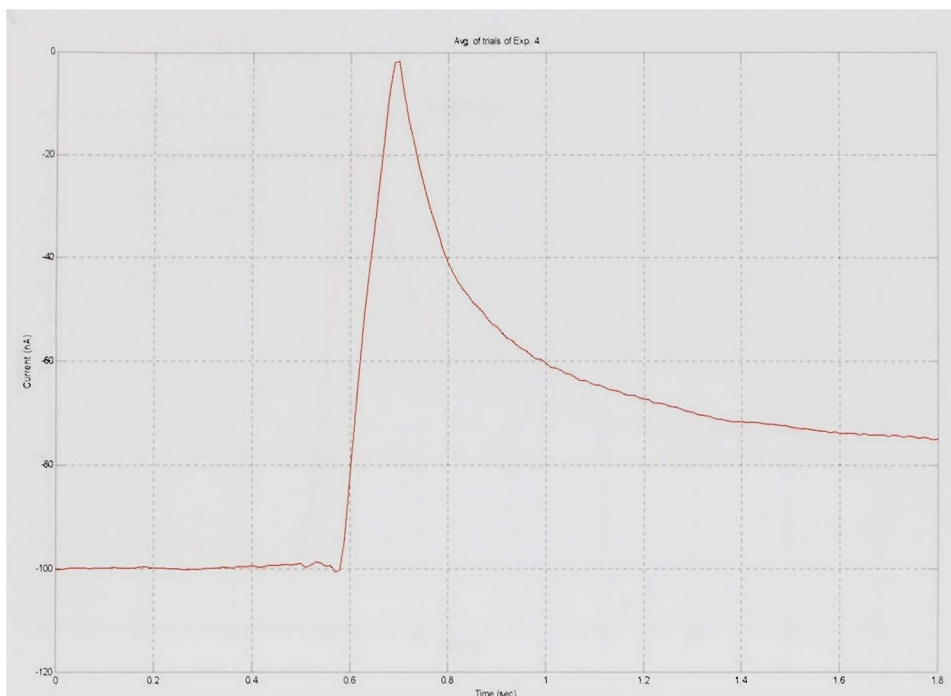


Figure 45. Normalized Data for Silica Polymer by titration of 1mM $[\text{PO}_4^{3-}]$ Solution.

4.2.4.2.2 CuCrNiAg Alloyed with CNT

Figure 46 is normalized data for 1mM phosphate titration by employing the enzyme-linked CuCrNiAg alloyed with CNT. As exhibited in Figure 46, the steady state was achieved between 0 to ~0.38 seconds. Consequently, the titration was performed and a change in current magnitude was experienced between ~0.57 to ~0.72 seconds. The signal then went in to transition period following the current peak shown at around 0.72 second to 1.2 seconds. The current came to the steady state at 1.2 seconds and stayed on

for the rest of the data collection. Previously literatures report the cause of the difference between the steady state baseline and concentration change was because of the phosphate titration (Christine Mousty 2001), (Fisher 2008), (N. Conrath 1995). The difference was calculated via Mat-Lab software. The current magnitude change was determined to be 26.35nA.

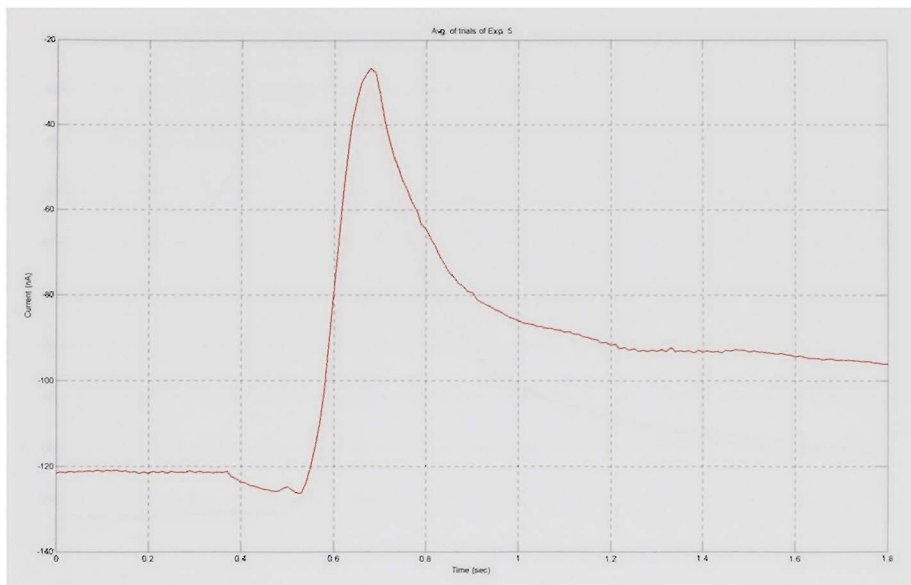


Figure 46. Normalized Data for CuCrNiAg Alloyed with CNT by titration of 1mM $[\text{PO}_4^{3-}]$ Solution.

4.2.4.2.3 CuCr Alloyed with MWCNT

The normalized data for CuCr Alloyed with MWCNT titrated by 1mM phosphate solution is demonstrated in Figure 47. The same conditions were applied for experiments of all three replications and the average results are obtained. In the figure, the steady state was accomplished between 0 to ~0.58 seconds. Later, the phosphate titration was completed and an observation of change in current magnitude was made between ~0.58 to 0.7 seconds. The transition period followed the current peak shown at around 0.7

seconds to 1.6 seconds. The final steady state was attained at 1.6 seconds and remained constant for the rest of the data collection. Mousty et al. described this as the concentration change due to the phosphate titration which caused an increment on the steady state baseline. (Christine Mousty 2001) (Fisher 2008) (N. Conrath 1995). Mat-Lab software was utilized to calculate the current difference and determined to be 26.94nA.

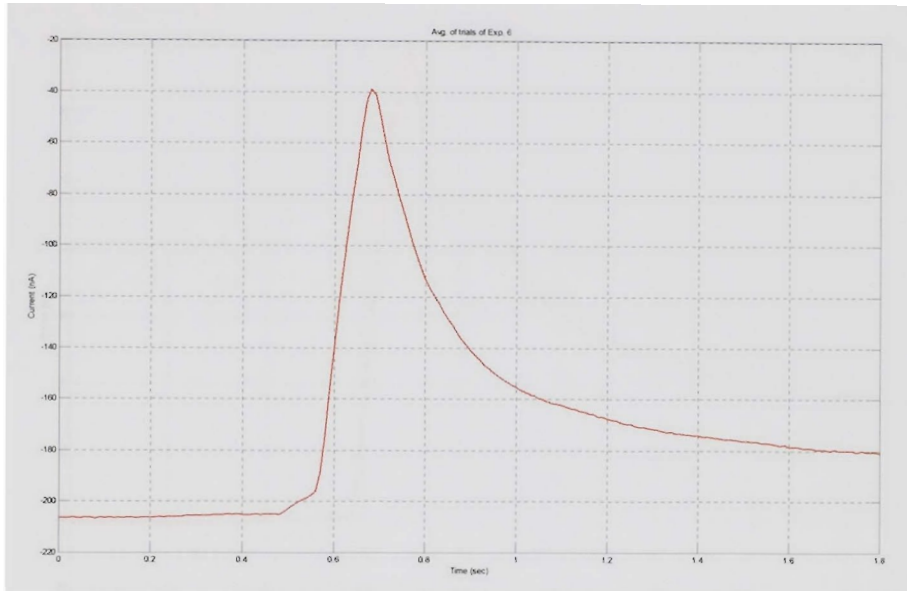


Figure 47. Normalized Data for CuCr Alloyed with MWCNT by titration of 1mM $[\text{PO}_4^{3-}]$ Solution.

4.2.4.3 Normalized signal for 0.01mM Phosphate Titration Responses

4.2.4.3.1 Silica Polymer Results

Figure 48 depicts the normalized data for silica polymer as a result of 0,01mM phosphate titration. As seen in the figure, the steady state is achieved between 0 to ~0.6 seconds. Then, the titration was conducted and in return, a change in current magnitude is observed between 0.6 seconds to 0.9 seconds. Following the current peak a transition period is shown from 0.9 seconds to 1.6 seconds. After the change in current magnitude,

the steady state is accomplished with difference between the steady state baseline and concentration change due to the phosphate titration. The current magnitude change was determined to be 18.11nA. This current difference was obtained through the difference of the phosphate concentration as it is reported (Christine Mousty 2001), (Fisher 2008), (N. Conrath 1995).

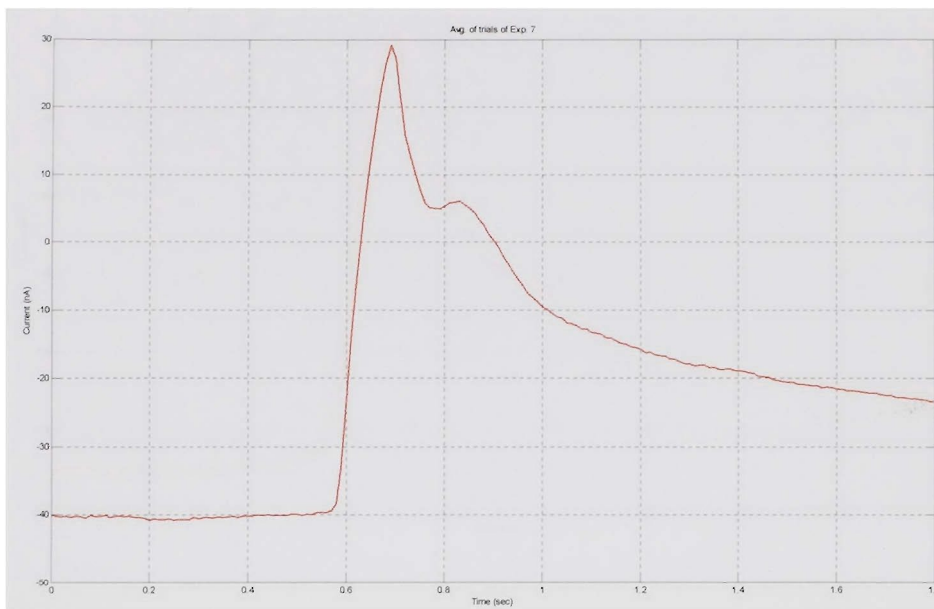


Figure 48. Normalized Data for Silica Polymer by titration of 0.01mM $[PO_4^{3-}]$ Solution.

4.2.4.3.2 CuCrNiAg Alloyed with CNT

Figure 49 exhibits the titration of CuCrNiAg alloyed with CNT by 0.01mM phosphate solution. From this experiment, the steady state was achieved between 0 to ~0.56 seconds. Afterward, the titration change in current magnitude was detected in between ~0.56 to 0.68 seconds. The transition period followed the current peak shown at around 0.68 seconds to 1.5 seconds. At this point, the current came to the steady state at 1.5 seconds and remained constant till the rest of the data collection. The difference between

the steady state baseline and the concentration change is attributed to the phosphate titration as it is stated (Christine Mousty 2001), (Fisher 2008), (N. Conrath 1995). The current change at this point is calculated by using the Mat-Lab software and it is obtained as 20.72nA.

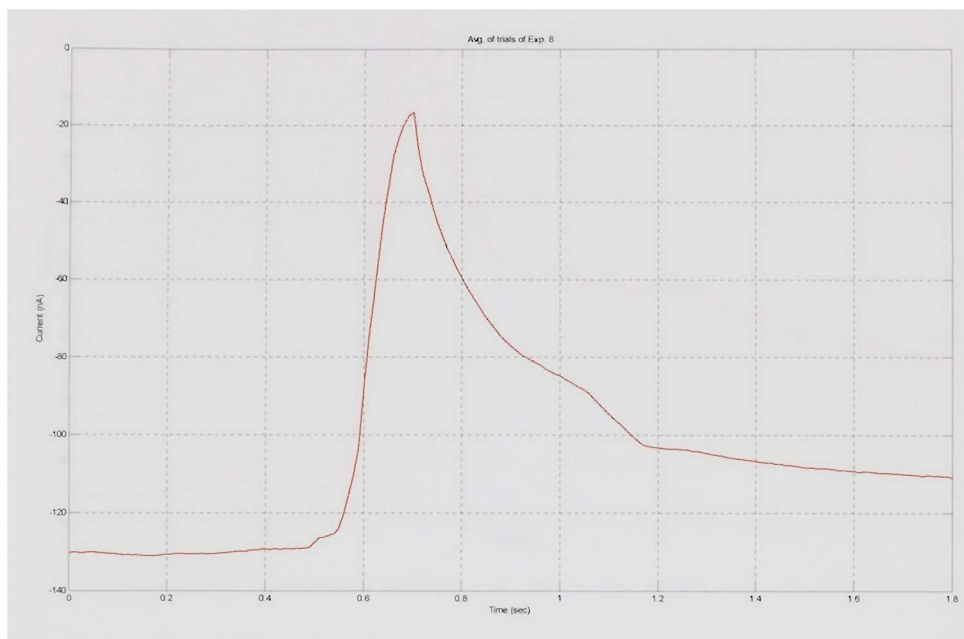


Figure 49. Normalized Data for CuCrNiAg Alloyed with CNT by titration of 0.01mM $[\text{PO}_4^{3-}]$ Solution.

4.2.4.3.3 CuCr Alloyed with MWCNT

In this investigation CuCr alloyed with MWCNT was titrated with 0.01mM phosphate solution and the normalized data is demonstrated in Figure 50. As indicated in the figure , the steady state was accomplished between 0 to ~0.5 seconds. Later, the phosphate was titrated and a change in current magnitude was observed between ~0.5 to 0.8 seconds. The transition period followed the current peak shown at around 0.8 second to 0.9 seconds and the response signal came to steady state at 0.9 seconds. The difference between the steady state baseline and concentration change was attributed to the

phosphate titration as it is revealed (Christine Mousty 2001), (Fisher 2008), (N. Conrath 1995). The data from this result was calculated via Mat-Lab software and determined to be 23.10nA.

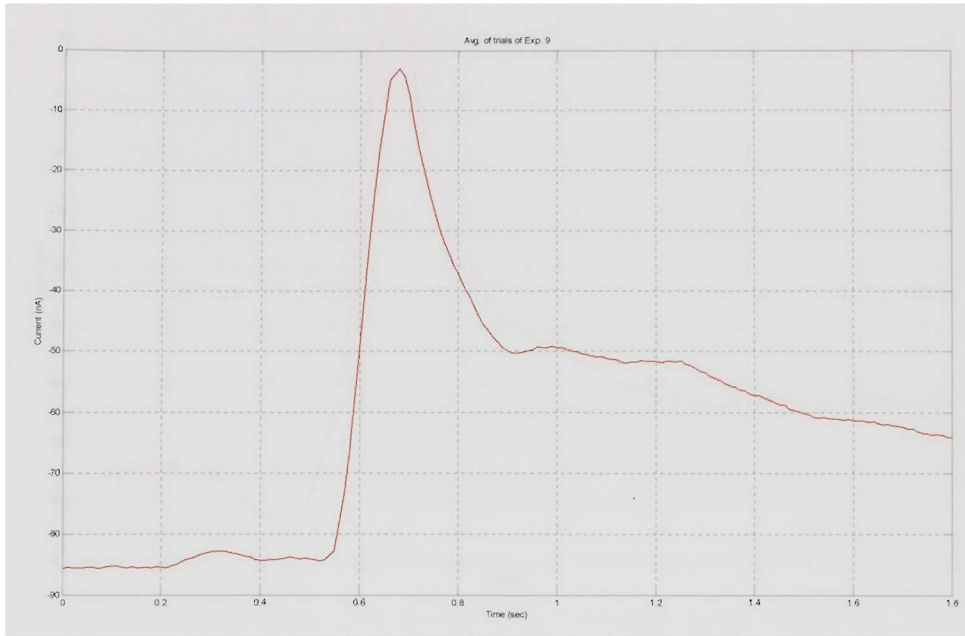


Figure 50. Normalized Data for CuCr Alloyed with MWCNT by titration of 0.01mM $[\text{PO}_4^{3-}]$ Solution.

4.2.4.4 Normalized signal for 0.0001mM Phosphate Titration Responses

4.2.4.4.1 Silica Polymer Results

Figure 51 exhibits the normalized data as a result for silica polymer by the titration of 0.0001mM phosphate. In addition, the figure shows the steady state between 0 to ~0.5 seconds. After, the phosphate was titration, a change in current magnitude is observed between approximately 0.5 to 0.67 seconds. Following the current peak, a transition period is seen from 0.67 seconds to 1.2 seconds. The difference was calculated via Mat-Lab software and it is determined to be 13.07nA. This current difference was caused by

the phosphate concentration change as previously reported (Christine Mousty 2001), (Fisher 2008), (N. Conrath 1995).

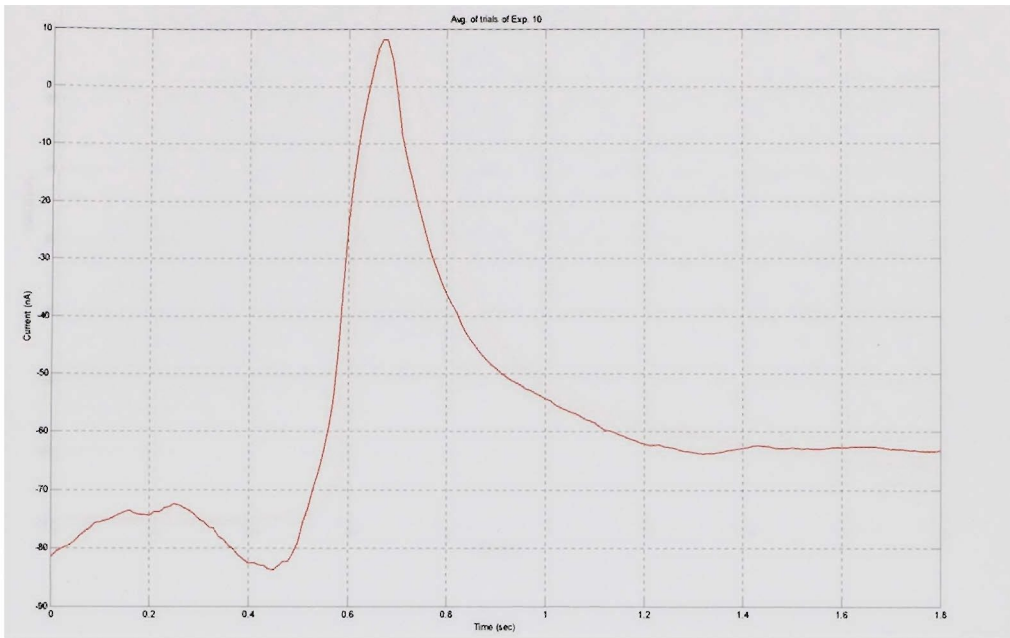


Figure 51. Normalized Data for Silica Polymer by titration of 0.0001mM [PO₄³⁻] Solution.

4.2.4.4.2 CuCrNiAg Alloyed with CNT

Figure 52 depicts the normalized data for 0.0001mM phosphate titration by employing the enzyme-linked CuCrNiAg alloyed with CNT. The steady state was achieved between 0 to ~0.58 seconds as it is shown in the figure. Followed by, the titration was performed at ~0.58 to ~0.7 seconds and the transition period was shown at around 0.7 second to 1.3 seconds. Previously literatures report the cause of the difference between the steady state baseline and concentration change was because of the phosphate titration (Christine Mousty 2001), (Fisher 2008), (N. Conrath 1995). For this material, the difference was 16.75 from the Mat-Lab software calculations.

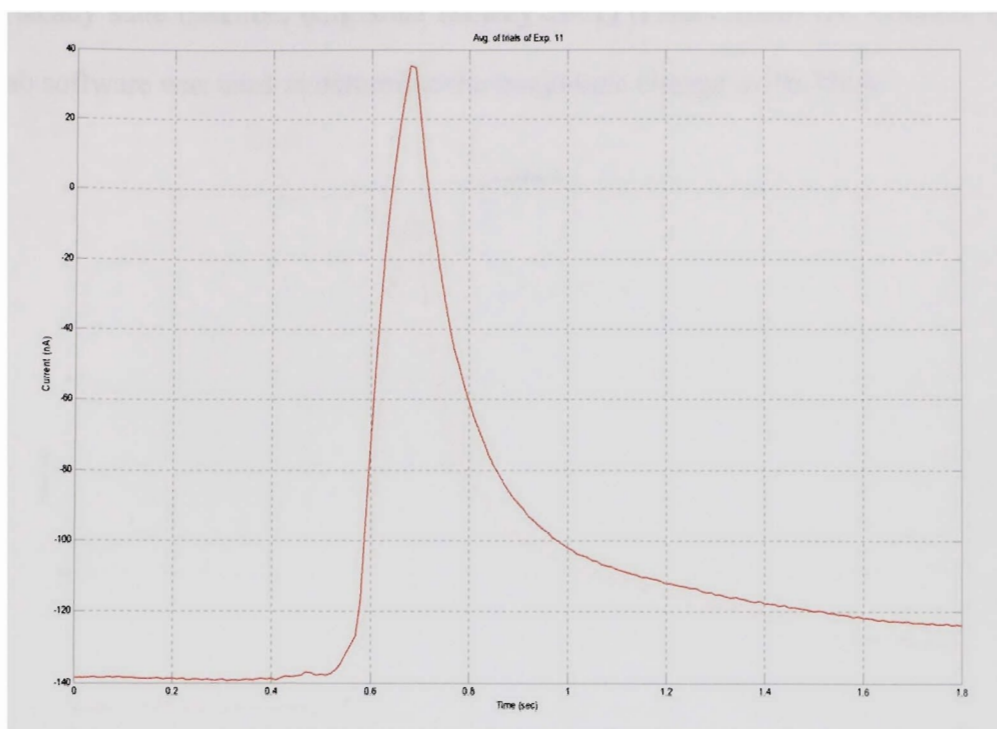


Figure 52. Normalized Data for CuCrNiAg Alloyed with CNT by titration of 0.0001mM $[\text{PO}_4^{3-}]$ Solution.

4.2.4.4.3 CuCr Alloyed with MWCNT

The response of amperometric measurements for 0.0001mM phosphate titration by employing CuCr alloyed with MWCNT are filtered and normalized as demonstrated in Figure 53. As seen in the figure, the steady state was accomplished between 0 to ~0.58 seconds and observation of change in current magnitude was made between ~0.58 to 0.7 seconds. The transition period followed the current peak shown at around 0.7 seconds to 1.5 seconds and again steady state was attained at 1.5 seconds. Mousty et al. described this as the concentration change due to the phosphate titration which caused an increment

on the steady state baseline. (Christine Mousty 2001) (Fisher 2008) (N. Conrath 1995).
Mat-Lab software was used to determine the magnitude change as 16.75nA.

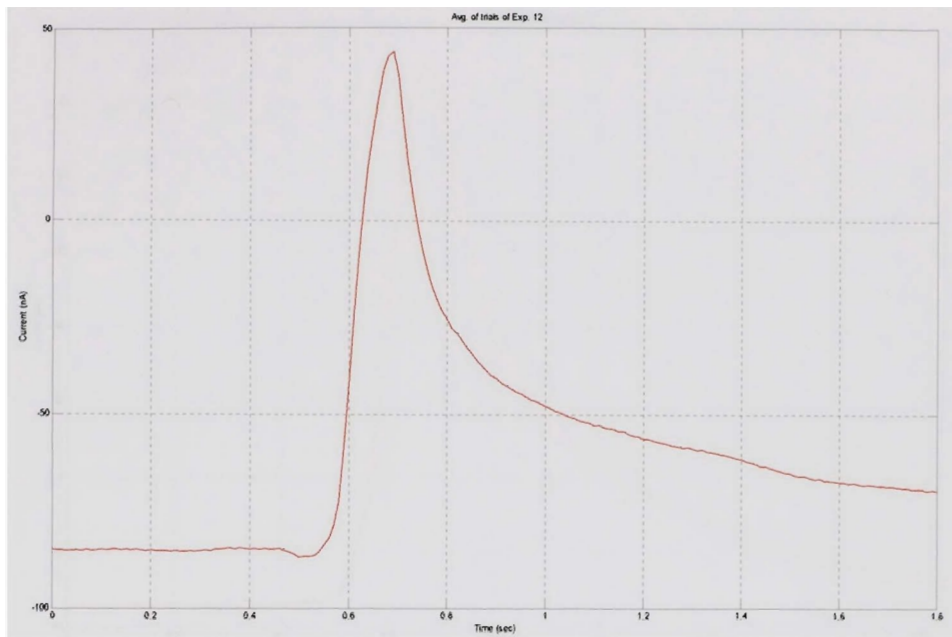


Figure 53. Normalized Data for CuCr Alloyed with MWCNT by titration of 0.0001mM [PO₄³⁻] Solution.

4.2.4.5 Normalized signal for 0.00001mM Phosphate Titration Responses

4.2.4.5.1 Silica Polymer Results

Figure 54 depicts the normalized amperometric responses for 0,00001mM phosphate titration. In the figure, the steady state was achieved between 0 to ~0.5 seconds and the titration was conducted between 0.6 seconds to 0.7 seconds. The transition period is seen from 0.7 seconds to 1.6 seconds and the steady state was again accomplished. The difference between the steady state baseline and concentration change due to the phosphate titration was distinguished. The current magnitude change was determined to

be 6.57nA. This current difference was due to the phosphate concentration change as previously reported (Christine Mousty 2001), (Fisher 2008), (N. Conrath 1995).

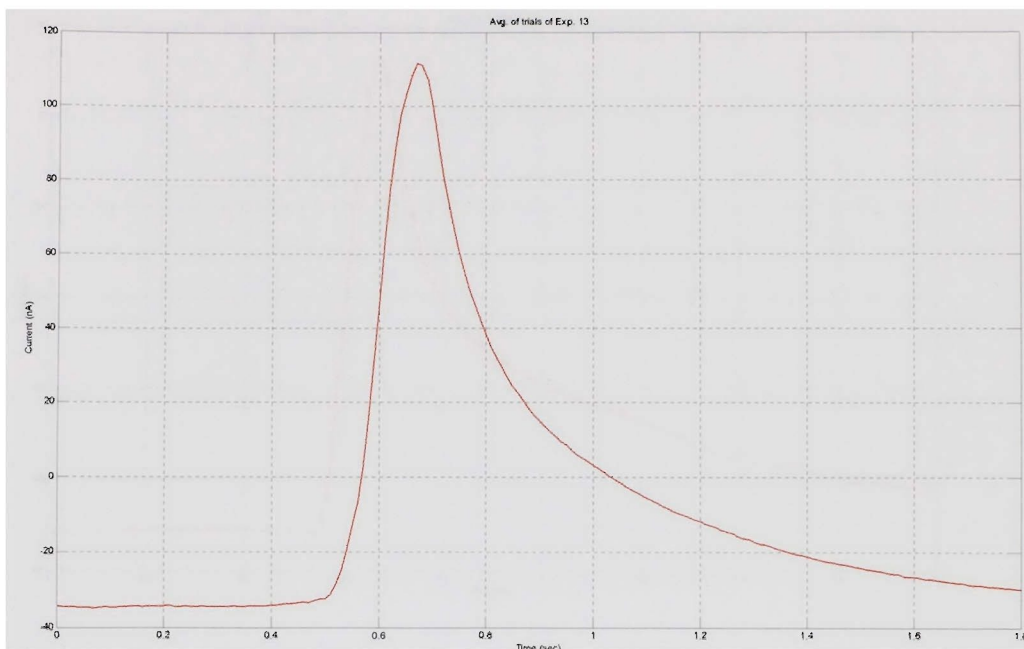


Figure 54. Normalized Data for Silica Polymer by titration of 0.00001mM $[\text{PO}_4^{3-}]$ Solution.

4.2.4.5.2 CuCrNiAg Alloyed with CNT

Figure 55 is the normalized data of amperometric recordings for 0.00001mM phosphate titration via employment of CuCrNiAg Alloyed with CNT. It is shown in figure that the steady state was achieved between 0 to ~0.55 seconds. Afterward, the titration change in current magnitude was detected in between ~0.55 to 0.68 seconds. At around 0.68 seconds to 0.8 seconds, the transition period took place. The current came to the steady state at 0.8 seconds and remained the same till the end of the data collection. The difference between the steady state baseline and concentration change was attributed to

the phosphate titration (Christine Mousty 2001), (Fisher 2008), (N. Conrath 1995). Mat-Lab software calculated the difference as 10.64nA.

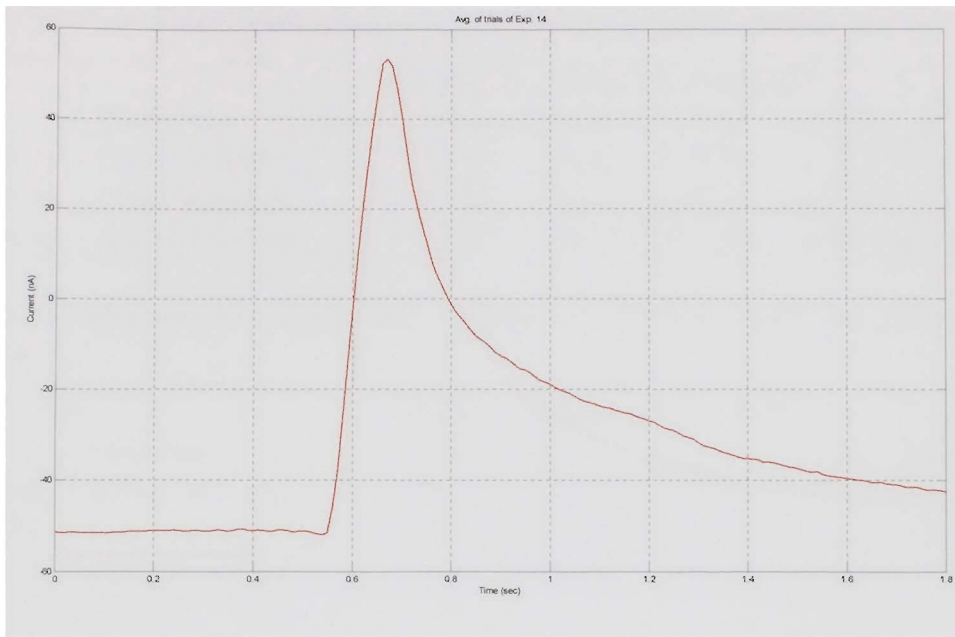


Figure 55. Normalized Data for CuCrNiAg Alloyed with CNT by titration of 0.00001mM $[\text{PO}_4^{3-}]$ Solution.

4.2.4.5.3 CuCr Alloyed with MWCNT

Figure 56 shows the current responses of 0.00001mM phosphate titrations. The figure clearly states that the steady state was accomplished between 0 to ~0.54 seconds. The change in current magnitude was observed between ~0.54 to 0.68 seconds after, the phosphate was titrated. The transition period followed the current peak shown at around 0.68 second to 1.6 seconds and the response signal came to steady state at 1.6 seconds. In the recent studies, the difference between the steady state baseline and concentration change was attributed to the phosphate titration (Christine Mousty 2001), (Fisher 2008),

(N. Conrath 1995). This current magnitude difference was calculated via Mat-Lab software and determined to be 12.13nA.

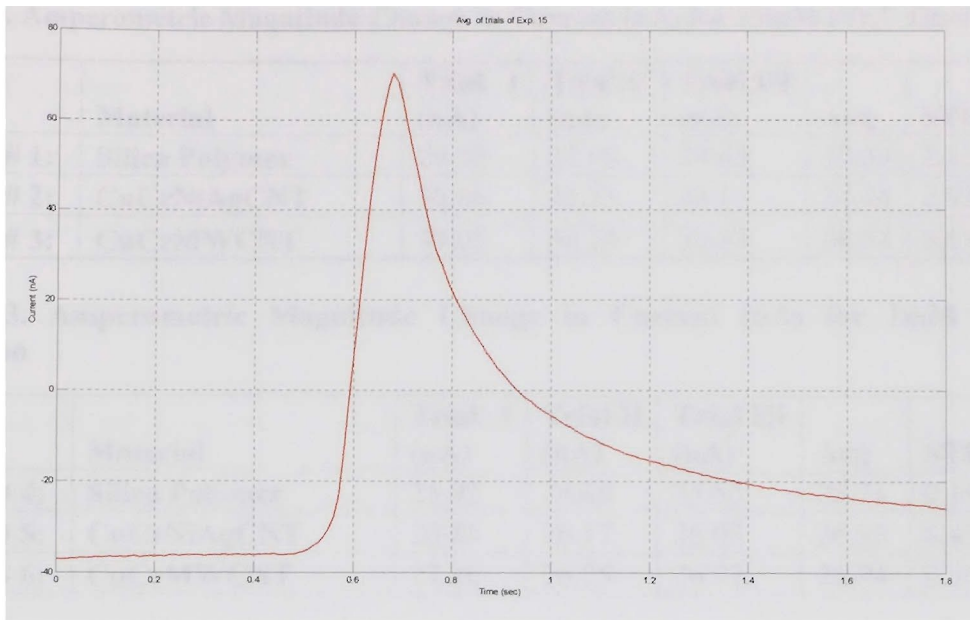


Figure 56. Normalized Data for CuCr Alloyed with MWCNT by titration of 0.0001mM [PO₄³⁻] Solution.

4.2.5 Current magnitude change obtained from amperometry

Table 2 summarizes the current magnitude changes due to the phosphate concentrations for all three materials (Silica Polymer- CuCrNiAg alloyed with CNT and CuCr Alloyed with MWCNT). 10mM phosphate concentration was tested with those materials and each material was tried three times for comparison reasons. In addition all these three trials were averaged and standard deviation was calculated.

Table 3 below also summarizes the current magnitude changes due to the phosphate concentrations for the same three materials (Silica Polymer- CuCrNiAg alloyed with CNT and CuCr Alloyed with MWCNT). However in this section 1mM phosphate concentration was detected by utilizing those materials. Same as above each material was tried three times

for comparison reasons. Moreover, all these three trials were averaged and standard deviation was calculated.

Table 2. Amperometric Magnitude Change in Current (nA) for 10mM PO₄³⁻ Titration

	Material	Trial I (nA)	Trial II (nA)	Trial III (nA)	Avg	STDV
Exp# 1:	Silica Polymer	29.39	27.96	24.65	27.33	2.43
Exp# 2:	CuCrNiAgCNT	36.66	35.55	31.11	34.44	2.93
Exp# 3:	CuCrMWCNT	39.05	38.74	37.83	38.54	0.63

Table 3. Amperometric Magnitude Change in Current (nA) for 1mM PO₄³⁻ Titration

	Material	Trial I (nA)	Trial II (nA)	Trial III (nA)	Avg	STDV
Exp# 4:	Silica Polymer	25.92	25.66	25.55	25.71	0.19
Exp# 5:	CuCrNiAgCNT	26.85	26.17	26.03	26.35	0.43
Exp# 6:	CuCrMWCNT	27.36	26.75	26.72	26.94	0.36

Table 4. Amperometric Magnitude Change in Current (nA) for 0.01mM PO₄³⁻ Titration

	Material	Trial I (nA)	Trial II (nA)	Trial III (nA)	Avg	STDV
Exp# 7:	Silica Polymer	15.8	14.55	8.87	13.07	3.69
Exp# 8:	CuCrNiAgCNT	16.23	16.1	16.05	16.13	0.09
Exp# 9:	CuCrMWCNT	17	16.68	16.58	16.75	0.21

Table 5. Amperometric Magnitude Change in Current (nA) for 0.0001mM PO₄³⁻ Titration

	Material	Trial I (nA)	Trial II (nA)	Trial III (nA)	Avg	STDV
Exp# 7:	Silica Polymer	18.94	17.91	17.48	18.11	0.75
Exp# 8:	CuCrNiAgCNT	21.93	21.06	19.18	20.72	1.40
Exp# 9:	CuCrMWCNT	23.85	23.02	22.42	23.1	0.71

Since five different phosphate concentrations were investigated, the

Table 4 was used for the summary of the current magnitude changes for the same three materials (Silica Polymer- CuCrNiAg alloyed with CNT and CuCr Alloyed with MWCNT). 0.01mM concentration was the detection subject in this part of the experiment. The three trails for each material were kept consistent for comparison reasons. Again, all these three trials were averaged and standard deviation was calculated as shown in the last column of

Table 4.

Table 5 is the summary of the investigation for 0.0001mM phosphate concentrations. The current magnitude changes for the same three materials (Silica Polymer- CuCrNiAg alloyed with CNT and CuCr Alloyed with MWCNT) are listed. The experiments were tested in three trails for each material. Lastly, average of all these three trials and standard deviation was calculated as seen in the last column of Table 5.

Table 6 below is the last concentration summary of phosphate concentrations. The current magnitude changes for the same three 00001mM materials (Silica Polymer- CuCrNiAg alloyed with CNT and CuCr Alloyed with MWCNT) were listed in the table. In this section the concentration of phosphate was 0.00001mM. Each material was again tried three times for comparison reasons and the averages of those materials as well as the standard deviations were calculated. In Table 7, those averages current magnitude changes from Table 2 through Table 6 were summarized. The table was designed to indicate the average differences of all three materials.

In Table 8 through Table 10, parameters for different materials' average current magnitude changes versus the concentration were summarized. Based on this table the calibration curves below were obtained.

Table 6. Amperometric Magnitude Change in Current (nA) for 0.00001mM PO₄³⁻ Titration

	Material	Trial I (nA)	Trial II (nA)	Trial III (nA)	Avg	STDV
Exp# 7:	Silica Polymer	N/D	N/D	N/D	N/A	N/A
Exp# 8:	CuCrNiAgCNT	11.08	11.02	9.81	10.64	0.71
Exp# 9:	CuCrMWCNT	12.57	12.4	11.41	12.13	0.62

Table 7. Summary of Current Change versus Concentration

MATERIAL	[PO ₄ ³⁻] CONCENTRATION				
	10mM	1mM	0.01mM	0.0001mM	0.00001mM
Silica Polymer	28.23	25.84	16.14	15.62	N/D
CuCrNiAgCNT	34.83	26.10	22.28	15.92	11.07
CuCrMWCNT	38.15	26.53	22.78	18.11	11.68

The conductivity of the materials is listed below for comparison purposes:

Silica Polymer: Not conductive

CuCrNiAgCNT: 5.96E+07

CuCrMWCNT: 8.61E+07

Gold : 45.2E+6

4.2.6 Calibration Curves

Table 8. Current Magnitude Changes (nA) for Silica Polymer in Various Concentrations

CONCENTRATION	Silica Polymer
10mM	28.23
1mM	25.84
0.01mM	16.14
0.0001mM	15.62
0.00001mM	N/D

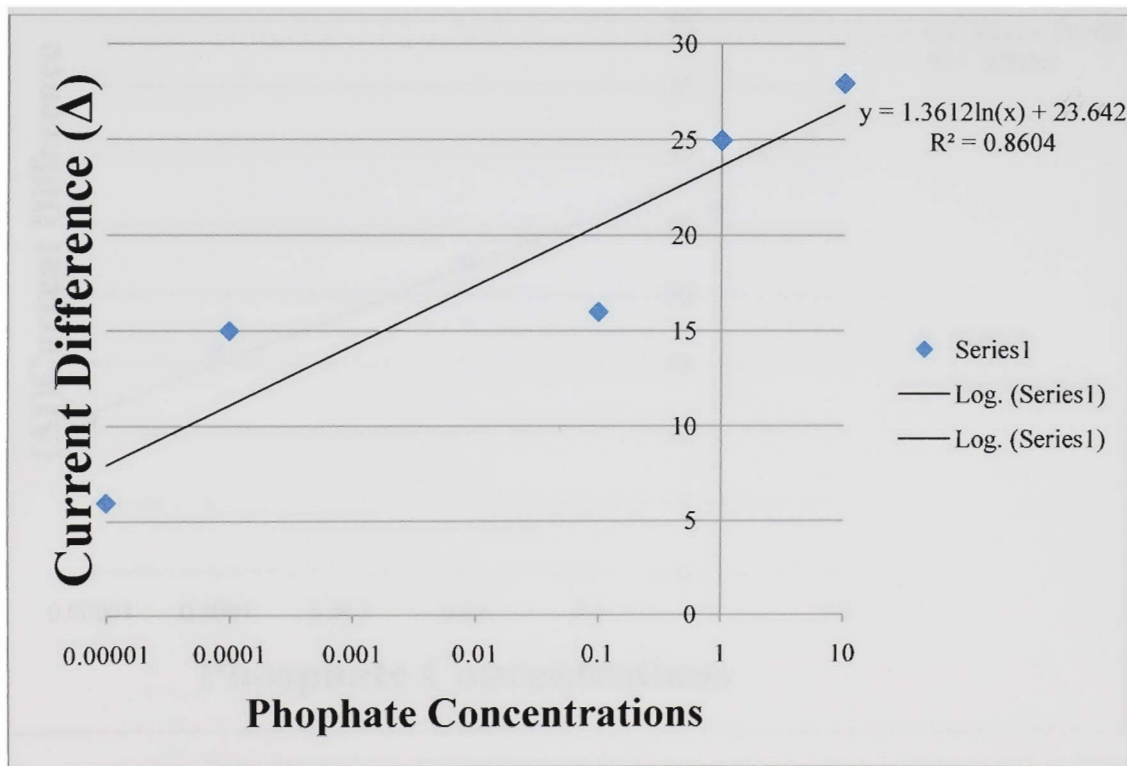


Figure 57. Phosphate Calibration Curve for Silica Polymer

Table 9. Current Magnitude Changes (nA) for CuCrAgNi Alloyed CNT in Various Concentrations

CONCENTRATION (mM)	Cu,Cr, Ag,Ni, CNT (nA)
10	34.83
1	26.10
0.01	22.28
0.0001	15.92
0.00001	11.07

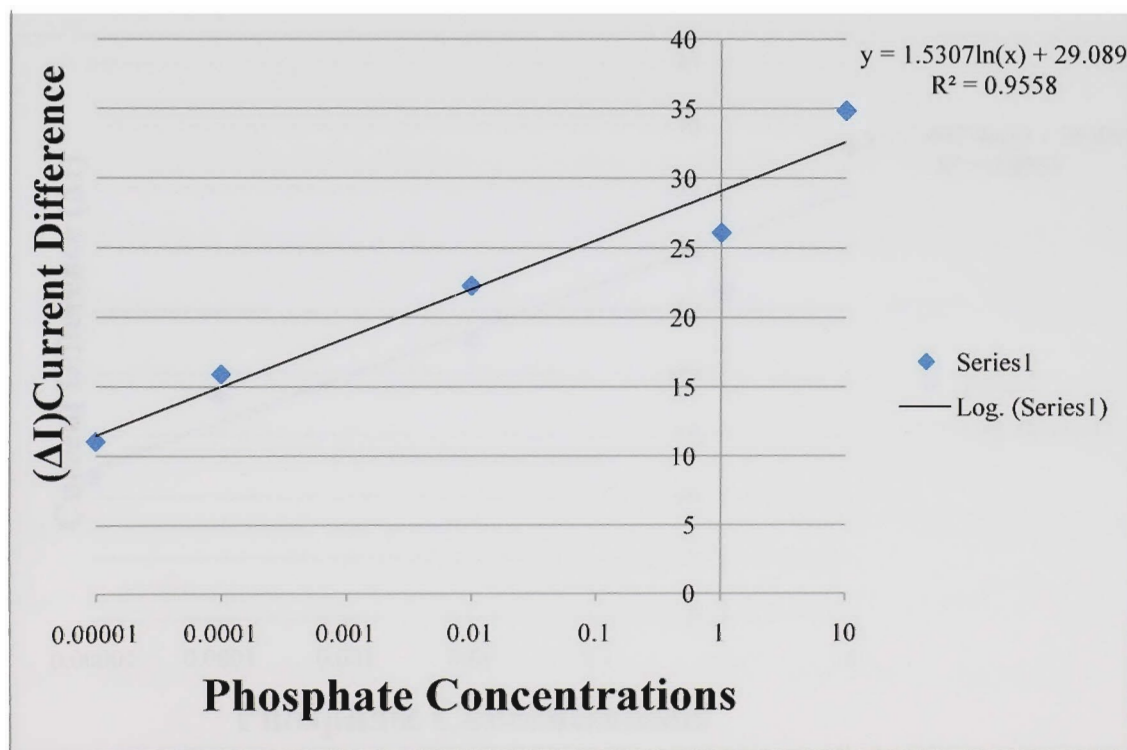


Figure 58. Phosphate Calibration Curve for CuCrAgNi Alloyed with CNT

Table 10. Current Magnitude Changes (nA) for CuCr Alloyed MWCNT in Various Concentrations

CONCENTRATION (mM)	Cu,Cr, MWCNT (nA)
10	38.15
1	26.53
0.01	22.78
0.0001	18.11
0.00001	11.68

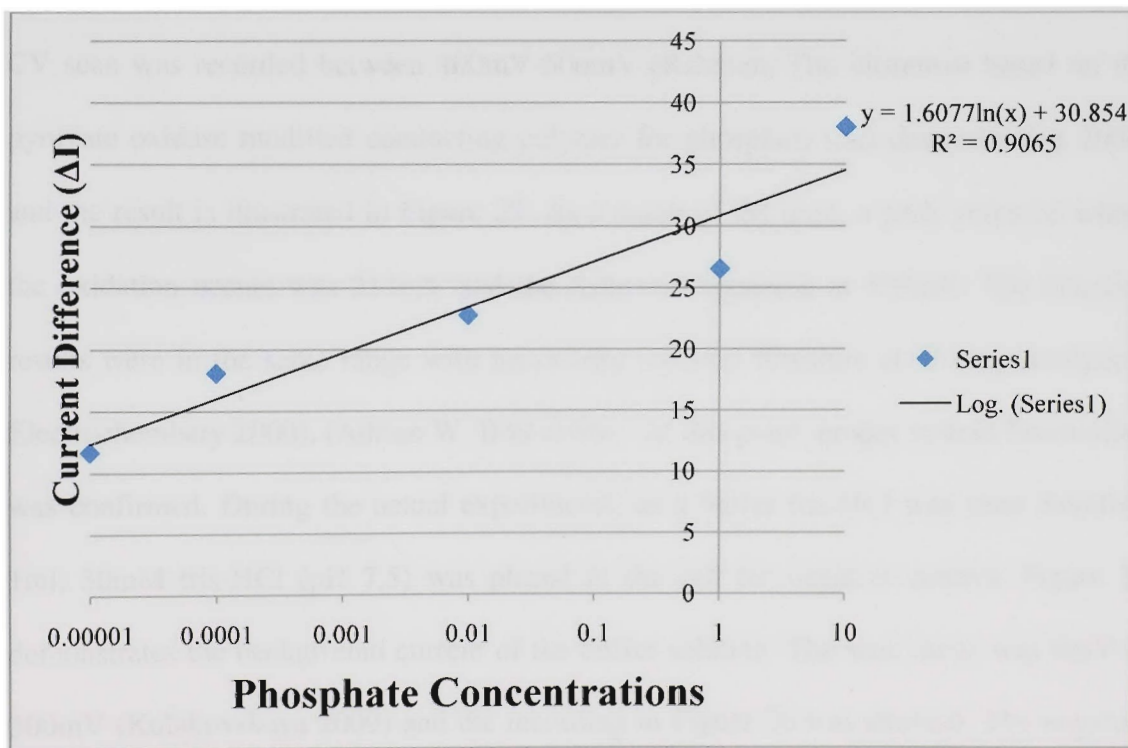


Figure 59. Phosphate Calibration Curve for CuCr Alloyed with MWCNT

4.3 Discussions

In this research, three different enzyme-linked materials were employed and the detection range of titrated phosphate concentration was assessed between 10mM to 0.00001mM (10nM). In order to take advantage of high conductivity properties, both CuCrNiAg-CNT and CuCr-MWCNT are composed of multi wall carbon nano tubes. Prior to the conduction of any experiments, a system check was performed. Cyclic voltammetry (CV) is widely utilized tool for electrochemical tests (Adrian W. Bott 1996). Before the electrolyte test, the functionality of the instrument components such as electrodes, cyclic voltammetry, amperometry and the connections must be tested. Ferricyanide scan is one of the most common electrolytes to test the system functionality (E. D. Moorhead 1980).

4.3.1 CV System and Background Test (Negative Control)

CV scan was recorded between 100mV-500mV (Rahman, The biosensor based on the pyruvate oxidase modified conducting polymer for phosphate ions determination 2006) and the result is illustrated in Figure 25. As a result of the scan, a peak potential where the oxidation occurs was 213mV and the reduction appeared at 338mV. The obtained results were in the same range with previously reported literature (J. Wang, Analytical Electrochemistry 2000), (Adrian W. Bott 1996). At this point, proper system functioning was confirmed. During the actual experiments, as a buffer tris-HCl was used therefore 1ml, 50mM tris-HCl (pH 7.5) was placed in the cell for negative control. Figure 26 demonstrates the background current of the buffer solution. The scan range was 0mV to 500mV (Kulakovskaya 2009) and the recording in Figure 26 was attained. The negative control was observed similar to the Kulakovskaya et al. (Kulakovskaya 2009).

Purpose of this background test was to ensure that the test cell did not contain any chemical substance other than tris-HCl solution (to rule any impurities). If any chemical compound were present in tris-HCl, there would be a redox reaction with voltage peak as indicated in Figure 25 (Sebastian Buchingera 2010).

4.3.2 Amperometric System and Background (Negative Control) Test

The system was tested for proper functionality by amperometric methods once again. A background test (negative control) was recorded for 1ml, 50mM tris buffer and the result is illustrated in Figure 27. During the experiment, the ions in tris buffer solution get charged with constantly applied potential of 450mV. Steady state is achieved approximately at 60th second. There were no observations of change in the current magnitude noted after the constant current state was reached. This was an indication of only tris-HCl being present in the cell which was consistent with results reported by Buchingera et al (Sebastian Buchingera 2010). The modus operandi for H₂O₂ recording was as follows:

As demonstrated in Figure 30, approximately at 150th second, the charged ions of 1ml, 50mM tris-HCl pH 7.5 were at steady state. At that moment, a single titration was performed and as a result, 500nA of alteration in current magnitude was recorded. The current stayed constant for about 80 seconds and began to decline which was attributed to dissipation of hydrogen and oxygen atoms Equation 5 as they electrooxidised.

It is concluded that the single titration technique has more advantages over multiple titration methods. According to the Equation 6 and Figure 29, H₂O₂ is produced in just one time.

Applied potential for the H₂O₂ solution was set at 450mV (Rahman, The biosensor based on the pyruvate oxidase modified conducting polymer for phosphate ions determination 2006). Figure 28 exhibits a change in magnitude of the current which is a clear indication of concentration change in the solution. Also, observed in the same figure that the difference in current magnitude decreases with each titration. This decline was attributed to the H₂O₂ saturation in 1ml, 50mM tris-HCl pH7.5.

4.3.3 Amperometric Results for Phosphate Detection

Results for phosphate detection are illustrated in Figure 31 through Figure 56. As described in detail in section 4.1, the results are divided in to three sections (raw, filtered and normalized data). The results were organized in the order of higher concentration starting with 10mM [PO₄³⁻] to lower concentration with 0.00001mM (10nM) [PO₄³⁻]. In this part, only normalized data will be discussed since the raw data and the filtered data are a process to obtain the normalized data (Wu 2009). In the normalized results section, only steady state and the current magnitude change were shown (refer to section 4.2.5). Recordings indicate a current change shortly after the steady state. This current change is an indication of H₂O₂ production occurring in the cell as seen in Figure 31 thru Figure 35 (Yuehe Lin 2004), (Christine Mousty 2001), (Akyilmaz, Construction of an Amperometric Pyruvate Oxidase Enzyme Electrode for Determination of Pyruvate and Phosphate 2007), (Gavalas 2001), (Gavalas 2001), (Kwan 2005), (Rahman, The biosensor based on the pyruvate oxidase modified conducting polymer for phosphate ions determination 2006), (Villalba, Bioelectroanalytical determination of phosphate 2009). In

the results section, Equation 6 outlines the H_2O_2 production due to the phosphate addition. The concentration of phosphate was determined based on the increments of current magnitudes and listed in the Table 2 through Table 6. (Kwan 2005), (Akyilmaz, Construction of an Amperometric Pyruvate Oxidase Enzyme Electrode for Determination of Pyruvate and Phosphate 2007), (Christine Mousty 2001), (Rahman, The biosensor based on the pyruvate oxidase modified conducting polymer for phosphate ions determination 2006). The results summary is also listed in Table 7. Calibration curves were determined based on these tables. The curves give a linear line between 0.00001mM and 0.01mM which is consistent with previously reported by Rahman et al (Rahman, The biosensor based on the pyruvate oxidase modified conducting polymer for phosphate ions determination 2006) (Fumio Mizutani 2000). It also showed saturation after the 0.01mM phosphate concentration. These findings were confirmed with the literature (Masayasu Suzuki 1998), (Fumio Mizutani 2000), (Christine Mousty 2001).

Response time of the biosensor for phosphate detection was determined from the time phosphate solution titrated in to the cell and the response signal reached to the steady state (Christine Mousty 2001). Experiments that utilized silica polymer showed overall one second of response time, CuCrNiAg with CNT 0.7seconds and CuCr with MWCNT 0.6seconds. A recent study published by Zhang et al. states that the response time of the sensor was 2-3 seconds (Ming Zhang 2009).

In addition, the detection of the phosphate concentration at 10mM – 100 μ M was relatively unchallenging to measure. On the other hand, obtaining results at the lower concentrations such as nano level (10^{-9}) was quite complex. The same difficulty for the low concentration detection of PO_4^{3-} such as 10nM was reported in literature (Villalba,

Bioelectroanalytical determination of phosphate 2009), (Mozaz 2006). This problem was surmounted by repeating the experiments for the lower phosphate concentrations by using the phosphate sensor which is developed for this thesis. Moreover, it must be stated that the conducting nano materials indicated less complexity in lower phosphate concentrations. A previous conference proceeding done by Akar et al reported the detection limits of the existing amperometric biosensors (Akar, Development of a biosensor for detection of phosphate species in uranium contaminated groundwater and wastewater sediments 2010). The Table 11 below summarizes the latest phosphate sensors detection methods and their limits.

Furthermore, selectivity of the biosensor is as important as the response time and the lower detection limit. In this research, pyruvate oxidase enzyme which specifically uses phosphate was employed to catalyze the reaction indicated in Equation 6. The reaction occurs only in the presence of phosphate and pyruvate which was consistent with literature (Akyilmaz, Construction of an Amperometric Pyruvate Oxidase Enzyme Electrode for Determination of Pyruvate and Phosphate 2007), (Engblom, The phosphate sensor 1998), (Fumio Mizutani 2000), (Gavalas 2001).

From the results it is concluded that the conductivity plays an important role in electron transfer (Munroe 2008). Similarly, the nano-structured highly conductive materials have higher current magnitude change than the non-conductive silica polymer. Correspondingly, CuCr alloyed MWCNT when compared to the CuCrAgNi alloyed CNT shows higher magnitude in current. Also Munroe et al. reported a comparison study that the CuCr alloyed MWCNT has superlative contribution in terms of the sensitivity. These results obtained in this research are compatible with the previously reported (Munroe

2008) as a conductivity theory. It is stated that as the conductivity increases, the sensitivity increases proportionally (Rahman, The biosensor based on the pyruvate oxidase modified conducting polymer for phosphate ions determination 2006). Based on the performed experiment for this thesis and the analyzed data as described in detail in the 2.3.6, the CuCrMWCNT has the highest conductivity. In order to enhance the biosensor, the further study is suggested.

Table 11. Phosphate Concentration Detection Limits with Different Methods (Akar, Development of a biosensor for detection of phosphate species in uranium contaminated groundwater and wastewater sediments 2010)

Method	Detection Limit (μM)
FIA-P	100
ISE Molybdate complex	0.06
Amperometric Molybdate complex	0.30
Amperometric POD/O ₂	1.00
Amperometric POD/H ₂ O ₂	3.60
Amperometric NP, XOD, AP	0.01
Amperometric MP, MR, GOX, AP	0.01
Ion chromatography	0.10
Capillary electrophoresis	0.10
Luminescent plate Europium–tetracycline	3.00
Fluorescent probe NP, XOD, HRP	0.05
Fluorescent PVC matrix Al-morin ionophore	0.20

5.0 CONCLUSION

In this thesis, an amperometric enzyme linked phosphate biosensor was successfully developed. Main focus of this investigation was to design and develop an enzyme linked biosensor to detect and quantify phosphate species. Pyruvate Oxidase (POX) (EC. 1.2.3.3, 100 units mg⁻¹) enzyme was immobilized on to three different materials to study their conductivity properties. These materials were; silica polymer, highly conductive carbon nano-tube (CNT) with nickel (Ni) and silver (Ag) and highly conductive multi wall carbon nano-tube (MWCNT) with copper (Cu) and chromium (Cr). All these three materials were evaluated in terms of their electron transfer rate which has an effect on biosensor's sensitivity, selectivity and response time. The biosensor then tested with phosphate solution with five various concentrations (10mM, 1mM, 0.01mM, 0.0001mM and 0.00001mM). As explained in detail (section 4.3) lower detection limit (sensitivity) was attained compared to the reported publications. In particular, a noticeable increase was observed in sensitivity of newly constructed biosensor more with highly conductive multi wall carbon nano-tube (MWCNT) alloyed copper (Cu) and chromium (Cr). Although many draw backs issues were noticed with silica polymer at low concentrations, highly conductive materials (CuCrAgNi with CNT and CuCr MWCNT) did not encounter these draw back issues.

Additionally, the response time was advanced one to two seconds in comparison to the recent study (Villalba, Bioelectroanalytical determination of phosphate 2009). In addition, the selectivity of the sensor was increased when compared to bi-enzyme and the multi enzyme employed in development of biosensors. It is also important to report that multi enzyme dependent (PO_4^{3-}) sensors have number of difficulties including

complicated immobilization process, storage predicament due to the life spans of various enzymes and so forth just to name a few (Villalba, Bioelectroanalytical determination of phosphate 2009).

From all these observations, it was concluded that the conductivity plays an important role in sensitivity and the response time of the sensor. The employed enzyme also plays an important role in the phosphate selectivity of the sensor. In this study, the pyruvate oxidase (single enzyme) was attached to the gold-coated material's surfaces and stored over three months of period. A few experiments with stored enzymes were repeated after a month and in two months period. The results showed slight de-naturation in enzymes and loss of conductivity in nano materials due to the elemental copper leaching to the solution it was stored in. According to these results, the one month storage period after the enzyme attachment on these nano-materials showed an insignificant effect. However, a significant amount of decay observed in selectivity and sensitivity on the developed sensor after the two months of storage period. Therefore, we concluded that, the shelf life of the developed sensing system was longer than the expected time period but it is limited between one to two months. Since the longer life span is one of the important aspects of the advanced bio-sensors, further investigation is needed to be performed to improve the shelf-life of the developed system.

The results obtained showed that using the developed biosensor, it is possible to detect lower concentrations of phosphate in ground water, waste water and many other organisms where phosphate is the major element.

6.0 FUTURE WORK

The recently produced protein, antibody and enzyme which are utilized for immobilization on the surface of the novel materials and the artificial bio-materials can contribute to improve the existing biosensors. Even these materials can be used to develop numerous new sensors with their high efficiency in terms of their advanced sensitivity and the selectivity. This contribution to the field of the health and the environmental detection may be invaluable. Also, field deployability of the sensor could be further studied with the developed experimental cell. Moreover, the sensor may even be miniaturized and multi channel may be added for multiple species detection.

BIBLIOGRAPHY

A.T. Lawal, S.B. Adeloju. "Comparison of enzyme immobilisation methods for potentiometric phosphate biosensors." *Biosensors and Bioelectronics*, 2009: 406–410.

Adrian W. Bott, Brad P. Jackson. "Study of Ferricyanide by Cyclic Voltammetry Using the CV-50W." *Bioanalytical Systems*, 1996: 25-30.

Akar, Serkan. "Development of a biosensor for detection of phosphate species in uranium contaminated groundwater and wastewater sediments." *Waste Management*. Phoenix: Waste Management, 2010.

Akyilmaz, Erol. "Construction of an Amperometric Pyruvate Oxidase Enzyme Electrode for Determination of Pyruvate and Phosphate." *Electrochimica Acta*, 2007: 7972-7977.

Allan, Ian J. "A "toolbox" for biological and chemical monitoring requirements for the European Union's Water Framework Directive." *Talanta* , 2006: 302–322.

Care, GE Health. "General Electric." *General Electric Corporation Website*. November 2007. <http://www5.gelifesciences.com> (accessed February 14, 2010).

Christine Mousty, Serge Cosnier, Dan Shan, Shaolin Mu. "Trienzymatic biosensor for the determination of inorganic phosphate ." *Analytica Chimica Acta*, 2001: 1-8.

Daykin, R. N. C. "Development of micro flow injection manifold for the determination of orthophosphate." *Analytica Chimica*, 1995: 155-159.

E. D. Moorhead, M. M. Stephens, G. A. Bhat. "An Improved Vibrating Wire Electrode Configuration: Voltammetric Reduction of Acidified Ferricyanide and I₂-Catalyzed Iodate." *Analytical Letters*, 1980: 167-179.

Engblom, Sten O. "The phosphate sensor." *Biosensors and Bioelectronics*, 1998: 981-994.

Facility, Chemistry Research. *Sungkyunkwan University*. 2005.

<http://chem.skku.ac.kr/~skkim/reseach-facility.htm> (accessed February 14, 2010).

Fisher, Thermo. "Thermo Scientific." *Thermo Scientific Web site*. 2008. (accessed February 12, 2010).

Fumio Mizutani, Soichi Yabuki, Yukari Sato, Takahiro Sawguchi, Seiichiro Iijima. "Amperometric determination of pyruvate, phosphate and urea using enzyme electrode based on pyruvate oxidase containing poly/polyioncomplex bilayer membrane." *Electrochimica Acta*, 2000: 2945-2952.

Gavalas, V.G. "Phosphate biosensor on Polyelectrolyte-Stabilized Pyruvate Oxidase." *Analytica Chimica Acta*, 2001: 271-277.

Guilbalut, G.G. *Analytica Chimica Acta*, 1975: 69.

Instrument, Pine Resarch. *Material Source Disclamer*. Glassy carbon information, Raleigh, NC: www.pineinst.com, 2005.

Jager, H. De. "Study of the hydrolysis of sodium polyphosphate in water using Raman spectroscopy." *Applied Spectroscopy*, 1998: 808-814.

Khan, Fareed. "Eutrophication: An Ecological Vision." *The Botanical Review*, 2002: 449-482.

Kim, Jin Hyuk. "Effect of local background intensities in the normalization of cDNA microarray data with skewed expression profiles." *EXPERIMENTAL and MOLECULAR MEDICINE*, 2002: 224-232.

Kubo, Inagawa I. "Immobilized Pyruvate Oxidase." *Analytical Letters*, 1991: 1711-1727.

Kulakovskaya, S.I. "Electrochemical Study of Au(III)–Luteolin Flavonoid System in Tris-Buffer." *Russian Journal of Electrochemistry*, 2009: 1135-1144.

Kwan, Roger C. H. "A screen printed biosensor using pyruvate oxidase for rapid determination of phosphate in synthetic water." *Applied Microbial Biotechnology*, 2005: 377-383.

Liu, Chuanjun. "Covalent immobilization of glucose oxidase on films prepared by electrochemical copolymerization of 3-methylthiophene and thiophene-3-acetic acid for amperometric sensing of glucose: Effects of polymerization conditions on sensing properties." *European Polymer Journal*, 2007: 3264-3276.

M. Sánchez-Paniagua López, F. Tamimib, E. López-Cabarcosc, B. López-Ruiz. "Highly sensitive amperometric biosensor based on a biocompatible calcium phosphate cement." *Biosensors and Bioelectronics*, 2009: 2574–2579.

Mak, Wing Cheung. "Biosensor for Rapid Phosphate Monitoring in a Sequencing Batch Reactor (SBR) system. ." *Biosensors and Bioelectronics*, 2003: 233-237.

Masayasu Suzuki, Hironobu Kurata, Yoshihiro Inoue. "Reagentless Phosphate Ion Sensor for Environmental Monitoring." *Journal of The Electrochemical Society*, 1998: 579-583.

McGraw, Christina M. "Autonomous microfluidic system for phosphate detection." *Talanta*, 2007: 1180-1185.

Merkel, B.J. *Uranium in the Environment: Mining Impact and Consequences*. New York: Springer, 2006.

Ming Zhang, Limiao Li, Zhifang Du. "Fast Response Amperometric Biosensor for H₂O₂ Detection based on Horse Radish peroxidase Titinia nano wires ." *Sensor Letters*, 2009: 543-549.

Mozaz, Sara Rodriguez. "Biosensors as useful tools for environmental analysis and monitoring." *Anal Bioanal Chemistry*, 2006 : 1025–1041.

Munroe, N. D. H. "Effect of Addition of Ni and Ag on Cu-CNT Composites Electrical Conductivity." *Materials Science and Technology*. Pittsburgh: MS&T, 2008. 2298-2308.

N. Conrath, B. Grundig, St. Huwel, K. Camman. "A novel enzyme sensor for the determination of inorganic phosphate." *Analytica Chimica Acta* , 1995: 47-52.

Ragothama, K. G. "Phosphate acquisition." *Plant Physiology and Plant Molecular Biology*, 1999: 665-693.

Rahman, Md. Aminur. "The biosensor based on the pyruvate oxidase modified conducting polymer for phosphate ions determination." *Biosensors and Bioelectronics*, 2006: 1116-1124.

Risse, Bernhard. "Stability and reconstitution of pyruvate oxidase from *Lactobacillus plantarum*: Dissection of the stabilizing effects of coenzyme binding and subunit interaction. ." *Protein Science*, 1992: 1699-1709.

Schropp, Diana M. "Phosphorous and phosphate metabolism in veterinary patients." *Journal of Veterinary Emergency and Critical Care* , 2007: 127-134.

Sebastian Buchingera, Pia Grillb, Valeri Morosowb, Hadar Ben-Yoavc, Yosi Shacham-Diamandc, Alva Birand, Rami Pedahzurd, Shimshon Belkind and Georg Reifferscheid. "Evaluation of chrono-amperometric signal detection for the analysis of genotoxicity by a whole cell biosensor ." *Analytica Chimica Acta*, 2010: 122-128.

Serge Cosnier, Chantal Gondran, Jean-Christophe Watelet, Wagner De Giovanni, Rosa P. M. Furriel, Francisco A. Leone. "A Bienzyme Electrode (Alkaline Phosphatase-Polyphenol Oxidase) for the Amperometric Determination of Phosphate." *Analytical Chemistry*, 1998: 3952-3956.

Shiber, Josph R. "Serum phophate abnormalities in the emergency department." *Clinical Laboratory in Emergency Medicine*, 2002: 395-400.

Sigmond, Reidar Svein. "Faraday Cage Profiles Giving Self-similar Charge Drift and Conduction in Insulator Samples." *IEBE Transactions 011 Dielectric and Electrical Insulation*, 2000: 197-203.

Smith, David M. *Engineering Computation with MatLab*. Addison Wesley, 2009.

Susana Campuzano, Maria Pedrero, Jose M. Pingarron. "A peroxidase-tetrathiafulvalene biosensor based on self-assembled monolayer modified Au electrodes for the flow-injection determination of hydrogen peroxide." *Talanta*, 2005: 1310-1319.

USEPA. *Use of Uranium Drinking Water Standards under 40 CFR 141 and 40 CFR 192 as Remediation Goals for Groundwater at CERCLA sites*. Government Agency Yearly Report, Washington, DC: United States Environmental protection Agency, 2001.

Villalba, Maria Marti. "Bioelectroanalytical determination of phosphate." *Journal of Molecular Catalysis B:Enzymatic*, 2009: 1-8.

Wang, Joseph. *Analytical Electrochemistry*. New York: Wiley-VCH, 2000.

Wang, Peng. "Amperometric phenol biosensor based on polyaniline." *Sensors and Actuators*, 2009: 577-584.

Weiner, M.L. "Toxicological review of inorganic phosphates." *Food and Chemical Toxicology*, 2001: 759-786.

Weisinger, Jose R. "Magnesium and Phosphorus ." *Electrolyte Quintet*, 1998: 391-396.

Wellman, Dawn M. "Synthesis and characterization of sodium meta-autunite, Na [UO₂PO₄]₃H₂O." *Radiochim. Acta* , 2005: 393-399.

Wu, Yunfeng. "Filtering electrocardiographic signals using an unbiased and normalized adaptive noise reduction system." *Medical Engineering and Physics*, 2009: 17-26.

Yaico D. Tanimoto de Albuquerque, Lucas Franco Ferreira. "Amperometric biosensing of carbamate and organophosphate pesticides utilizing screen-printed tyrosinase-modified electrodes." *Analytica Chimica Acta*, 2007: 210-221.

Yamamoto, Kazumi. Pyruvate oxidase and an analytical method using the same . Japan Patent 4965194. August 19, 1987.

Yuehe Lin, Fang Lu, Joseph Wang. "Disposable carbon nanotube modified screen printed biosensor for amperometric detection of organophosphorus pesticides and nerve agents ." *Electroanalysis*, 2004: 16.

Zhang, P.C. "Geochemistry of Soil Radionuclides." *Soil Science Society of America*, 002.